Novel water shutoff treatment using PDMS elastomer

Ma, Baoguang

Publication date:
2014

Document Version
Publisher's PDF, also known as Version of record

Novel water shutoff treatment using PDMS elastomer

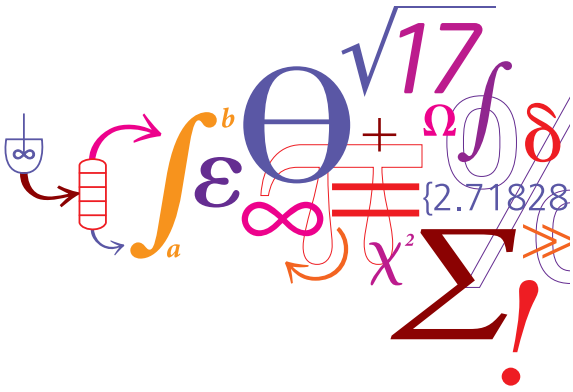

Baoguang Ma
Ph.D. Thesis
October 2014

DTU Chemical Engineering
Department of Chemical and Biochemical Engineering

Novel water shutoff treatment using PDMS elastomer

Baoguang Ma

October 2014

Supervisor: Anne Ladegaard Skov

Co-supervisor: Søren Hvilsted

PhD Thesis

Danish Polymer Centre, DTU, Kgs.Lyngby

DTU Chemical Engineering
Department of Chemical and Biochemical Engineering

Address: The Danish Polymer Centre
Department of Chemical and Biochemical Engineering
Technical University of Denmark
Building 227
DK-2800 Kgs. Lyngby
Denmark
Phone: +45 4525 6801
Web: www.dpc.kt.dtu.dk

Print: J&R Frydenberg A/S
København
January 2015

ISBN: 978-87-93054-59-2

PREFACE

The thesis is written in partial fulfillment of the requirements for obtaining a PhD degree. The work has been carried out at the Danish Polymer Centre (DPC), Department of Chemical and Biochemical Engineering at the Technical University of Denmark (DTU) from August 1 2011 to July 31 2014. The PhD study has been funded by Mærsk Oil and Gas, Qatar.

I would like to convey my sincere gratitude to my supervisor Anne Ladegaard Skov for her endless support, enthusiasm and knowledge for the completion of this work. I would also like to thank my co-supervisor Søren Hvilsted for his fruitful comments and inspiring advices.

I am grateful to my fellow colleagues Lidia Gonzalez, Li Li, Qian Huang, Irakli Javakhishvili, Liyun Yu and Malgorzata Kostrzewska for the wonderful research environment and for their insightful thoughts and comments. A special thanks to Jens Henrik Hansen of Maersk Oil Research and Technology Centre for the guidance of this project.

I dedicate this thesis to my parents and wife.

Baoguang Ma

Oct, 2014

Abstract

Many matured water-flooding reservoirs are suffering excessive water production and low oil sweep efficiency due to the fractures in reservoir rocks. Thus, water shutoff treatment for fractured reservoirs is urgently required to improve the efficiency. Despite many successful treatments, failures are also common for three main reasons as follows. The first reason can be a too efficient plugging effect due to for example that gels are able to form a macroscopic gel inside pore and fractures after penetrating deep into the rock, leading to water inaccessible oil inside the porous rock and thereby low efficiency of oil recovery. The second reason is the formation of macroscopic gel during the transportation arose from the crosslinking reaction taking place not in a controlled manner. The last reason to failure can be a weak plugging effect due to the healing macroscopic gel can not withstand the harsh environment in the oil field, leading to the slide of the macroscopic gel from the fracture.

The objective of this thesis is to solve the above-mentioned problems, namely to block fracture selectively and efficiently. For selective plugging, the healing materials should block the fractures without affecting the pores and form a macroscopic gel inside the fracture in a controlled manner. For efficient plugging, the macroscopic gel should block the fracture and withstand the high pressure difference for a long period. Vinyl functional polydimethylsiloxane (PDMS) microspheres with diameter ranging from 2µm-500µm have been prepared by emulsion polymerization in surfactant solution. The size of the PDMS microspheres allows them to flow into the fracture without affecting the porous rock, while the vinyl groups confer them further crosslinking reaction with hydride crosslinker and yielding macroscopic PDMS elastomer. Moving towards the controlled crosslinking reaction, it has been achieved by the encapsulation of hydride crosslinker in poly (methyl methacrylate) (PMMA) microcapsule. The mixture containing the PMMA microcapsules and the vinyl terminated PDMS allows for storage at 50℃. Upon heating up to 120℃, the hydride crosslinker is released from the microcapsule, reacting with PDMS microsphere and yielding PDMS elastomer. This allows a fast and efficient delivery of elastomeric plug to the fracture. As the criteria for selective and efficient plugging have been fulfilled, core flow experiments are employed to evaluate the water shutoff performance of the elastomeric plug. In the evaluation, macroscopic PDMS elastomer is obtained from vinyl functional PDMS microspheres and hydride crosslinker and filled into the fracture core sample. Compared to the high permeability of the fractured core sample, the water permeability of the treated core sample is significantly lower. Furthermore, the water permeability of the treated core sample is similar to that of the core sample without fracture and remains constant for a long period, indicating that selective and efficient plugging has been achieved.

Resume på dansk

Mange modne, vand-oversvømmede olie-reservoirer lider under for stor produktion af vand og for lav olie-udvindingsgrad på grund af frakturer i undergrunden. Derfor er behandlingsmetoder til at lukke for frakturerne krævet for at øge olie-udvindingsgraden. Til trods for mange succesfulde behandlinger, har fiaskoerne også været almindelige på grund af følgende tre grunde. Første årsag kan være, at frakturlukningen har været for effektiv forstået på den måde, at den også har lukket for porøsiteten i omkringliggende klippe- eller sandsten (kerne) og dermed har forårsaget lav olie-udvindingsgrad. Den anden årsag kan være, at det blokerende materiale ikke har nået frakturen, men i stedet har blokeret undervejs til eller efter frakturen, eller slet ikke har blokeret. Den sidste årsag er for hurtigt tab af blokeringsevne over tid i det ekstreme miljø i oliefeltet.

Formålet med denne afhandling er at løse ovenstående problemer, altså at blokere frakturer selektivt og effektivt. Ved en selektiv blokering menes der, at materialet er i stand til at blokere udelukkende frakturen og ikke poresystemet på en kontrolleret måde. Ved en effektiv blokering forstås en blokering, der kan modstå det ekstreme miljø over tid foruden modstå enorme trykforskelle.

Vinylfunktionelle polydimethylsiloxan (PDMS) mikrokugler med diametre i intervallet 2-500 µm er blevet fremstillet via emulsionspolymerisering i en vandig opløsning af opløsningsmiddel. Størrelsen af mikrokuglerne tillader dem at flyde ind i frakturen, men ikke at flyde ind i den porøse kerne. Vinylgrupperne på overfladen af mikrokuglerne gør mikrokuglerne i stand til krydsbinding ved tilstedeværelsen af en hydridfunktionel krydsbinder og dermed danne en makroskopisk PDMS elastomer. Den kontrollerede krydsbinding opnås ved at indkapsle krydsbinderen i poly(methylmethacrylat) (PMMA) i såkaldte mikrokapsler. Disse kapsler kan blandes med PDMS mikrokuglerne og lagres ved temperaturer under 50^{o}C uden krydsbinding. Ved opvarming til glasovergangstemperaturen for PMMA frigives krydsbinderen og reagerer med mikrokuglerne, hvormed en PDMS elastomer fås. Dette muliggør en hurtig og effektiv placering af den frakturblokerende elastomer.

For at vurdere kvaliteten af blokeringen er kernestrømningsforsøg gennemført. En kerne påføres en fraktur, hvormed vand-permeabiliteten øges kraftigt. Dermed udføres behandlingen med mikrokugler og krydsbinder, og målingen gentages. Permeabiliteten er tilnærmelsesvist identisk med den oprindelige kerne, hvormed det er bevist, at elastomeren effektivt blokerer frakturen og samtidigt ikke forårsager lav-permeabilitets-zoner i omkringliggende kerne. Blokeringsevnen er tilmed vist at være konstant over lang tid, hvilket beviser effektiviteten af blokeringsmetoden.

Contents

PREFACE i

Abstract ii

Resume på dansk iii

Contents iv

1. Introduction 1

1.1. Fracture characteristics 1

1.1.1. Width 1

1.1.2. Orientation 2

1.1.3. Length 2

1.1.4. Nature of fracture 3

1.1.5. Fracture density and intensity 3

1.2. Current methods in oil field treatment 4

1.2.1. Inorganic gel system 4

1.2.2. Thermosetting synthetic resin system 4

1.2.3. Monomer-based system 5

1.2.4. Polymer gel system 5

1.2.5. Polymeric microsphere system 6

1.3. Novel method in oil field treatment 6

1.3.1. Criteria for physical properties of healing material 6

1.3.2. Criteria for size of healing material 9

1.3.3. Criteria for initiation of crosslinking reaction 9

1.4. Thesis outline 10

2. PDMS microspheres with PMMA coating: modeling, preparation and characterization 11

2.1. Mean diameter predicted by Hinze-Kolmogorov theory 11

2.2. Size distribution described by population balance model, maximum entropy formalism and normal distribution 12

2.2.1. Population balance model 12

2.2.2. Maximum entropy formalism 14

2.2.3. Normal distribution 15

2.3. Experimental section 15

2.3.1. Materials 15
2.3.2. Experimental procedure 16
2.3.3. Apparatus 16
2.4. Modeling 17
2.5. Results and discussion 18
2.5.1. Experimental mean diameter and size distribution of PDMS microspheres 18
2.5.2. Comparison of theoretical predictions with experimental results 20
2.5.3. Characterization of PMMA coated PDMS microspheres 24
2.6. Conclusions 27
3. Surface vinyl concentration of PDMS microspheres and their further crosslinking reaction 28
3.1. Quantification of surface vinyl concentration of PDMS microspheres 28
3.2. Crosslinking reaction between PDMS microspheres and hydride crosslinker 29
3.3. Experimental section 29
3.3.1. Materials 29
3.3.2. Apparatus 29
3.3.3. Experimental procedure 30
3.4. Results and discussion 31
3.4.1. Size distribution of vinyl functional PDMS microspheres 31
3.4.2. Soluble fraction of vinyl functional PDMS microspheres 32
3.4.3. Surface vinyl concentration of PDMS microspheres 33
3.4.4. Crosslinking reaction between PDMS microspheres and hydride crosslinker 36
3.4.5. Terminal storage moduli of resulting macroscopic PDMS network 39
3.5. Conclusions 41
4. Control of PDMS crosslinking by encapsulating a hydride crosslinker in a PMMA microcapsule 42
4.1. Control of PDMS crosslinking reaction 42
4.2. Experimental section 43
4.2.1. Materials 43
4.2.2. Apparatus 43
4.2.3. Microcapsule preparation 43
4.2.4. Soluble fraction determination 44
4.3. Results and discussion 44
4.3.1. Morphological characterization 44
4.3.2. Size distribution 45

4.3.3. Determination of the HMS-301 weight fraction in microcapsules 46
4.3.4. Reactivity of PMMA/HMS-301 microcapsules in a vinyl-terminated PDMS polymer 47
4.3.5. Soluble fraction 49
4.3.6. Influence of stoichiometric imbalance on the equilibrium storage modulus 50
4.4. Conclusions 55
5. Water shutoff performance of macroscopic PDMS elastomer 56
5.1. Water permeability 56
5.2. Experimental section 57
5.2.1. Materials 57
5.2.2. Apparatus 57
5.2.2. Experimental procedure 58
5.3. Results and discussion 60
5.3.1. Properties of PDMS microspheres and their crosslinking reaction 60
5.3.2. Mechanism of water shutoff using macroscopic PDMS elastomer 60
5.3.3. Evaluation of water shutoff performance of macroscopic PDMS elastomer 61
5.3.4. Comparison with other water shutoff systems 63
5.4. Conclusions 64
6. Conclusions and future work 65
6.1. Conclusions 65
6.2. Future work 66
References 67
Symbols and abbreviations 77
Publication list 80
Copyright 81
Appendix I 83
Appendix II 115

1. Introduction

Water injection is widely employed in reservoirs to increase the oil production rate, and ultimately, oil recovery. The mechanism of water injection is to displace oil from pores and to push it towards a production well[1]. However, for fractured reservoirs, injected water can break through rapidly along the fractures, resulting in problematic oil production due to a high water cut and a decline in the oil production rate. Thus, it is highly important to block the fractures to increase the efficiency of oil recovery[2]. In the following, the characteristics of fractures will be explained and current methods for oil field treatment will be discussed.

1.1. Fracture characteristics

Oil field treatment is affected by many factors, including properties of the healing material, fracture characteristics, reservoir temperature and pressure, etc. Despite many successful treatments, failure cases, which result in huge economic losses and the potential shutdown of reservoirs, are not rare[3]. To avoid failure treatment and to block fractures efficiently, a proper understanding of fracture characteristics is required. Fracture characteristics are usually described by five parameters: width, orientation, length, nature of fracture as well as fracture density and intensity. These parameters are explained in the following sections in greater detail.

1.1.1. Width

The distance between fracture walls is defined as fracture width. Fracture width usually varies from 1µm to 4mm[4], depending on the type of rock and reservoir pressure. In general, the most common types of rock in reservoir are sandstone and limestone. The average fracture width in a limestone reservoir is often smaller than that in a sandstone reservoir in the same district[5,6].

Fracture width is also related to reservoir pressure, which is defined as the pressure of fluids within the pores of a reservoir. Reservoir pressure correlates to an increase in fracture width by 10%-80%[5]. Upon the release of reservoir pressure, the fracture expands, resulting in the increase of fracture width. Thus, the fracture width measured in the lab at atmospheric pressure is larger than that in the reservoir[3].

Compared to a fracture width of around 1µm, pore size in porous rocks is much smaller, mostly below 1µm. The permeability of porous rock increases significantly due to the presence of fractures with a width larger than 10µm. For instance, Zhao *et al*[7] reported that the permeability of a 4-cm core sample increased by 100 times due to an 800-µm fracture under lab conditions. In comparison, the permeability of porous rock increases by only 20% due to the presence of a fracture with a width of less than 10µm[8]. Hence, from a commercial point of view, fractures larger than 10µm are of particular interest in our application.

1.1.2. Orientation

Fracture orientation plays an important role in oil recovery, and it is usually described according to the direction between the injection well and the production well. When fracture orientation is parallel to the direction between the injection well and production well, the injected water will flow through the high permeable fractures instead of the porous rocks, resulting in low efficiency of oil recovery. This orientation of the fractures is described as 'unfavorable direction'. When fracture orientation is normal to the direction between the injection well and the production well, the permeability of the porous rock increases slightly. Therefore, the efficiency of oil recovery will not be significantly affected. The orientation of the fractures is described as 'favorable direction'[4,9]. Figure 1.1 schematically shows the top view of fractures in favorable and unfavorable directions in reservoirs.

Dyes *et al*[10] reported that the water permeability of a 13-mm width core sample increased by more than 100% when a 200-μm wide fracture was located in unfavorable direction. In comparison, water permeability increases just under 10% due to the presence of a 200-μm fracture in the favorable direction.

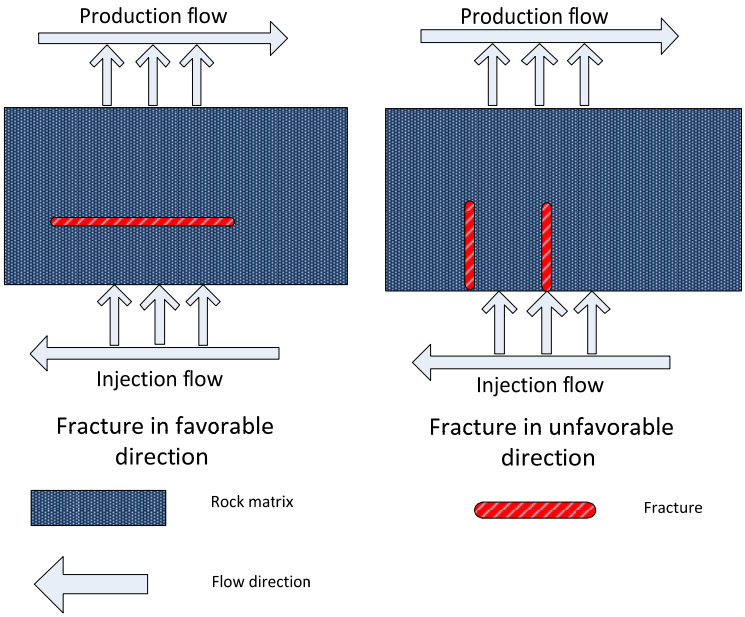

Figure 1.1. Top view of fractures in favorable direction and unfavorable direction in oil reservoirs.

1.1.3. Length

Fracture length is defined as the distance between two fracture openings. Fracture lengths range from meters to thousands of meters, depending on the type of rock and reservoir pressure. Fractures can also be grouped into two types by length: first-order fractures, which traverse more than one reservoir layer and have a very large extension, often on the order of 10-100 meters, and second-order fractures, which have a length less than that of a single layer of the reservoir.

In the evaluation of effects of fracture length on oil recovery, fracture orientation should also be considered simultaneously. For fractures in favorable direction, Fisher *et al*[11] reported that the efficiency of oil recovery was not affected markedly, even though they are first-order fractures. For fractures in unfavorable direction, the efficiency of oil recovery decreased by at least 50% when fractures are longer than half of the distance between the injection well and the production well[12,13].

1.1.4. Nature of fracture

The nature of fracture can be described according to several parameters. First, the nature of fracture can be described by the filling minerals. The volume and the type of the filling minerals are numerous in different reservoir layers, depending on the location of the fracture openings. Compared to the volume of oil and porous rock in an oil reservoir, the volume of the filling minerals is fairly small. As the filling minerals will be easily washed away by the injection of water, the influence of the filling minerals is therefore limited in oil recovery. Secondly, the nature of fracture can also be described by the fracture walls, which can be rough or smooth. The properties of fracture walls are related to the velocity of the injection water and the stability of the healing chemicals inside the fracture. Olsson *et al*[14] reported that the velocity of injected water increased by 20% inside a smooth fracture and decreased by 40% inside a rough one. When water passes through fractures with smooth walls, the flow rate of water is higher than that through rough walls, resulting in the production of more water during oil recovery. Moreover, the smooth surface of the fracture may lead to the sliding of the healing material and, in turn, unsuccessful treatment[15]. Thirdly, the location of the fracture opening can also be used to describe the nature of fracture. When the fracture opening is located in the joint of two different layers, the injection water may flow into other layers in the reservoir instead of driving oil from the porous rock, resulting in a low oil production rate[9].

1.1.5. Fracture density and intensity

Fracture density is the ratio between the number of fractures and the length of the rock matrix. For sandstone reservoirs, the fracture density is between 9.0-50.0 fractures per meter. For limestone reservoirs, the fracture density ranges from 12.0-33.0 fractures per meter[4].

The fracture intensity is the ratio between the fracture density and the thickness of the reservoir layer. According to Ruhland[16], the reservoir layers can be divided into three categories by fracture intensity: layers with fracture intensities of less than 1 are defined as average fractured layers, and layers with fracture intensities ranging from 5-50 are strongly fractured layers, while layers with fracture intensities of larger than 100 are defined as breccia layers. The average fractured layer is beneficial for oil recovery because the limited number of fractures usually does not cause water channeling. For the strongly fractured layers, treatments are usually required before oil recovery. Otherwise, water may flow through the high permeable fractures, resulting in the production of an excessive amount of water during oil recovery[17]. In the breccia layer, oil recovery should be avoided because the treatment cost of the layer is usually fairly high[4,18].

1.2. Current methods in oil field treatment

As discussed in Section 1.1, fractures not only reduce the efficiency of oil recovery, but also result in excessive production of water. It is estimated that the unwanted production of water costs about $45 billion every year, including the expense of lifting, disposing and reinjection of water, as well as the purification of the produced oil[19].

Numerous attempts have been made to address the excessive production of water. Most attempts involve the pumping of chemicals into the oil field in order to block the fractures and reduce unwanted production of water. Several types of widely employed chemicals are discussed in the following sections:

1.2.1. Inorganic gel system

Sodium silicate gel is one of the most frequently used inorganic gels in oil field treatment. Due to its low viscosity, the sodium silicate solution can penetrate deeply into the rock matrix easily[20]. After being activated by a catalyst, the sodium silicate can crosslink and form a strong gel, which is stable at up to 150℃[21]. Compared to other chemical methods, the sodium silicate gel treatment is fairly economical. Therefore, the treatment is often applied to abandoned oil reservoirs, which produce less than 5% oil in the producing fluid before treatment.

However, there are drawbacks to the use of inorganic gel. First, the gelation of sodium silicate gel is rapid. Control of gelation is therefore difficult to achieve. If gelation takes place before arriving at the fracture, the gel may block the rock matrix instead of healing the fractures. Secondly, the silicate gel is not stable in an acidic environment. In the presence of caustic chemicals, the gel will dissolve slowly and lose its strength, resulting in invalidation of the treatment.

1.2.2. Thermosetting synthetic resin system

Thermosetting synthetic resins are polymers cured irreversibly. With superior physical strength and thermal stability, thermosetting synthetic resins are widely used for sand consolidation and blocking fractures in sandstone reservoirs[22]. Amongst all resins, phenolic resins are most commonly used.

Moradi *et al*[23] reported that the water permeability of a sandstone reservoir decreased by 57.5% after the treatment of phenolic resin. Initially, the solution contains 2,000ppm phenol and 2,000ppm formaldehyde in fresh water. When the solution is pumped down and cured, the fractures are blocked within 1.1days at 93℃, and the resulting water permeability decreases significantly. Steven *et al*[24] also reported that successful oil field treatment achieved at the reservoir temperature ranged from 60℃ to 140℃ by using the phenolic resin. The reaction leading to the formation of phenolic resin is shown in Figure 1.2[25].

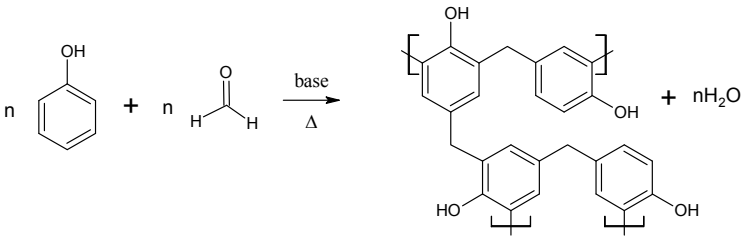

Figure 1.2. Polycondensation of phenol and formaldehyde.

1.2.3. Monomer-based system

Monomeric systems have also been used in oil field treatment. Initially, monomers are stored as low-viscosity solutions. After being pumped into the oil field, the monomers will penetrate into the rock matrix and flow into the fractures. When monomers are activated by a catalyst, they will polymerize and form a strong gel. Amongst all monomeric systems, the acrylamide (AM) system is the most commonly used.

Larry *et al*[26] reported that the efficiency of oil recovery increased by 100% after the treatment of an AM system in a fractured reservoir. The AM system used in the literature is activated by azo initiators at 50℃ and validates in reducing water permeability after a period of 24h. Dalrymple *et al*[27] further found that the polymerization of AM was not sensitive to the ions in the solution, indicating that the AM system was compatible with brine. As brine costs less than fresh water, the AM system is more commercially feasible. However, the AM system has been gradually substituted by polymeric gel systems because of the high cost and the high toxicity of AM.

1.2.4. Polymer gel system

The polymer gel system usually consists of a high molecular weight polymer with functional groups and a crosslinker. The polymer gel, which is obtained from the crosslinking reaction between the polymer and the crosslinker, can be used to block fractures in the oil field. Amongst all polymer gel systems, the polyacrylamide (PAM) gel system is most widely used in oil field treatment[28,29].

Anazi *et al*[30] reported a successful treatment using PAM gels in a fractured core at 80℃ under lab conditions. Initially, the solution contains a 5,000-ppm PAM gel and a 500-ppm crosslinker in brine. When the solution is pumped into the fractured core and cured for 18h, the water permeability of the fractured core decreases from 800mD to 8mD. Due to the wide applicability of a PAM system in blocking fractures, the effects of PAM concentration on the crosslinking reaction has been investigated in many studies. For instance, Jia *et al*[31] reported that no visible gel can be obtained with a PAM concentration lower than 0.5%, regardless of the concentration of the crosslinker and the molecular weight of the PAM. To obtain a strong gel, the PAM concentration should be above 1.5% and a moderate concentration of crosslinker should be used.

1.2.5. Polymeric microsphere system

Different types of polymeric microspheres have been used in oil field treatments[32–38]. Yao *et al*[39] reported that the oil production rate of a reservoir increased from 72.5 tons/day to 132.2 tons/day after the treatment of PAM microspheres. The mean diameter of the PAM microspheres is approximately 12μm, and the size of the PAM microspheres ranges from 4μm to 40μm. The PAM microspheres are dispersed in brine at a concentration of 2,000mg/L and then pumped down into the oil field over a period of 65 days. In another study, Zhang *et al*[35] investigated the plugging efficiency of polyacrylamide/polyacrylic copolymer microspheres in fractured cores at room temperature and at atmospheric pressure. The polyacrylamide/polyacrylic copolymer microspheres are dispersed at a concentration of 1,000mg/L in brine to yield a solution. The solution is then injected into fractured cores at a flow rate of 5mL/min-30mL/min. It has been shown that the water permeability of the fracture decreases by up to 80% after the injection of the microsphere solution.

1.3. Novel method in oil field treatment

As discussed in Section 1.2, most of the current methods in oil field treatment involve the pumping of low-viscosity chemicals into the oil field. The chemicals with functional groups can further react with crosslinkers, yielding a macroscopic gel in the fracture. The macroscopic gel will act as physical barrier, thus significantly reducing the water permeability of the oil field. On the other hand, the chemicals pumped down into the oil field can also penetrate into the porous rock, yielding a macroscopic gel inside it. This will result in oil inaccessible to water, potentially shutting down the oil field. Thus, this thesis will focus on designing a novel system for blocking fractures without affecting the porous rock. In the design of the system, several criteria should be satisfied and will be discussed as follows:

1.3.1. Criteria for physical properties of healing material

The first objective of this thesis is to design a new system for blocking fractures in reservoirs. Regarding the physical properties of the healing material, the new system should fulfill several requirements. First, the system should contain chemicals that can react with crosslinkers, yielding a macroscopic gel to block the fractures. Secondly, the macroscopic gel from the crosslinking reaction should be thermally and chemically stable in the oil field. Thirdly, the macroscopic gel should be able to sustain the high hydraulic pressure inside the fracture, which is caused by the injection of water during oil recovery.

Based on the requirements above, polydimethylsiloxane (PDMS) elastomers are selected as the healing materials due to their high thermal stability, high durability and excellent mechanical properties[40–43]. The properties of the PDMS elastomer will be discussed in the following based on the requirements of blocking the fractures.

The first requirement of the new system is the ability to obtain macroscopic gel from the crosslinking reaction between the chemicals and the crosslinkers. The PDMS elastomer can be obtained from the crosslinking reaction between PDMS polymers and crosslinkers. Grouped by the mechanisms of the crosslinking reactions[43], there are two types of silicone elastomer: Room Temperature Vulcanizing (RTV) and High Temperature Vulcanizing (HTV) silicones. In this study, RTV silicone is used. The RTV silicone elastomer is formed via two reactive components, namely PDMS polymer with terminal vinyl groups and

crosslinkers with hydride groups. In the presence of a platinum catalyst, the vinyl groups react with the hydride groups through a hydrosilylation reaction, yielding a three-dimensional PDMS network. The mechanism of the crosslinking reaction of RTV silicone is shown in Figure 1.3[44].

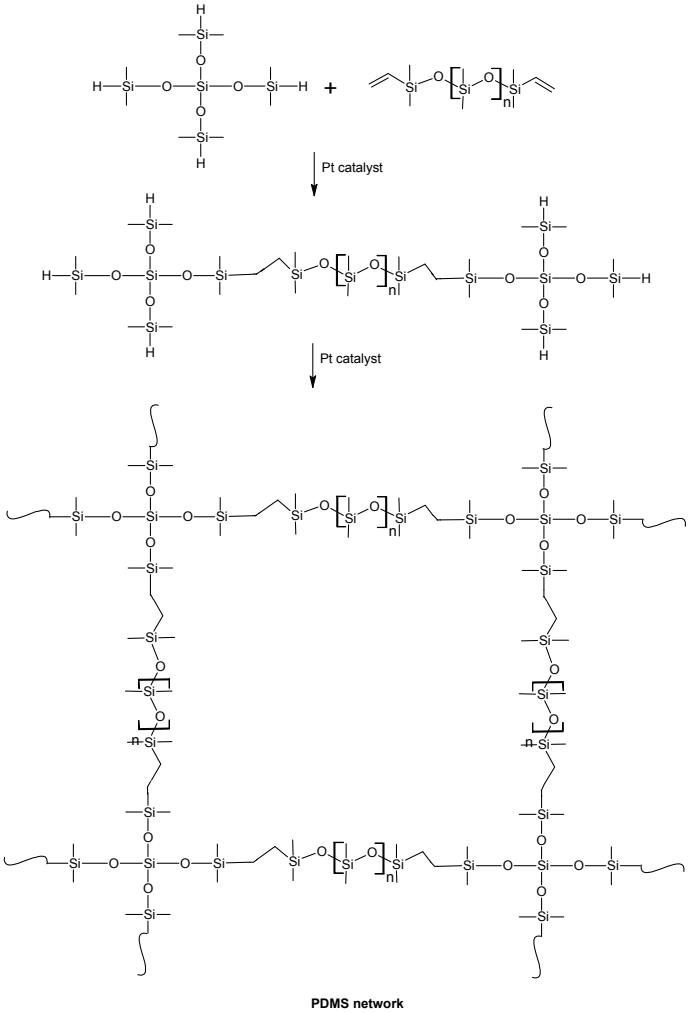

Figure 1.3. Formation of a crosslinked PDMS elastomer through hydrosilylation reaction between vinyl-terminated PDMS and four-functional hydride crosslinker.

As discussed above, the reactivity of PDMS allows for a crosslinking reaction and obtaining a macroscopic PDMS elastomer. To determine whether the PDMS elastomer satisfies other requirements in oil field treatment, the properties of the PDMS elastomer will be compared with those of PAM gels, which have been widely used in oil field treatment.

The second requirement of the macroscopic gel is high durability at high temperature. The high durability of PAM gel makes it a suitable material for use in oil field treatment. The thermal stability of the PAM gels is therefore investigated in many studies[29,45–48]. For instance, Dupuis *et al*[49] investigated the thermal stability of a PAM gel system in an oxygen-free oven at 60℃, 100℃ and 140℃. The PAM gels in the literature are obtained from the crosslinking reaction between 7,000-ppm PAM and 1,400-ppm crosslinker in brine. The thermal stability of the PAM gels is evaluated by measuring the viscosity of the PAM gels. It has been shown that the viscosity of the PAM gels remains constant at 60℃ and 100℃ and decreases by 60% at 140℃ over a period of four months, indicating that the thermal stability of the PAM gels is less than 140℃. Many studies have further shown that the backbone of the PAM gels undergoes hydrolysis from 70℃ to 105℃[7,28,29,45,46,50,51].

Compared to the thermal stability of PAM gels, the thermal stability of the PDMS elastomer is significantly higher. According to reported data from the ShinEtsu Silicone Company and Dow Corning[52,53], PDMS elastomers can be used indefinitely at 150℃ and for more than several years at 200℃ with almost no changes in properties under both ambient and oxygen-free conditions, suggesting high thermal stability of the PDMS elastomer at 200℃. Thus, PDMS elastomer should be qualified to sustain high temperatures in the oil field.

The third requirement of the macroscopic gel is high chemical stability to sustain the corrosion of chemicals in the oil field. As a representative material in oil field treatment, PAM gels are expected to be chemically stable. The chemical stability of the PAM gels is therefore investigated in several studies. Russell *et al*[54] investigated the chemical stability of the PAM gels synthesized from solutions containing 2,000-ppm PAM and 2,000-ppm crosslinker by measuring the viscosity of the PAM gels in an oxygen-free environment. In a period of two months, the viscosity of the PAM gel system decreases by 50% at a pH of 8.0 at 50℃ due to the hydrolysis of the PAM gels. Yang *et al*[55] also reported that the viscosity of a similar PAM gel system decreased by 65% at 50℃ in the presence of ferrous ion and oxygen over a period of two weeks. Compared to the PAM gel system, the chemical stability of PDMS elastomer is markedly higher. For most fully crosslinked PDMS elastomer, they can sustain a pH range of 5-9 for more than one year regardless of the presence of oxygen[56–59]. Hence, PDMS elastomers should be suitable to sustain the corrosive chemicals in the oil field.

The fourth requirement of the macroscopic gel is good mechanical properties. The mechanical properties can be described by many parameters, such as hardness, tensile strength and gel strength. Amongst all parameters, gel strength is the most important one, as it describes the ability of a material to retain shape based on its resistance to force. The gel strength of PAM gels has been investigated in many cases because PAM gels are the most widely used material in blocking fractures. Kakadjian *et al*[60] investigated the gel strength of PAM gels used in blocking fractures at concentrations of 5%-20% in brine at room temperature and at atmospheric pressure. The gel strength of the PAM gels is characterized by the frequency sweep rheological measurement at a strain rate of 1%. It has been shown that the complex modulus of the crosslinked PAM gels is approximately 400Pa at a concentration of 20% and 100Pa at a concentration of 5% at a frequency of 1Hz.

Compared to the complex modulus of the PAM gel systems, the PDMS elastomer has a much higher complex modulus, usually ranging from 10^4 to 10^6 Pa[41,61]. The high complex modulus of the PDMS

elastomer allows for sustaining much higher hydraulic pressure in the fracture during the oil recovery. Hence, PDMS elastomer should be suitable for the water shutoff application.

1.3.2. Criteria for size of healing material

Numerous attempts, most of which involve the pumping of crosslinkable chemicals as described in Section 1.2.1-1.2.4, have been made for addressing this problem[62]. The chemicals usually have low viscosity and, therefore, are able to penetrate deep into the oil field, yielding a gel inside the fracture to hinder the flow of water. Despite many successful treatments, failures are also common, resulting in huge economic loss and in the potential shutdown of the well[29]. A reason for failure can also be due to an overly efficient plugging effect as a result of, for example, the formation of a macroscopic gel inside pores and fractures simultaneously after penetrating deep into the rock, leading to water-inaccessible oil inside the porous rock and, thus, low efficiency of oil recovery[32,49].

Another objective of this thesis is to solve the above-mentioned problem, namely to block fractures without affecting the porous rock. One way is to prevent the healing materials from flowing into the porous rock. This requires that the size of the healing material should be larger than that of the pores, i.e. larger than approximately 1µm. Meanwhile, the size of the healing material should also be smaller than the width of the fracture, which ranges from 1µm to 4mm, such that the healing materials are able to flow into the fracture and yield a macroscopic gel inside it. As discussed in Section 1.2.5, polymeric microspheres constitute one of the materials that fulfill the size requirements and are able to block fractures without affecting the pores inside the rocks[35,39,63]. Though microspheres have not been applied in blocking fractures, they have been widely used in profile control since they can reduce the high permeability of an oil field without affecting the pores in the rock. The studies in Section 1.2.5 suggested that the mechanism behind the microspheres blocking the high-permeability zone without affecting the pores was that the size of the microspheres fell between the size of pores and that of the high permeability zone.

The similarities between using microspheres for profile control and for fracture blocking are numerous, but for the efficient blocking of fractures, the microspheres should be assembled covalently to yield a macroscopic gel inside the fracture. PDMS microspheres are employed in the application of blocking fractures due to their high thermal stability, high reactivity and hydrophobicity. The high thermal stability of the PDMS microspheres, which arises from the flexible backbone of the PDMS molecule, allows the PDMS microspheres to maintain the mechanical properties at over 200°C for several years[53]. This enables the PDMS microspheres to facilitate water shutoff despite the harsh environment of the oil field. The reactivity of the investigated PDMS microspheres can be attributed to the vinyl groups on the surface, which allows for the extensive crosslinking reaction in the presence of crosslinker to yield a macroscopic PDMS elastomer. The high and efficient reactivity is favorable because otherwise the PDMS microspheres can be washed away due to the injection of water. Finally, the hydrophobicity of the PDMS microspheres will prevent water from penetrating the PDMS elastomer, resulting in the long-term validity of the treatment[24].

1.3.3. Criteria for initiation of crosslinking reaction

As discussed in the first two objectives, the excellent physical properties and the moderate size of the PDMS microspheres enable its fracture blocking without affecting the porous rock. To introduce the

macroscopic gel into the fracture, it is also important to prevent the covalent assembly of the PDMS microspheres before flowing into the fracture. Thus, the crosslinking reaction of the PDMS microspheres should be controlled.

The last objective of this thesis is to design a responsive system for oil field treatment, namely the control of PDMS microsphere crosslinking. One way to achieve this goal is to encapsulate the hydride crosslinker in polymeric microcapsules. When the hydride crosslinker is sequestered inside the microcapsules, the microcapsules can be mixed with the PDMS microspheres without undergoing a crosslinking reaction, thereby ensuring that the PDMS microspheres have not reacted.

To initiate the crosslinking reaction and obtain a macroscopic gel, the hydride crosslinker should be released from the polymeric shell, which is capable of changing its morphology or structure upon external stimulus. Thermal initiation is one of the most commonly used stimuli that cause changes in the structure of amorphous polymer. At temperatures lower than the glass transition temperature (T_g) of the polymeric shell, the shell remains rigid, and the hydride crosslinker is sequestered inside it; therefore, the PDMS microspheres will remain separate due to the absence of the crosslinking reaction. Upon heating of the system, the structure of the polymeric shell changes when the temperature is higher than its T_g, resulting in the release of the hydride crosslinker and the initiation of the crosslinking reaction.

1.4. Thesis outline

The thesis is organized as follows. **Chapter 2** deals with the preparation, modeling and coating of the PDMS microspheres.

In **Chapter 3**, the vinyl concentration of the PDMS microspheres is determined by a novel titration method exploiting monofunctional hydride, while the crosslinking reaction of the PDMS microspheres is analyzed by rheological measurement.

In **Chapter 4**, the control of PDMS crosslinking by encapsulating a hydride crosslinker will be analyzed.

The topic of **Chapter 5** is the water shutoff performance of macroscopic PDMS elastomer in a core flow experiment.

Finally, the conclusions of this thesis and opportunities for future work will be discussed in **Chapter 6**.

2. PDMS microspheres with PMMA coating: modeling, preparation and characterization

As discussed in Section 1.3.1 and 1.3.2, the size of the healing materials used in oil field treatment should fall between 1μm and 4mm, such that the healing materials can block the fracture without affecting the porous rock in the oil field. In this chapter, PDMS microspheres with diameter ranging from 2μm to 500μm are prepared by emulsion polymerization in surfactant solution. The influences of surfactant concentration on the mean diameter and the size distribution of the PDMS microspheres are also investigated. Furthermore, the experimental mean diameter is compared with the theoretical mean diameter predicted by Hinze-Kolmogorov theory, which will be discussed in Section 2.1. The experimental size distribution is compared with the theoretical size distribution described by population balance model and maximum entropy formalism, which will be discussed in Section 2.2. The PDMS microspheres are coated with a poly (methyl methacrylate) (PMMA) shell to protect the surface vinyl groups by a novel spin coating method. The efficiency of the PMMA shell in protecting the vinyl groups on the surface of the PDMS microspheres is investigated by rheological measurement. The results presented in this chapter have been submitted to Canadian Journal Chemical Engineering and is attached as Appendix I.

2.1. Mean diameter predicted by Hinze-Kolmogorov theory

Many industrial processes involve liquid-liquid dispersion in stirred vessels and the knowledge of the resulting drop size distribution characteristic with changes of external mechanical energy input. Much work has been done to investigate the mean diameter and size distribution in turbulent liquid-liquid dispersions subjected to mechanical stirring, and most of them investigate the concept of turbulent energy cascaded to predict the mean diameter of droplets, referring to the Hinze-Kolmogorov theory[64]. This theory presents a decreasing power law for the dependence of the mean diameter on the average turbulent energy dissipation. Applying this approach, similar equations have been derived for systems where energy dissipation occurred[65–67]. A recent version of the resulting formula is:

$$\frac{D_{32}}{D} = k \cdot We^{-0.6}(1 + a \cdot Vi(\frac{D_{32}}{D})^{\frac{1}{3}})^{0.6}(1 + b \cdot \phi) \tag{2.1}$$

where *We* is the Weber number given by equation (2.2) and *Vi* is the viscosity number given by equation (2.3)

$$We = \frac{\rho \cdot \omega^2 \cdot D^3}{\sigma} \tag{2.2}$$

$$Vi = \frac{\mu_d \cdot \omega \cdot D}{\sigma} \tag{2.3}$$

where D_{32} is the Sauter mean diameter, D is impeller diameter, k is an empirical constant, a is a proportionality factor, b is an empirical system-dependent constant, ρ is the density of the continuous

phase, φ is the volume fraction of the dispersed phase, μ_d is the viscosity of the continuous phases, ω is the rotational speed of the impeller and σ is the surface tension of the aqueous solution.

2.2. Size distribution described by population balance model, maximum entropy formalism and normal distribution

The particle size distribution has been predicted by numerous methods in turbulent systems. Amongst the methods, population balance model, Monte Carlo simulation and maximum entropy formalism were most commonly used. The population balance model deals with systems containing particles in a continuous phase. In this model, the basic assumption is that there exists a number density of particles in a continuous phase[68]. By coupling conservation equations with this assumption, the population balance model is used to depict the number density and the size distribution of particles at given conditions. The population balance model has been applied in various studies, in which the number density and the particle distribution play an important role. For instance, this model has successfully predicted the size distribution of droplets in water-in-oil systems[69,70] and oil-in-water systems[71,72]. As the population balance model is concerned about the particle size distribution on a macroscopic level, Monte Carlo simulation has also been used for describing the particle size distribution by means of statistics[73]. Compared to the other methods, the Monte Carlo simulation describes the particles with various degrees of freedom, such as temperature, pressure and density. Also, the simulation provides a realistic way to understand a system in a dynamic way. For instance, Monte Carlo simulation has been used to predict the particle size distribution by combining the behavior of individual particle in the system[74]. While the Monte Carlo simulation describes the particle size distribution in a dynamic way, maximum entropy formalism depicts the particle size distribution in a thermodynamic way[75]. The maximum entropy formalism suggests the least biased solution in the prediction of the particle size distribution, given that the statistical entropy in the system is maximized. For instance, the drop size distribution in a spraying process has been successfully predicted by this formalism[76]. In this study, the population balance model and the maximum entropy formalism are used to describe the size distribution of the PDMS microspheres.

2.2.1. Population balance model

Consider a suspension that contains a large number of particles, each consisting of a number of primary particles. Due to the high speed mechanical stirring in the vessel, there is a great possibility that the particles will collide with each other and form larger particles in the suspension; but it is also possible that the particles break and divide into smaller particles or primary particles due to the mechanical stirring until a dynamic equilibrium is established[77,78].

Let the number of particles in the system be N, the number of primary particles be N_0 and the number of particles with size equal i be N_i. Then it can be written as:

$$N = \sum_{i=1} N_i$$
$$N_0 = \sum_{i=1} i \cdot N_i \qquad (2.4)$$

where *i* is the number of primary particles in a particle. By assuming that the fragmentation and the aggregation process of the particles occur randomly and independently, the particle size distribution is determined solely by the stochastic combination of the primary particles[79,80]. When the dynamic equilibrium is achieved, the particle size distribution can be predicted by using various methods or assumptions, such as self-similarity[81], breakage-domination[82], aggregation-domination[83] or maximum entropy[84]. Here, the maximum entropy assumption is used to depict the particle size distribution in the dynamic equilibrium in our system. From Boltzmann's equation, *S* can be expressed as:

$$S = k_B \ln \Omega \tag{2.5}$$

where k_B is the Boltzmann constant and Ω is the degeneracy or the total number of ways in which the particles can be distributed into all particles. According to the statistical mechanics[85], Ω can be expressed as:

$$\Omega(N_1, N_2, N_3 \ldots) = \frac{N_0!}{\prod_{i=1}^{N_0} N_i ![i!]^{N_i}} \tag{2.6}$$

Since the value of Ω is constrained by (2.4) and (2.6), the Lagrange multipliers λ_1 and λ_2 are introduced in order to obtain the maximum value of Ω.

$$\frac{\partial}{\partial N_i}(\ln \Omega + \lambda_1 N_0 + \lambda_2 N) = 0 \tag{2.7}$$

In an isotropic turbulent system, where all particles are primary particles or a single large particle in the solution, Ω is minimized. When the number of particles is suitable, Ω becomes maximized. By solving equations. (2.4)-(2.7), we obtain the Poisson type size-distribution probability function[86]:

$$p(i) = \exp(-Z)\frac{Z^i}{i!} \tag{2.8}$$

where *Z* is the characteristic parameter of N_0, and it satisfies the following equation:

$$N_0 = Z \exp Z \tag{2.9}$$

The primary particle size is denoted d_{min} to describe the relation between drop size distribution and particle size using the mathematical definition of D_{32}:[79,80]

$$\frac{\sum_{i=1}^{N_0} i \cdot p(i)}{\sum_{i=1}^{N_0} i^{2/3} \cdot p(i)} = \frac{D_{32}}{d_{\min}} \tag{2.10}$$

2.2.2. Maximum entropy formalism

In the prediction of the particle size distribution in a turbulent system, an alternative way is to use Shannon's entropy function[87]. The relation between the Shannon entropy *S'* and the particle diameter D_p can be expressed as:

$$S' = -k\int_0^\infty f_n(D_p)\ln[f_n(D_p)]dD_p \tag{2.11}$$

where $f_n(D_p)$ is the number-based particle size distribution. Here, we assumed that the entropy function *S'* is maximized in the dynamic equilibrium in our system. In order to obtain the maximum value of the entropy function S', the relation between the mean diameters D_{q0} and the particle diameter D_p is used as constraint[76]:

$$\int_0^\infty f_n(D_p)D_p^q dD_p = D_{q0}^q \tag{2.12}$$

According to the definition of $f_n(D_p)$, another constraint exists:

$$\int_0^\infty f_n(D_p)dD_p = 1 \tag{2.13}$$

By solving equations. (2.11), (2.12) and (2.13), we get:

$$f_n(D_p) = \exp(-a_0 - a_1 D_p^q) \tag{2.14}$$

where a_0 and a_1 are Lagrange multipliers, which satisfy the following equations:

$$\exp(a_0) = q^{\frac{1-q}{q}} D_{q0}\Gamma(\frac{1}{q}) \tag{2.15}$$

$$a_1 = \frac{1}{qD_{q0}^q} \tag{2.16}$$

where Γ is the Gamma function. In order to compare the experimental data with the simulation data, $f_v(D_p)$ is introduced as the volume based distribution. The relation between the $f_v(D_p)$ and the $f_n(D_p)$ is

$$f_v\left(D_p\right) = \frac{D_p^3}{D_{30}^3} f_n\left(D_p\right) \tag{2.17}$$

where D_{30} is the mean volumetric diameter. Therefore, we can obtain the final expression for volume-based distribution by assuming that the Shannon's entropy function is maximized:

$$f_v\left(D_p\right) = \frac{D_p^3}{D_{30}^3} f_n\left(D_p\right) \tag{2.18}$$

From the Hinze-Kolmogorov theory, we obtain the Sauter mean diameter D_{32}. From the definition of D_{32}, we have:

$$D_{32} = \frac{D_{30}^3}{D_{20}^2} \tag{2.19}$$

where D_{20} is the mean surface diameter. Then we can obtain the relation between the D_{32} and the D_{q0} by combining equation (2.12) and (2.19):

$$D_{32} = D_{q0} \cdot \sqrt[q]{q} \frac{\Gamma(4/q)}{\Gamma(3/q)} \tag{2.20}$$

Here, the parameter q is related to the width of the distribution and equals the distribution parameter of the Rosin-Rammler distribution[76]. In order to estimate the value of q, the Rosin-Rammler distribution is introduced:

$$1 - Q_i = \exp(-\frac{d_i}{Y})^q \tag{2.21}$$

where Q_i is cumulative volume fraction for particle smaller than d_i. Y is a size parameter, which measures the particle size below 63.2% of total volume[75,88]. By plotting $\ln(1-Qi)^{-1}$ versus d_i/Y , we can obtain the value of q.

2.2.3. Normal distribution

In order to compare with the size distribution predicted by the population balance model and the maximum entropy formalism, normal distribution is introduced. Several studies showed that the normal distribution fit the experimental size distribution in the turbulent system fairly well[67,89,90]:

$$f(D) = \frac{1}{\sqrt{2\pi}\sigma_d} \exp[-\frac{(\mathrm{D} - D_{32})^2}{2\sigma_d^{\,2}}] \tag{2.22}$$

where $f(D)$ is the particle size distribution, D_{32} is the mean diameter and σ_d is the standard deviation.

2.3. Experimental section

2.3.1. Materials

The materials used in the experiments were listed below: Sylgard 184 consisting of vinyl functional PDMS (Batch A) and curing agent (Batch B) (RTV silicone elastomer, Dow Corning), 25-35% (methylhydrosiloxane) with 65%-70% (dimethylsiloxane) copolymer (HMS-301) (M_w=2,000g/mol 8-functional crosslinker, Gelest), platinum-cyclovinylmethylsiloxane complex (SIP6832.2 catalyst) (Gelest), polyvinyl alcohol (PVA) (M_w=22,000g/mol, Fluka), poly (methyl methacrylate) (PMMA) (M_w=15,000g/mol, Aldrich), dimethyl

fomamide (DMF) (>99%, Aldrich), sodium dodecyl sulphate (SDS) (>99%, BDH), non-reactive silicone oil (20cSt, Dow Corning) and deionized water.

2.3.2. Experimental procedure

PDMS microsphere preparation

8g Sylgard 184 vinyl functional PDMS (Batch A) and respective amounts of curing agent (Batch B) were mixed in a container in a ratio of 10:1 and 20:1 (recommended ratio is 10:1 according to the manufacturer) by using a Speed mixer at 3500rpm for 2min. The mixture was then poured into a conical flask with 200g of aqueous surfactant solution, which contained 3% (wt) SDS and 1% (wt) PVA. A 2.0 cm diameter impeller with two inclined blades was used to stir in the solution for 2min at 2000rpm to produce an emulsion. After the emulsion was formed, the stirring speed was reduced to 500rpm and the system was cured at 80℃ for 2h in water bath. The PDMS microspheres were then obtained by filtering after the curing process. The PDMS microspheres were then dried in an oven at 80℃ for overnight and weighed to calculate the yield of PDMS microspheres.

PDMS microspheres coated with PMMA

0.4g PDMS microsphere with a ratio of vinyl functional PDMS to curing of 20:1 were added to a watch glass (radius 22mm). PMMA was dissolved in DMF to yield a solution of 10%, 20%, 50% (wt), which was dropped into the watch glass with a syringe. The watch glass was then placed in the spin coater. Spin coating was performed at 5000rpm for 1min, with an acceleration of 1000rpm/s from 0 to 5000rpm. After the coating, the coated PDMS microspheres were inserted into an oven at 80℃ to remove the residual DMF.

2.3.3. Apparatus

Size distribution

PDMS microsphere size distribution was measured by Mastersizer (Malvern, UK) in a jar tester. In the measurement, PDMS microspheres in aqueous solution were pumped through a transparent tubing with an internal diameter of 5mm by a peristaltic pump at a flow rate of 10mL/min and then back to the conical flask. The instrument was equipped with a laser with a wavelength of 633nm, and the size range was 1μm-1000μm in the measurement.

Surface tension

The surface tension was measured by Nelder-Mead simplex method using a Data Physics OCA20 tension meter. The sample was loaded into a syringe mounted to a stepper motor, which was used to control the rate of the advancing and receding drop front. 10μL samples were dispensed at a rate of 2μL/s using a needle with a diameter of 1.67mm. The pendant drop was illuminated from behind by a white-light projector. A CCD camera was used to capture the images for analysis.

Viscosity measurement

The viscosity of PDMS emulsion was measured using an AR-2000 Rheometer (TA Instruments, USA) at room temperature using a conical tank. 100mL PDMS emulsion was tested at shear rates ranging from $100s^{-1}$ to $0.1s^{-1}$.

Spin coating

Spin coating was performed by using Spin150 (SPS coating, Netherland). 0.4g PDMS microsphere on a watch glass were subjected to spin-coating with different concentration PMMA solution in DMF for 1min at 5000rpm.

Thermogravimetric analysis

The thermogravimetric behavior of coated PDMS microspheres was analyzed by using a TGA Q500 (TA Instruments, USA). Typically 20-50mg sample was used. The measurement was made from 30℃ to 800℃ in nitrogen at a heating rate of 10℃/min.

Rheological measurement

The rheological behavior of coated and uncoated PDMS microspheres was investigated by using AR-2000 using a time sweep procedure. 0.4g PDMS microsphere was mixed with 0.01g hydride 8-functional crosslinker (HMS-301) and 0.1g non-reactive silicone oil. For the amount of hydride crosslinker used in the measurement, see Section 3.4.3. Measurements were made using a parallel plate geometry consisting of a pair of 25mm plates at 50℃ with a strain rate of 2%. 2% of strain rate was set to ensure that the material to be within the linear regime.

2.4. Modeling

The mean diameter of PDMS microspheres can be calculated from equations. (2.1)-(2.3) with the following parameters:

k is an empirical number equal 0.100 for the systems with a viscosity ranging from 0.005 to 4 Pa·s[77,78], a equals 11.5 for the silicone oil-water system[66,67], b is an empirical number equal 4.47 for the system with concentrations between 1.5% and 5%[67,78]. The values of k, a and b are from the literatures while the following parameters are determined from the measurements. D is the impeller diameter (D=0.02m), ρ is the density of the continuous phase (993kg/m^3), φ is the volume fraction of PDMS mixture, φ≈3.5% as 7g PDMS mixture is dispersed in 200g solution, ω is the rotational speed of the impeller (2000rpm), μ_d is the viscosity of the continuous phase (μ_d =0.00528Pa·s, measured by AR-2000) and σ is the surface tension of the aqueous surfactant solution (σ=36.2mN·m^{-1})[91].

For the population balance model, the size distribution of PDMS microspheres can be described from equation (2.10). The primary particle size (d_{min}) is measured by using Mastersizer 2000 in the experiment. After substituting the value of D_{32} and d_{min}, the particle size distribution can be obtained.

For maximum entropy formalism, the size distribution of PDMS microspheres can be described from equation (2.18). The parameter q is estimated from a plot of $\ln(1-Q_i)^{-1}$ versus d_i/Y.

For normal distribution, the size distribution of the PDMS microspheres can be described from equation (2.22). Similar to the population balance model, the standard deviation (σ_d) equals the primary particle size (d_{min}).

2.5. Results and discussion

2.5.1. Experimental mean diameter and size distribution of PDMS microspheres

In order to investigate the PDMS microsphere size distribution with respect to diameter and the yield of the PDMS microspheres, eight samples were prepared by mixing Sylgard 184 in a recommended ratio of 10:1 with different surfactant concentrations. Sample ID, surfactant concentration, mean diameter and microsphere yield are listed in Table 2.1. The Sample ID indicates the surfactant concentration, e.g. S3P1 means that 3% (wt) SDS and 1% (wt) PVA are added to the aqueous solution.

The yield of the PDMS microspheres was calculated from equation (2.23). As shown in Table 2.1, the yield of PDMS microspheres increased from 41.4% (S1P0) to 54.4% (S5P0) and from 25.3% (S1P1) to 71.3% (S5P1), indicating that the yield of PDMS microspheres increased with the increase of surfactant concentration. This can be explained as follows: the increase in surfactant concentration allowed for more surfactant molecules to organize themselves around the PDMS droplets, eventually preventing them from aggregation or being stick to the edge of the conical flask. The PDMS droplets would therefore remain separate, resulting in increase in yield of PDMS microspheres.

$$Y_{PM} = \frac{m_{PM}}{m_{tot}} \cdot 100\% \tag{2.23}$$

where Y_{PM} is the yield of PDMS microspheres, m_{PM} is the mass of PDMS microspheres and m_{tot} is the mass of vinyl functional PDMS and curing agent.

Table 2.1. Mean diameter and yield of PDMS microspheres from varying surfactant concentrations

Sample ID	SDS (%)	PVA (%)	σ (mN/m)	D_{32} (μm)	Y_{PM} (%)
S0P0	0	0	72.9	/	0
S1P0	1	0	37.3	120	41.6
S3P0	3	0	32.3	104	47.4
S5P0	5	0	32.0	102	54.4
S0P1	0	1	52.4	/	0
S1P1	1	1	37.9	105	25.3
S3P1	3	1	36.2	107	69.4
S5P1	5	1	36.1	89	71.3

Figure 2.1 and Figure 2.2 show the volume frequency and the accumulated volume frequency of the PDMS microspheres in different surfactant solutions. As shown in Figure 2.1, the diameter of the PDMS microspheres fell between 30μm and 300μm and the mean diameter is approximately 100μm.

As shown in Figure 2.1, the samples with PVA exhibited narrower size distribution than those without PVA, indicating that the emulsions created from the mechanical stirring were more stable at the presence of PVA. This was in agreement with that the stability of the emulsion could be increased by using PVA as an assistant surfactant[92]. On the other hand, no PDMS microsphere were obtained in Sample S0P1, suggesting that the PVA could not be used solely in the preparation of the PDMS microspheres and should be added to the solution as assistant surfactant.

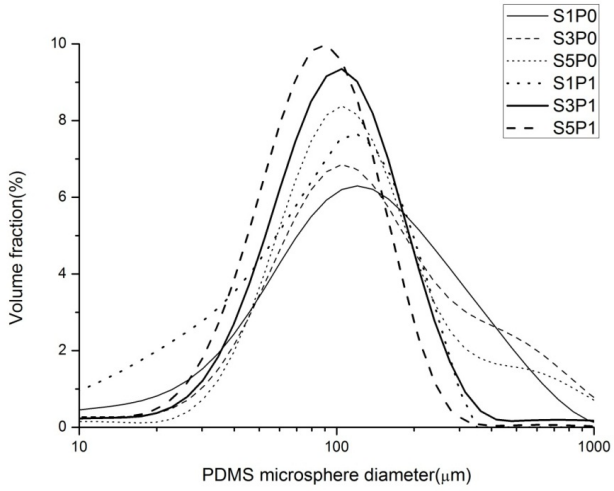

Figure 2.1. Experimental relative volume fraction versus microsphere diameter for different surfactant concentrations.

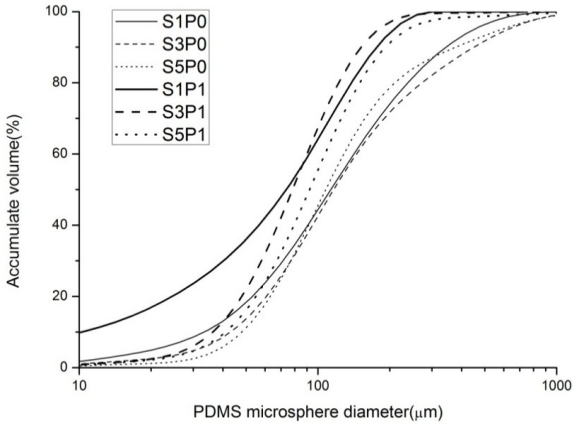

Figure 2.2. Experimental accumulated volume fraction versus microsphere diameter for different surfactant concentrations.

2.5.2. Comparison of theoretical predictions with experimental results

2.5.2.1. Comparison of the population balance model simulation with the experimental results

As discussed in Section 2.1 and 2.4, the theoretical mean diameter of the PDMS microspheres was calculated from equation (2.1). By substituting the parameters from the measurements and the literatures,

the theoretical mean diameter of the PDMS microspheres could be obtained. Table 2.2 shows the experimental and the theoretical mean diameter of the PDMS microspheres. It can be seen that the experimental mean diameter varied from 89μm to 120μm, while the predicted mean diameter was approximately 99μm. The maximum deviation between the experimental value and the theoretical value was 20μm and the average deviation was approximately 7μm, indicating that the theoretical values fit the experimental results quite well.

Table 2.2. Comparison between the experimental and the theoretical mean diameter of the PDMS microspheres in different surfactant solutions

Sample ID	S1P0	S3P0	S5P0	S1P1	S3P1	S5P1
Exp. mean diameter (μm)	120	104	102	105	107	89
Theo. mean diameter (μm)	98.1	99.5	99.6	97.9	98.4	98.4
Deviation between exp. and theo. (μm)	21.9	4.5	2.4	7.1	8.6	9.4

In Section 2.2, population balance model was used to describe the size distribution of the PDMS microspheres based on equation (2.10). Normal distribution was introduced in order to compare with the size distribution predicted by the population balance model. Table 2.3 shows the volume frequency of the most probable distribution from the experiment, the population balance model and the normal distribution. It can be seen that the deviation of the volume frequency of the most probable distribution between the experiment and the population balance model was approximately 5%, while the deviation between the experiment and the normal distribution was substantial, indicating that the population balance model provided realistic solution in prediction of the volume frequency of the most probable distribution.

Table 2.3. Comparison of the volume frequency of the most probable distribution between the experiment, the population balance model and the normal distribution of the PDMS microspheres in different surfactant solutions

Sample ID	S1P0	S3P0	S5P0	S1P1	S3P1	S5P1
Exp. most probable distribution (%)	6.3	6.9	8.4	7.6	9.4	10
Theo. most probable distribution (%)	8.3	11	11	6.6	11	11
Normal distribution (%)	36.4	36.4	36.4	36.4	36.4	36.4

The size distribution of the PDMS microspheres between the experiment, the population balance model and the normal distribution are compared and shown in Figure 2.3. It can be seen that the size distribution obtained from the population balance model was similar to that from the experiment. Meanwhile, the experimental size distribution indicated that there was small possibility of primary particles forming

particles smaller than 30μm or larger than 300μm, which could not be predicted by the population balance model.

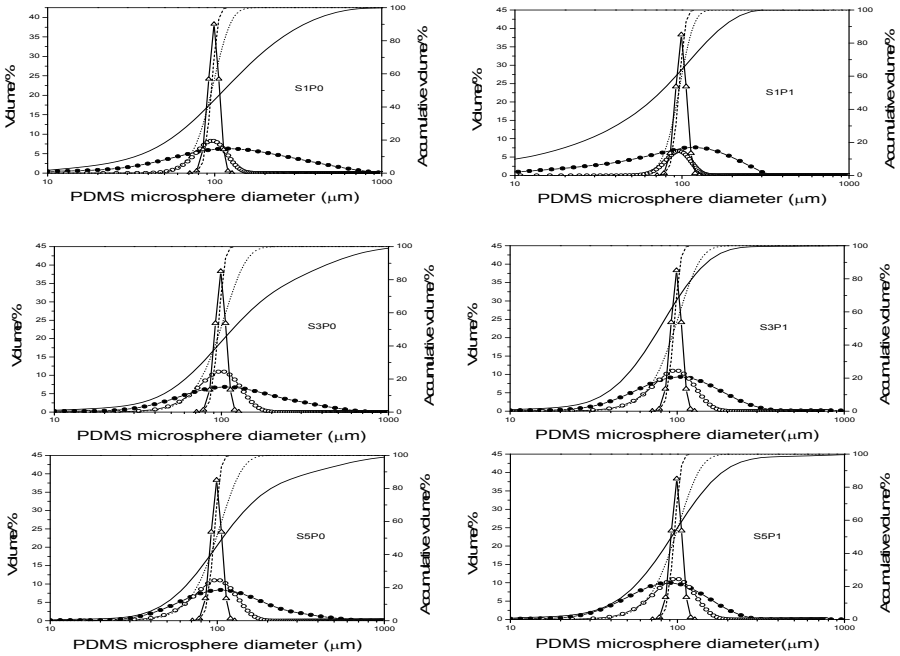

Figure 2.3. Comparison between experimental (solid circle and solid line), population balance model (open circle and dotted line) and normal distribution (triangle and dash line) of the PDMS microspheres in size distribution and cumulative volume fraction.

There was good agreement between the experimental values and the modeling values, demonstrating that the Hinze-Kolmogorov theory and population balance model based on dilute systems provided realistic values for the mean diameter and size distribution of the PDMS microspheres. A lot of experiments and simulations based on the Hinze-Kolmogorov theory have been reported[66,77,78], however, to the best of our knowledge, none of them involved chemical reactions and irreversible crosslinking in the system. The good agreement between the experimental and the theoretical values in our experiment showed that the applicability of the Hinze-Kolmogorov theory to determine mean diameter could be fairly broadened.

2.5.2.2. Comparison of the maximum entropy formalism simulation with the experimental results

As described in section 2.2, the mean diameter and the size distribution of the PDMS microspheres could also be predicted by the maximum entropy formalism using equation (2.18). The mean diameter obtained from the simulation is compared with the experimental values and shown in Table 2.4. As shown in Table 2.4, the deviation of the mean diameter of the PDMS microspheres between the experiment and the

simulation was approximately 20μm, meaning that the agreement between the experiment and the simulation was reasonably good.

Table 2.4. Comparison between the experimental and the theoretical mean diameter of the PDMS microspheres in different surfactant solutions

	S1P0	S3P0	S5P0	S1P1	S3P1	S5P1
Exp. mean diameter (μm)	120	104	102	105	107	89
Theo. mean diameter (μm)	118	120	121	120	138	122
Deviation between exp. and theo. (μm)	2	16	19	15	29	33

In equation (2.18), the size distribution predicted by the maximum entropy formalism was relevant to the distribution parameter q. In some studies, the value of q was arbitrarily set to 1, providing the size distribution in terms of linear mean diameter[76,93]. In this study, the value of q could also be determined by using equation (2.21), namely that q equaled the slope of $\ln(1-Qi)^{-1}$ versus d_i/Y[75,88]. The value of the size parameter Y and the distribution parameter q are shown in Table 2.5.

In order to compare with the maximum entropy formalism model, the normal distribution was also introduced. Table 2.5 shows the volume frequency of the most probable distribution of the PDMS microspheres from the experiment, the maximum entropy formalism and the normal distribution in different surfactant solutions. It can be seen that the deviation of the volume frequency of the most probable distribution between the experiment and the maximum entropy formalism was approximately 5%, while the deviation between the experiment and the normal distribution was phenomenal, demonstrating that the maximum entropy formalism also provided fairly realistic solution in the prediction of the volume frequency of the most probable distribution.

Table 2.5. Comparison of the volume frequency of the most probable distribution between the experiment, the population balance model and the normal distribution of the PDMS microspheres as well as the value of the size parameter Y and the distribution parameter q in different surfactant solutions

	S1P0	S3P0	S5P0	S1P1	S3P1	S5P1
Exp. most probable distribution (%)	6.3	6.9	8.4	7.6	9.4	10
Theo. most probable distribution (%)	11	9.7	8.4	8.4	11	8.4
Normal distribution (%)	36.4	36.4	36.4	36.4	36.4	36.4
Y value (size below 63.2%) (μm)	152	158	135	184	124	113
q (slope of $\ln(1-Qi)^{-1}$ versus d_i/Y)	1.1	0.8	0.6	2.7	1.0	0.6

Figure 2.4 shows the size distribution of the PDMS microspheres from the experiment, the maximum entropy formalism and the normal distribution. It can be seen that the normal distribution showed a remarkable difference in distribution trend, thus was not suitable to describe the experimental data. Meanwhile, the size distribution predicted by the maximum entropy formalism described the distribution trend of the experimental data as well as showed inevitable difference in the peak. This demonstrated that the entropy in the experimental systems was not maximized, resulting in the deviation between the predicted values and the experimental values.

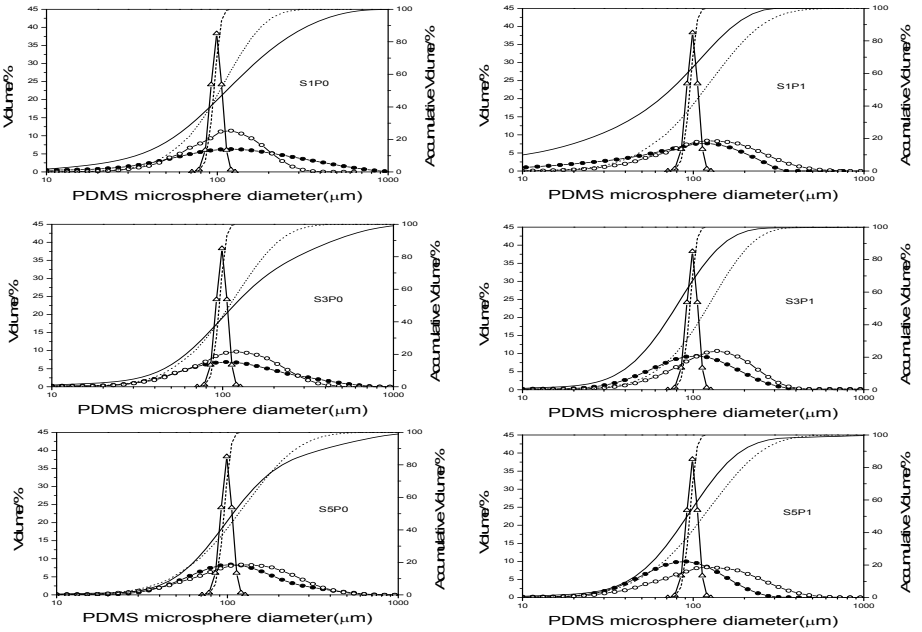

Figure 2.4. Comparison between experimental (solid circle and solid line), maximum entropy formalism (open circle and dotted line) and normal distribution (triangle and dash line) of the PDMS microspheres in size distribution and cumulative volume fraction.

2.5.3. Characterization of PMMA coated PDMS microspheres

2.5.3.1. Thermogravimetric analysis

In order to investigate the content of PMMA in the coated PDMS microspheres, four samples were coated in presence of various concentrations of PMMA. Sample ID, PMMA concentrations and char yield at 800℃ are summarized in Table 2.6. The sample ID indicates the coating concentration of PMMA, e.g. 10PD mean the coating solution is 10% PMMA in DMF.

In the thermogravimetric analysis, the PDMS microspheres degraded simultaneously with the PMMA. Since the PMMA degraded completely at 430℃, the char yield at 800℃ only depended on the content of the PDMS microspheres. As shown in Table 2.6, the char yield of the coated PDMS microspheres decreased when higher concentration of PMMA was used in the spin coating process as expected. This indicated that the content of the PMMA in the coated PDMS microspheres increased with the increase of PMMA concentration in the solution.

Table 2.6. Thermogravimetric analysis (TGA) of PDMS microspheres coated with different concentration of PMMA by spin coating

Sample ID	PMMA	non-coated PDMS microspheres	PDMS microspheres - 10PD	PDMS microspheres - 20PD	PDMS microspheres - 50PD
PMMA concentration in solution (%)	/	0	10	20	50
Char yield at 800℃ (wt%)	0	37.7	27.5	18.3	11.4

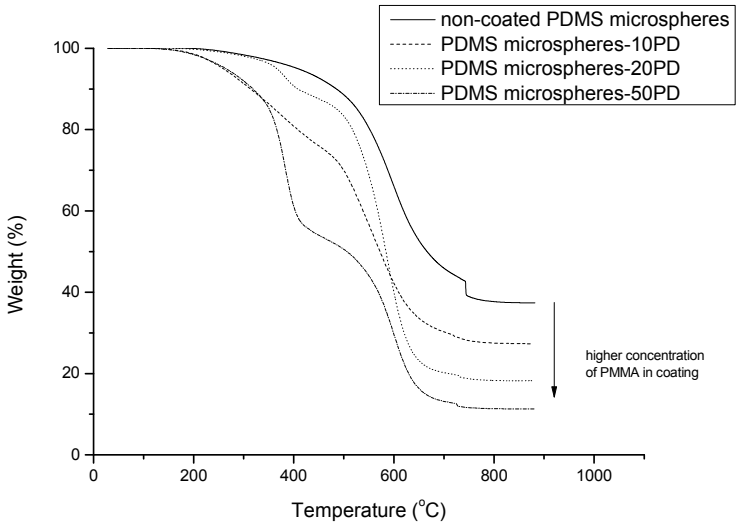

Figure 2.5. TGA thermograms in a N_2 atmosphere of PDMS microspheres coated with PMMA and non-coated PDMS microspheres.

As a commercial available technique, spin coating was frequently used to produce thin films on a planar substrate. However, it has not been reported that spin coating could be used to produce coated

microspheres. There was no solid evidence to prove that PMMA could be coated perfectly onto PDMS microspheres, therefore further studies (e.g. rheology) were required.

2.5.3.2. Rheological measurement

In the preparation of the PDMS microspheres, excess vinyl terminated PDMS was added to the mixture to obtained the vinyl functional PDMS microspheres. The vinyl groups on the surface of the PDMS microspheres were able to react with the crosslinker at the presence of catalyst. As the reaction between the PDMS microspheres and the crosslinker increased the crosslinking density of the system, the storage modulus of the mixture would also increase.

The objective of the rheological measurement was to investigate the quality of the coated PMMA layer, namely that whether the coated PMMA was sufficient to prevent the vinyl functional PDMS microspheres from reacting with the crosslinker. If the PDMS microspheres were completely coated with PMMA, the crosslinker could not penetrate the PMMA shell and the modulus remained constant, vice versa.

In the measurement, 0.4g PMMA-coated vinyl functional PDMS microsphere was mixed with 0.01g HMS-301 crosslinker and 0.1g non-reactive silicone oil. The uncoated PDMS microspheres were used as a reference sample. Meanwhile, the rheological measurements were made at 50℃ for two reasons: first, the measuring temperature was lower than the T_g of the PMMA such that the coated PMMA remained rigid; secondly, the PDMS microspheres reacted with the crosslinker at a moderate rate if the crosslinking reaction occurred.

Figure 2.6 shows the rheological behavior of the PDMS microspheres with and without coating over a period of 10h. For the PDMS microspheres without coating, the storage modulus increased from 10kPa to 38kPa, indicating that the PDMS microspheres underwent crosslinking reaction with the crosslinker. The slope of the storage modulus curve was relatively steep at first hour, showing a relatively high rate of the crosslinking reaction. Afterwards, the storage modulus leveled out, meaning that the vinyl groups on the surface of the PDMS microspheres were consumed. For the coated PDMS microspheres, the storage modulus increased slightly, demonstrating that the crosslinking reaction occurred to a small degree. In the comparison of the uncoated and the coated PDMS microspheres, the difference in rheological behavior suggested that the PMMA shell hindered the crosslinking reaction greatly.

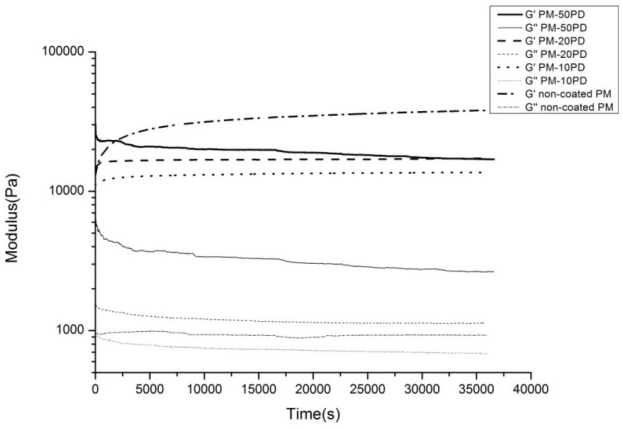

Figure 2.6. Rheological behavior of PDMS microspheres with and without PMMA coating in silicone oil at 50℃.

2.6. Conclusions

PDMS microspheres have been prepared by mechanical stirring in a series of surfactant solutions. The mean diameter of the PDMS microspheres is approximately 100μm and 90% PDMS microspheres fall between 30μm and 300μm. The experimental mean diameter of the PDMS microspheres is in line with the theoretical mean diameter predicted by Hinze-Kolmogorov theory, indicating that the applicability of the Hinze-Kolmogorov theory can be fairly broadened in the prediction of the mean diameter of droplets in turbulent system. Meanwhile, the experimental size distribution is compared with the theoretical size distribution predicted by population balance model and maximum entropy formalism. The agreement between the experimental result and the prediction is acceptable.

Vinyl functional PDMS microspheres have also been prepared by increasing the mixing ratio of vinyl terminated PDMS to crosslinking agent. The vinyl functional PDMS microspheres are coated in a newly developed spin coating procedure. According to the rheological results, the coated PDMS microspheres show much slower crosslinking reaction rate than the uncoated ones. This indicates that the PMMA shell is efficient in protecting the vinyl functional PDMS microspheres. In the next chapter, the surface vinyl concentration of the vinyl functional PDMS microspheres will be determined by a novel titration method and the crosslinking reaction between the uncoated vinyl functional PDMS and the hydride crosslinker will be investigated systematically.

3. Surface vinyl concentration of PDMS microspheres and their further crosslinking reaction

As discussed in Chapter 2, the surface vinyl groups of PDMS microsphere allow for further crosslinking reaction in the presence of hydride crosslinker and thus yielding macroscopic PDMS elastomer. The extent of the crosslinking reaction is determined by the surface vinyl concentration and the amount of hydride crosslinker. Thus, the surface vinyl concentration should be quantified. In this chapter, the surface vinyl concentration is determined by a novel titration method, which will be discussed in Section 3.1. Furthermore, the crosslinking reaction between the PDMS microspheres and the hydride crosslinker is also investigated systematically.

3.1. Quantification of surface vinyl concentration of PDMS microspheres

The surface vinyl groups confer PDMS microspheres with surface activity, which includes the potential for further chemical modification on the surface of the PDMS microspheres and the increase in the miscibility of the PDMS microspheres with other polymers, thereby broadening the applicability of the PDMS microspheres. For the potential in surface chemical modification, the surface vinyl groups allow for grafting a polymeric layer on the surface of PDMS microspheres and thus yielding multifunctional PDMS microspheres[94]. For the increase in the miscibility, the surface vinyl groups allow for blending incompatible polymers with the PDMS microspheres and thus obtaining reinforced materials[95]. Both the grafting density of the functional polymeric layer and the blending efficiency with the incompatible polymers correlate to the surface vinyl concentration of the PDMS microspheres. Thus, it is essential to quantify the surface vinyl concentration of the PDMS microspheres.

The quantification of the surface vinyl concentration of PDMS microspheres is challenging due to the highly crosslinked structure and the hydrophobicity of the PDMS microspheres. Common technique (e.g. ^{1}H NMR spectroscopy) and titration method (e.g. bromine titration) is not suitable for the quantification of the surface vinyl concentration. For ^{1}H NMR measurement, it requires samples to be completely dissolved in deuterated solvent[96]. However, the PDMS microspheres are highly crosslinked and thus not being soluble in any solvent, eventually preventing the characterization of the surface vinyl concentration from ^{1}H NMR measurement. For bromine titration, it utilizes the reaction between bromine and vinyl groups in aqueous solution to determine the vinyl concentration of polymeric microspheres[97]. However, the aqueous solution used in the bromine titration may alter the surface properties of the PDMS microspheres and extract the vinyl groups from the bulk to the surface, resulting in inaccuracy in the quantification.

Here, a novel titration method is employed to determine the surface vinyl concentration of PDMS microspheres. The titration method exploits that monofunctional hydride terminated PDMS reacts with the surface vinyl groups of the PDMS microspheres through hydrosilylation reaction in a ratio of 1:1[98,99]. The covalently bonded monofunctional hydride will result in weight increase in the PDMS microspheres, thus allowing for the quantification of the surface vinyl concentration. The titration method also takes advantage of the high miscibility between the monofunctional hydride and the PDMS microspheres, such

that the surface properties of the PDMS microspheres will not be altered and the vinyl groups in the bulk will not be extracted to the surface. Not only is the titration method applicable for PDMS microspheres to determine the surface vinyl concentration, but it can also be utilized in the determination of the surface vinyl concentration in other commercial silicone materials, i.e. RTV silicones and liquid silicone rubbers.

3.2. Crosslinking reaction between PDMS microspheres and hydride crosslinker

The surface vinyl groups on PDMS microspheres allow for further crosslinking reaction with hydride crosslinker and thus yielding macroscopic PDMS network. The extent of the crosslinking reaction and the properties of the resulting macroscopic PDMS network are influenced by the surface vinyl concentration of the PDMS microspheres, the amount of hydride crosslinker and surrounding medium. The surface vinyl concentration, which can be detected by monofunctional titration method, allow for the estimation of the amount of hydride crosslinker needed in the crosslinking reaction[100]. Both the surface vinyl concentration and the amount of the hydride crosslinker determine the density of the inter-particle crosslinking points in the macroscopic PDMS network. Regarding to the surrounding medium, non-reactive silicone oil with low molecular weight is used for the crosslinking reaction for the following reasons. First of all, the silicone oil promotes the diffusion of hydride crosslinker, allowing the hydride crosslinker to approach and react with the surface vinyl groups. Secondly, the silicone oil with low molecular weight does not entangle with the macroscopic PDMS network since the molecular weight of the silicone oil (2,000g/mol) is far below the molecular entanglement weight of PDMS (12,000g/mol)[101]. Accordingly, the properties of the macroscopic PDMS network depend solely on the weight fraction of the silicone oil. The crosslinking reaction between the surface vinyl groups and the hydride crosslinker allows for obtaining macroscopic PDMS network and thus delivering PDMS elastomer to a hard-to-reach place in oil reservoir, where elastic seals can be utilized to increase oil production[39,102,103].

3.3. Experimental section

3.3.1. Materials

The chemicals employed were: Sylgard 184 consisting of vinyl terminated PDMS (Batch A) and curing agent (Batch B) (RTV silicone elastomer, Dow Corning), 25-35% (methylhydrosiloxane) with 65%-70% (dimethylsiloxane) copolymer (HMS-301) (M_n=2,000g/mol, 8-functional hydride crosslinker, Gelest), monofunctional hydride (MCR-H21) (M_n=4,500g/mol, Gelest), platinum-cyclovinylmethylsiloxane complex (SIP6832.2 catalyst) (Gelest), polyvinyl alcohol (PVA) (M_w=22,000g/mol, Fluka), sodium dodecyl sulphate (SDS) (>99%, BDH), non-reactive silicone oil (20cSt, M_n=2,000g/mol, Dow Corning) and deionized water.

3.3.2. Apparatus

Homogeneous mixtures were made by mixing Batch A and B of Sylgard 184 using a Speed mixer (Synergy Devices Ltd, UK) at room temperature.

The size distribution of PDMS microspheres was measured by Mastersizer (Malvern, UK) in a jar tester. The instrument was equipped with a laser with a wave length of 633nm operational in the size range 1μm to 1000μm.

The morphology of the PDMS microspheres was analysed by Optical Microscope (Leica, German).

Rheological measurements were performed in AR2000 stress controlled Rheometer (TA instrument, US). The measurements were performed with a strain of 2% to ensure to be within the linear regime of the material as well as to minimize the disruption of the network[61]. Similar to other measurements of *in situ* crosslinking reaction, the frequency in the rheological measurements was set to 1Hz[104]. In order to have a moderate crosslinking reaction rate, measuring temperature was set to 50°C[105]. All measurements were performed in the presence of 10ppm platinum catalyst.

3.3.3. Experimental procedure

Preparation of vinyl functional PDMS microspheres

8g Sylgard 184 vinyl terminated PDMS (Batch A) and respective amounts of curing agent (Batch B) were mixed in a container in a ratio of 15:1, 20:1 and 25:1 (recommended ratio is 10:1 according to the manufacturer) by using Speed mixer at 3500rpm for 2min. The mixture was then poured into a conical flask with 200g of aqueous surfactant solution, which contained 3% (wt) SDS and 1% (wt) PVA. A 2.0 cm diameter impeller with two inclined blades was used to stir the solution for 2min at 2000rpm to produce an emulsion. Upon the formation of the emulsion, the stirring speed was reduced to 500rpm and the system was cured at 80°C for 2h in water bath. The PDMS microspheres were then obtained by filtering. To ensure that the crosslinking reaction in the PDMS microspheres was finished and to remove residual water, the PDMS microspheres were dried at 80°C overnight. The obtained vinyl functional PDMS microspheres are denoted as 15:1 PDMS microspheres, 20:1 PDMS microspheres and 25:1 PDMS microspheres. More details about the preparation procedure can be found in Gonzalez *et al*[106].

Determination of soluble fraction of vinyl functional PDMS microspheres

Approximately 0.5g vinyl functional PDMS microspheres were swelled in heptane for 48h (20-30 times excess, i.e. 15-25mL solvent to a sample of 0.5g). In all experiments, we ensure that the PDMS microspheres were fully covered in heptane for 48h[107]. After 48h, the PDMS microspheres were separated from the heptane solution. The residual heptane was removed by evaporation over 48h under atmospheric condition. Afterwards, the dry PDMS microspheres were weighted and the soluble fraction of PDMS microspheres was calculated.

Titration determination of surface vinyl concentration of PDMS microspheres

According to the information from Dow Corning, the Sylgard 184 Batch A contained vinyl terminated PDMS with a molecular weight of 22,000g/mol and silica particles. Since vinyl terminated PDMS in Batch A has functionality approximately 2, the vinyl concentration of the Batch A should equal $9.09 \cdot 10^{-5}$mol/g. The vinyl terminated PDMS from Batch A underwent crosslinking reaction with hydride crosslinker in the preparation of PDMS microspheres, the vinyl concentration of PDMS microspheres should be less than $9.09 \cdot 10^{-5}$mol/g. Thus, 0.5g of PDMS microspheres should have molar number of vinyl groups less than $4.54 \cdot 10^{-5}$mol. In the

titration experiment, 2.5g of monofunctional hydride, which has molar number of hydride approximate $5.5 \cdot 10^{-4}$mol, was used to ensure excess monofunctional hydride groups. The mixture containing 0.5g of PDMS microspheres and 2.5g of monofunctional hydride was reacted for 24h at 80℃ at the presence of 50ppm catalyst. Unreacted monofunctional hydride and soluble fraction were removed by swelling with heptane for 48h. After the 48h, the titrated PDMS microspheres were separated from heptane solution. The residual heptane was removed by evaporation over 48h under atmospheric conditions. Afterwards, the titrated PDMS microspheres were weight and the surface vinyl concentration of PDMS microspheres was calculated.

3.4. Results and discussion

3.4.1. Size distribution of vinyl functional PDMS microspheres

The diameter of 10:1 (reference sample), 15:1, 20:1 and 25:1 PDMS microspheres fell between 2μm to 500μm, indicating that highly polydisperse PDMS microspheres were obtained (Figure 3.1). It can be seen that the mixing ratio did not affect the mean diameter of the PDMS microspheres. This can be attributed to the mean diameter being mainly determined by the stirring rate of impeller and the resulting energy transferred to the suspension medium[64]. On the other hand, the PDMS microspheres displayed broader size distribution with increasing mixing ratio. This is due to a viscous PDMS suspension, which arose from the high mixing ratio of high viscosity vinyl terminated PDMS to low viscosity crosslinker, is hard to disperse and thus yielding PDMS microspheres with broad size distribution[108].

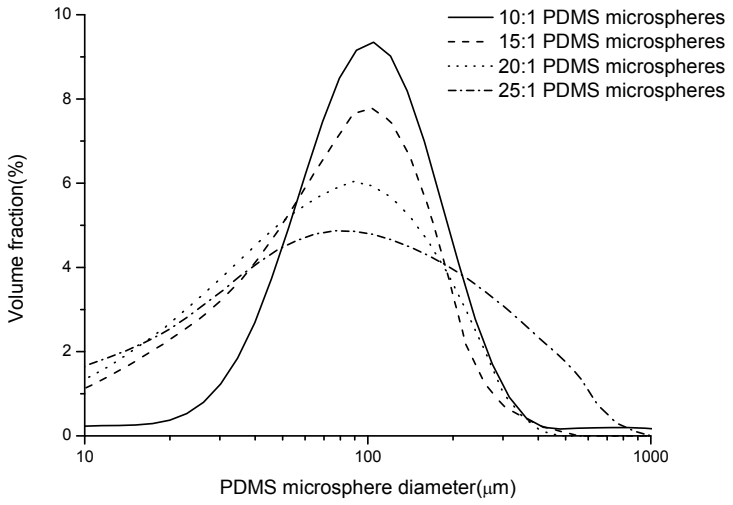

Figure 3.1. Size distribution of 10:1 (reference sample), 15:1, 20:1 and 25:1 PDMS microspheres prepared from emulsion polymerization.

3.4.2. Soluble fraction of vinyl functional PDMS microspheres

In the preparation of vinyl functional PDMS microspheres, unreacted PDMS was trapped in the network of the PDMS microspheres due to its physical interaction with the elastically active strands. Upon the swelling of the PDMS microspheres in heptane, the physical interaction decreased significantly and the unreacted PDMS was dissolved in heptane as soluble fraction.

To determine the soluble fraction of vinyl functional PDMS microspheres, the PDMS microspheres were swelled in heptane for 48h. After the swelling procedure, the PDMS microspheres were dried at ambient temperature for another 48h to remove the residual heptane and weight. The soluble fraction of the PDMS microspheres is calculated from the following equation:

$$w_{sol}\% = \frac{m_1 - m_2}{m_1} \cdot 100\% \tag{3.1}$$

where m_1 is the weight of vinyl functional PDMS microspheres before swelling in heptane, m_2 is the weight of vinyl functional PDMS microspheres after swelling in heptane and drying and $w_{sol}\%$ is the fraction of solubles.

The soluble fraction of the PDMS microspheres was lower than 17% in all samples (Table 3.1), indicating that the PDMS microspheres were highly crosslinked. Meanwhile, the soluble fraction of the PDMS microspheres increased from 7% to 16% when the mixing ratio increased from 15:1 to 25:1. This can be attributed to the amount of the unreacted PDMS in the PDMS microspheres increasing with the increase in the mixing ratio.

PDMS microspheres have larger surface area and higher amount of surface defects than pure PDMS elastomer. Thus, the soluble fraction of the PDMS microspheres should not be compared with that of the pure PDMS elastomer. This will be discussed in detail later.

Table 3.1. Soluble fraction of vinyl functional PDMS microspheres from different mixing ratio

Sample ID	Weight of PDMS microspheres (m_1g)	Weight of PDMS microspheres (m_2g) after swelling in heptane	Soluble fraction of PDMS microspheres ($w_{sol}\%$)*
15:1 PDMS microspheres	0.55±0.03	0.51±0.03	7±1
20:1 PDMS microspheres	0.53±0.02	0.48±0.02	9.3±0.2
25:1 PDMS microspheres	0.57±0.03	0.47±0.01	16±3

*The measurements were averaged from 3-4 samples.

3.4.3. Surface vinyl concentration of PDMS microspheres

The surface vinyl concentration of PDMS microspheres was analysed by titration with monofunctional hydride. Two types of surface vinyl concentration, namely surface vinyl concentration by weight ($c_{vinyl}(wt)$) and surface vinyl concentration by area ($c_{vinyl}(surface)$), are defined as follows:

$$c_{vinyl}(wt) = \frac{n_{vinyl}}{m_3} \tag{3.2}$$

$$c_{vinyl}(surface) = \frac{n_{vinyl}}{A_{PM}} \tag{3.3}$$

where n_{vinyl} and A_{PM} are the molar number and the surface area of PDMS microspheres, respectively, m_3 is the mass of PDMS microspheres before titration.

Since monofunctional hydride reacted with vinyl in a molar ratio of 1:1 via hydrosilylation reaction, the molar number of reacted monofunctional hydride ($n_{hydride}$) should equal the molar number of vinyl groups. Thus, we have

$$n_{vinyl} = n_{hydride} = \frac{m_{hydride}}{M_{hydride}} \tag{3.4}$$

where $m_{hydride}$ and $M_{hydride}$ are the mass and the molecular weight of monofunctional hydride, respectively. Upon the accomplishment of titration, titrated PDMS microspheres were swelled in heptane to remove unreacted monofunctional hydride and soluble fraction. The soluble fraction should therefore be subtracted from the weight of the PDMS microspheres in the calculation. Thus, we obtain

$$n_{vinyl} = \frac{m_4 - m_3 \cdot \left(1 - w_{sol}\%\right)}{M_{hydride}} \tag{3.5}$$

where m_4 is the mass of PDMS microspheres after reacting with monofunctional hydride and $w_{sol}\%$ is the soluble fraction of PDMS microspheres. According to equation (3.3), the surface vinyl concentration of the PDMS microspheres ($c_{vinyl}(surface)$) is also related to the surface area of the PDMS microspheres(A_{PM}). The surface area of PDMS microspheres is a sum over each PDMS microspheres and it can be written as:

$$A_{PM} = \sum n_i \cdot A_i \tag{3.6}$$

where A_i and n_i are the surface area and the number of PDMS microspheres with a diameter of d_i, respectively. Meanwhile, the volume of the PDMS microspheres (V_{PM}) is a sum over each PDMS microspheres and can also be written as follows:

$$V_{PM} = \sum n_i \cdot V_i \tag{3.7}$$

where V_i and n_i are the volume and the number of PDMS microspheres with a diameter of d_i, respectively. Based on the volume frequency measured by Mastersizer, the number of the PDMS microspheres (n_i) with a diameter of d_i can also be calculated:

$$n_i = \frac{V_{PM} \cdot f_i}{V_i} \tag{3.8}$$

By inserting (3.8) into (3.6), we can obtain:

$$A_{PM} = V_{PM} \cdot \sum \frac{f_i \cdot A_i}{V_i} \tag{3.9}$$

Meanwhile, the volume of PDMS microspheres can be calculated:

$$V_{PM} = \frac{m_{PM}}{\rho_{PM}} \tag{3.10}$$

where the m_{PM} and ρ_{PM} are the mass and the density of the PDMS microspheres. By inserting (3.10) into (3.9), we can obtain:

$$A_{PM} = \frac{m_{PM}}{\rho_{PM}} \cdot \sum \frac{f_i \cdot A_i}{V_i} \tag{3.11}$$

Equation (3.11) can be further simplified when the following is inserted:

$$\begin{aligned} V_i &= \frac{4}{3}\pi(\frac{d_i}{2})^3 \\ A_i &= 4\pi(\frac{d_i}{2})^2 \end{aligned} \tag{3.12}$$

Thus, the final expression of the surface area of PDMS microspheres is shown as following:

$$A_{PM} = \frac{6 \cdot m_{PM}}{\rho_{PM}} \cdot \sum \frac{f_i}{d_i} \tag{3.13}$$

And the vinyl concentration by surface area of the PDMS microspheres can be calculated as follows:

$$c_{vinyl}(surface) = \frac{n_{vinyl} \cdot \rho_{PM}}{6 \cdot m_{PM} \cdot \sum \frac{f_i}{d_i}} \tag{3.14}$$

In the titration, the swelling of PDMS microspheres was limited due to their highly crosslinked structure. Thus, the titration method ensured that only surface vinyl groups which were accessible for further crosslinking reaction could react with monofunctional hydride. The surface vinyl concentrations of the 15:1, 20:1 and 25:1 PDMS microspheres are summarized in Table 3.2. The surface vinyl concentration increased with mixing ratio due to larger amount of unreacted vinyl on the surface of the PDMS microspheres.

The theoretical vinyl concentrations in PDMS microspheres are estimated as follows. The vinyl groups in our system are from Batch A (contains vinyl functional PDMS and catalyst) and Batch B (contains vinyl functional PDMS and crosslinker). Thus we will have $n_{v,tot} = n_{vA} + n_{vB}$ where $n_{v,tot}$ is the total molar number of vinyl groups before reaction, n_{vA} and n_{vB} is the initial molar number of vinyl groups from Batch A and Batch B. Since the viscosity of Batch B is much lower than that of Batch A, we assume Batch B contains no more than 50% vinyl functional PDMS and that the vinyl-functional PDMS in Batch A and Batch B are identical. The molar number of vinyl groups in Batch A and Batch B can be then calculated:

$$n_{vA} = f_{PDMS} \cdot \frac{m_A}{M_{PDMS}}$$
$$n_{vB} = \frac{1}{2} f_{PDMS} \cdot \frac{m_B}{M_{PDMS}} \tag{3.15}$$

where the m_A and m_B is the mass of Batch A and Batch B, M_{PDMS} is the molecular weight of vinyl functional PDMS and f_{PDMS} is the number of vinyl groups on the PDMS chain. Here we use 20:1 PDMS microspheres as an example. The mass ratio of Batch A to Batch B in our system is 20:1 (m_A:m_B=20:1). After substituting into equation above, we have

$$n_{v,tot} = n_{vA} + n_{vB} = \frac{f_{PDMS}}{M_{PDMS}} \cdot (m_A + \frac{1}{2} m_B) = \frac{f_{PDMS}}{M_{PDMS}} \cdot (m_A + \frac{1}{40} m_A) \approx \frac{f_{PDMS}}{M_{PDMS}} \cdot m_A \tag{3.16}$$

According to the data provided by Dow Corning, the molecular weight of vinyl functional PDMS in Sylgard 184 Batch A should be 22,000g/mol[56]. As the vinyl groups are on both end of the PDMS chain, the vinyl concentration of the original PDMS is estimated to be $9.1 \cdot 10^{-5}$mol/g. Meanwhile, the recommended ratio between Batch A and Batch B is 10:1 and for that mixing ratio, we assume that the stoichiometric imbalance r equals 1.3[41], since an excess of crosslinker is usually applied. When the ratio of Batch A to Batch B is 20:1 as in our system, this will thus give an r=0.65. Then the molar number of vinyl groups left after reaction can be calculated as

$$n^{\#}_{v,tot} = n_{v,tot} - 0.65 \cdot n_{v,tot} = 0.35 \cdot n_{v,tot} \tag{3.17}$$

where $n^{\#}_{v,tot}$ is the molar number of vinyl groups after reaction in our system. By substituting the parameters into equation above, we can obtain $n^{\#}_{v,tot}$ equals $3.2 \cdot 10^{-5}$mol/g. Similarly, the vinyl concentration of 15:1 and 25:1 PDMS microspheres are estimated to be $1.2 \cdot 10^{-5}$mol/g and $4.4 \cdot 10^{-5}$mol/g, respectively.

The fractions of the surface vinyl of the total vinyl are also summarized in Table 3.2. The fractions of surface vinyl of the total vinyl ranged from 58% to 78%, indicating that the vinyl groups were located primarily on the surface of the PDMS microspheres. Such high fraction arises from the low efficiency of the crosslinking reaction on the surface of the PDMS microspheres in the preparation because the crosslinking reaction was unfavorable at aqueous interface and PDMS was immiscible in water[109].

Table 3.2. Surface vinyl concentration of PDMS microspheres from different mixing ratio

Sample ID	Weight of PDMS microspheres (m_3 g)	Weight of PDMS microspheres (m_4 g) after reacting with MCR-H21	Surface vinyl concentration ($c_{vinyl}(wt)$) of PDMS microspheres by weight (10^{-5} mol/g)*	Surface vinyl concentration ($c_{vinyl}(sur)$) of PDMS microspheres by surface area (10^{-3} mol/m^2)*	Total vinyl concentration of PDMS microspheres (10^{-5} mol/g)	Fraction of surface vinyl of total vinyl (%)
15:1 PDMS microspheres	0.62±0.06	0.57±0.05	0.7±0.2	0.6±0.2	1.2	58
20:1 PDMS microspheres	0.48±0.01	0.50±0.01	2.4±0.1	2.0±0.1	3.2	75
25:1 PDMS microspheres	0.53±0.05	0.53±0.05	3.4±0.4	2.9±0.3	4.4	78

*The measurements were averaged from 3-4 samples.

3.4.4. Crosslinking reaction between PDMS microspheres and hydride crosslinker

To evaluate the crosslinking reaction between PDMS microspheres and hydride crosslinker, a typical mixture containing 1g PDMS microsphere, hydride crosslinker and 0.5g non-reactive silicone oil was made. The needed amount of hydride crosslinker was estimated from the surface vinyl concentration of the PDMS microspheres based on stoichiometric imbalance, *r* calculated from:

$$r = \frac{n_{hydride}}{n_{vinyl}} = \frac{\frac{m_{HMS-301}}{M_{HMS-301}} \cdot f_{HMS-301}}{m_{PM} \cdot c_{vinyl}(wt)} \tag{3.18}$$

where *n* is the number of moles, *m* is mass, *M* is molecular weight, *f* is the functionality of hydride crosslinker and *c* is surface vinyl concentration by weight, where subscripts HMS-301 and PM denote hydride crosslinker and vinyl functional PDMS microsphere, respectively.

The mixture containing PDMS microspheres, hydride crosslinker and non-reactive silicone oil was cured at 50℃ for 5h. Figure 3.2a shows the PDMS microspheres before crosslinking reaction. It can be seen that the PDMS microspheres aggregated due to inter-particle physical interaction and remained spherical due to lack of the potential chemical crosslinking points between the PDMS microspheres, which allowed them to be separated again upon shear force or swelling. In contrast, Figure 3.2b shows that a macroscopic crosslinked network was obtained and the PDMS microspheres were deformed after the crosslinking reaction. This indicates extensive crosslinking reaction between the PDMS microspheres and the hydride crosslinker. After cooling down to room temperature, the macroscopic PDMS network remained in its gel state, indicating that gelation did not arise from the physical association between the PDMS microspheres.

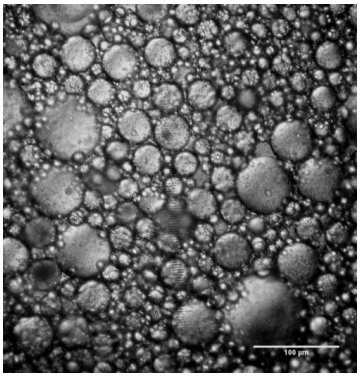

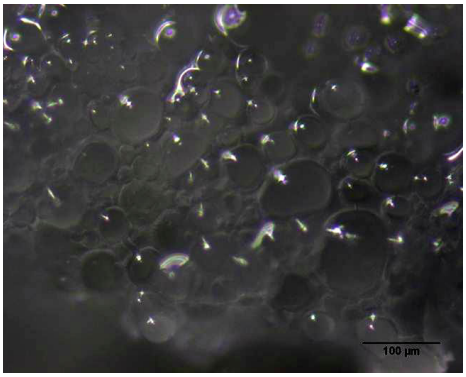

Figure 3.2a(left), 3.2b(right). Representative microscopic images of 20:1 PDMS microspheres before (left) and after (right) crosslinking reaction. The crosslinking reaction between 20:1 PDMS microspheres and hydride crosslinker was performed at 50°C and at *r*=5 with 35% (wt) non-reactive silicone oil in a period of 5h.

The crosslinking reaction between PDMS microspheres and hydride crosslinker was characterized quantitatively by rheological measurements. Stoichiometric imbalances of 1, 3 and 5 were employed to investigate the influences of the amount of hydride crosslinker on the crosslinking reaction. High stoichiometric imbalances (e.g. *r*=5) were used in the crosslinking reaction for the following reasons: firstly, some of the hydride crosslinker might be absorbed by the PDMS microspheres and then reacted with the vinyl groups in the bulk of the PDMS microspheres, resulting in increasing the crosslinking density of the bulk of the PDMS microspheres without yielding inter-particle crosslinking points. Secondly, the hydride crosslinker might react with surface vinyl groups from the same PDMS microsphere, rather than yielding inter-particle crosslinking points. This leads to increasing the surface crosslinking density of the PDMS microspheres rather than yielding macroscopic network.

In the crosslinking reaction between PDMS microspheres and hydride crosslinker, 10ppm platinum catalyst was added to the system. The concentration of the added platinum catalyst was much higher than the concentration of the residual platinum catalyst on the surface of the PDMS microspheres, thereby ensuring that the concentration of the platinum catalyst in each system was similar and the crosslinking reaction rate was not affected by the concentration of the platinum catalyst.

The storage moduli of the mixtures containing PDMS microspheres, hydride crosslinker and non-reactive silicone oil varied for small changes in the volume fraction of components[110]. Hence, the storage moduli of the mixtures were normalized by dividing with initial storage modulus (*G'(0)*) of respective mixture[111]. Figure 3.3 shows the evolution of the normalized storage moduli as a function of time with *r*=1 and *r*=5 (*r*=3 not shown for clarity but the results follow identical trend as *r*=1 and *r*=5 and falls in between). The curve of the normalized storage modulus of 15:1 PDMS microspheres at *r*=5 exhibits steeper slope than that at *r*=1, indicating that the crosslinking reaction rate increased with the amount of hydride crosslinker. Meanwhile, the curves of storage modulus of 20:1 and 25:1 PDMS microspheres show a steeper slope than that of 15:1 PDMS microspheres at identical stoichiometric imbalances, indicating that the crosslinking reaction rate also increased with the surface vinyl concentration.

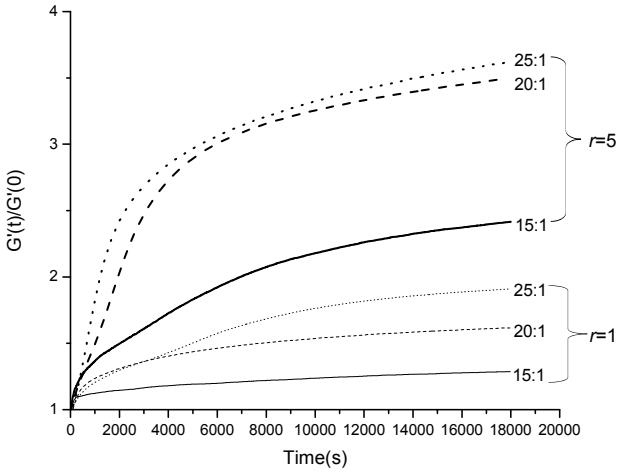

Figure 3.3. Normalized storage moduli of mixtures containing PDMS microspheres, hydride crosslinker and non-reactive silicone oil (35% (wt)) in a period of 5h at 50℃. The measurements were performed with strain of 2% and frequency of 1Hz.

The crosslinking reaction between 20:1 PDMS microspheres and hydride crosslinker at *r*=1 and *r*=5 was further evaluated in a period of 72h. The normalized storage moduli of the resulting macroscopic PDMS networks obtained at 5h, 24h, 48h and 72h are listed in Table 3.3. The value of *G'(24h)/G'(0)*, *G'(48h)/G'(0)* and *G'(72h)/G'(0)* were closely resembling, indicating that *G'(72h)* could be regarded as the equilibrium storage modulus of the macroscopic network. Meanwhile, the ratio between *G'(5h)* and *G'(72h)* was higher than 0.95, suggesting that most crosslinking reaction finished within a period of 5h[112]. Thus, it should be reasonable to use the storage modulus obtained after reacting for 5h to describe the crosslinking reaction between PDMS microspheres and hydride crosslinker. The storage moduli of the resulting macroscopic network obtained at 5h are denoted as terminal storage moduli.

Table 3.3. Normalized storage moduli of mixtures containing 20:1 PDMS microspheres, hydride crosslinker and non-reactive silicone oil (35% (wt)) obtained after reacting for 5h, 24h, 48h and 72h at 50℃. The measurements were performed with strain of 2% and frequency of 1Hz.

	G'(5h)/G'(0)	*G'(24h)/G'(0)*	G'(48h)/G'(0)	*G'(72h)/G'(0)*
Normalized storage modulus at *r*=1	1.61	1.63	1.63	1.63
Normalized storage modulus at *r*=5	3.49	3.61	3.63	3.64

The normalized terminal storage moduli (*G'(5h)/G'(0)*) are obtained from Figure 3.3 and shown in Figure 3.4 to compare the stiffness of the obtained macroscopic PDMS networks. The normalized terminal storage modulus increased with stoichiometric imbalance in 1<*r*<5, indicating that stronger macroscopic PDMS network was obtained in the presence of increasing amount of hydride crosslinker. Meanwhile, the

normalized terminal storage modulus also increased with mixing ratio, i.e. the macroscopic PDMS networks obtained from 20:1 and 25:1 PDMS microspheres exhibited higher normalized terminal storage moduli than that obtained from 15:1 PDMS microspheres at r=5[113]. This can be attributed to the surface vinyl concentration of the 20:1 and 25:1 PDMS microspheres being higher than that of the 15:1 PDMS microspheres.

The initial storage moduli of 20:1 and 25:1 PDMS microspheres as well as the terminal storage moduli were similar. Thus, the 20:1 PDMS microspheres were selected to investigate the influence of stoichiometric imbalance in a wider range and the weight fraction of non-reactive silicone oil on the terminal storage modulus of the obtained macroscopic PDMS network.

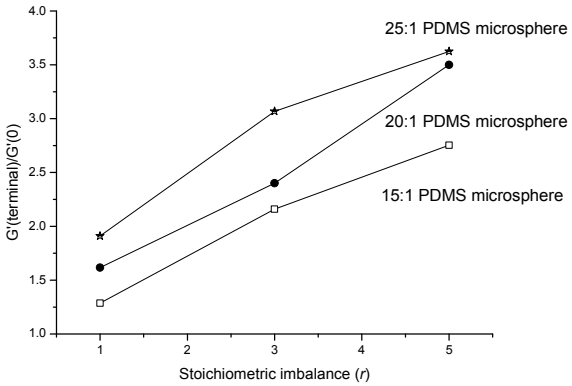

Figure 3.4. Normalized terminal storage moduli of macroscopic PDMS network obtained from the crosslinking reaction between 15:1, 20:1 and 25:1 PDMS microspheres, hydride crosslinker and non-reactive silicone oil (35% (wt)) as a function of r. (Solid lines are a guide to the eye only).

3.4.5. Terminal storage moduli of resulting macroscopic PDMS network

In this section, the terminal storage moduli of the obtained macroscopic PDMS network were investigated in a wider range of stoichiometric imbalance ($1<r<11$). Similar to previous section, the terminal storage moduli was also normalized by dividing the initial storage moduli of respective mixtures. Maximum normalized terminal storage modulus was obtained at r=7 (Figure 3.5), after which excess amount of hydride crosslinker did not increase the crosslinking density of the macroscopic network. The reasons for obtaining maximum normalized terminal storage modulus at high stoichiometric imbalances are explained as follows: firstly, part of the hydride crosslinker was absorbed by the PDMS microspheres and then reacted with the vinyl groups in the bulk of the PDMS microspheres. As a result, the absorbed hydride crosslinker only strengthen the PDMS microspheres without yielding inter-particle crosslinking points. Secondly, crosslinking reaction took place when the hydride crosslinker diffused to the surface vinyl groups attached on the PDMS microspheres. On the completion of the crosslinking reaction, the hydride crosslinker was also

covalently attached on the microspheres. Accordingly, some of the hydride groups in the crosslinker were unable to react with the surface vinyl groups due to steric effect, resulting in the high amount of hydride crosslinker needed to obtain the maximum terminal storage modulus.

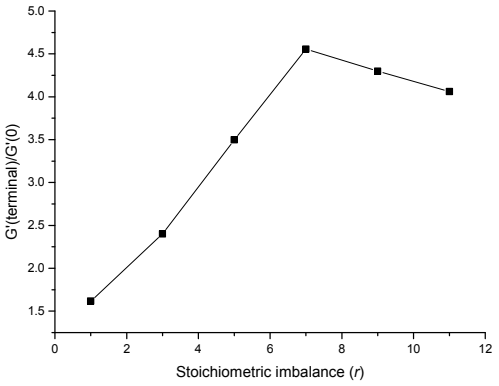

Figure 3.5. Normalized terminal storage moduli of macroscopic PDMS network obtained from the crosslinking reaction between 20:1 PDMS microspheres, hydride crosslinker and non-reactive silicone oil (35% (wt)) as a function of *r* ranging from 1 to 11. (Solid lines are a guide to the eye only).

To investigate the influence of the weight fraction of non-reactive silicone oil on the terminal storage modulus of macroscopic PDMS network, silicone oil with a molecular weight of 2,000g/mol was employed. The low molecular weight of the silicone oil ensured that it could not entangle with the macroscopic PDMS network. Consequently, the terminal storage modulus of the macroscopic PDMS network depended solely on the weight fraction of the silicone oil[114]. Similar to previous experiments, mixtures containing PDMS microspheres, hydride crosslinker and non-reactive silicone oil were made. To ensure sufficient amount of hydride crosslinker, high stoichiometric imbalances (*r*=5 and *r*=7) were used.

The normalized terminal storage moduli of the obtained macroscopic PDMS networks are plotted as a function of the weight fraction of silicone oil in Figure 3.6. The trends of the normalized terminal storage modulus curves between *r*=5 and *r*=7 were similar, indicating that the silicone oil influenced the mechanical properties of the macroscopic networks in a similar manner in the presence of different amount of hydride crosslinker. Meanwhile, the normalized terminal storage modulus increased with the weight fraction of the silicone oil in the range 15% (wt) to 35% (wt). This can be attributed to the increase of the weight fraction of the silicone oil enhancing the diffusion rate of hydride crosslinker and thus yielding stronger network. In the range 35% (wt) to 50% (wt), the normalized terminal storage modulus remained constant with the increase of the weight fraction of the silicone oil. This can be explained by the silicone oil promoting the diffusion rate of the crosslinker and diluting the polymer chains in the macroscopic PDMS network simultaneously. When the weight fraction of the silicone oil increased up to 90% (wt)[115], the PDMS microspheres in the mixture were diluted sufficiently to avoid inter-particle interactions. As a result, no crosslinking reaction between the PDMS microspheres took place and no macroscopic PDMS network could be obtained.

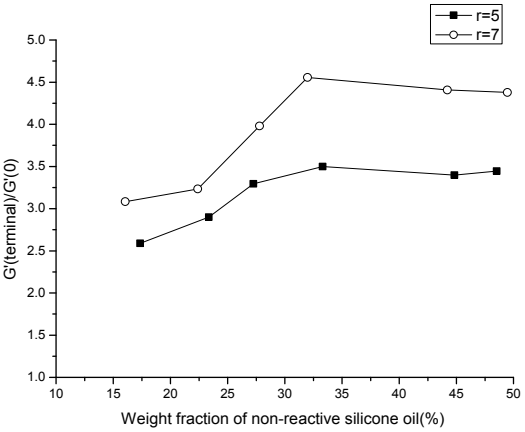

Figure 3.6. Normalized terminal storage moduli of macroscopic PDMS network obtained from the crosslinking reaction between 20:1 PDMS microspheres, hydride crosslinker and non-reactive silicone oil at *r*=5 and *r*=7 as a function of the weight fraction of silicone oil. (Solid lines are a guide to the eye only).

3.5. Conclusions

A novel titration method is introduced for the quantification of the surface vinyl concentration of PDMS microspheres. The titration method exploits the efficient and covalent bonding of monofunctional hydride to vinyl. The good reproducibility of the titration method implies that the titration method should be applicable to other commercial unstoichiometric silicone materials where surface vinyl concentration is of importance. The surface vinyl groups of the PDMS microspheres allow for further crosslinking reaction with hydride crosslinker in the presence of non-reactive silicone oil and thus yielding macroscopic PDMS network. The influences of stoichiometric imbalance and the weight fraction of non-reactive silicone oil on the storage modulus of the macroscopic network are investigated. It is found that the maximum storage modulus (~90kPa) is obtained at *r*=7 and 35% (wt) of silicone oil.

The system containing PDMS microspheres, hydride crosslinker and silicone oil can be used to introduce macroscopic PDMS elastomer to the fractures in oil field. For the application of blocking fractures, the modulus of the macroscopic PDMS elastomer is essential to the blocking efficiency as the macroscopic elastomer should withstand the pressure difference during oil recovery. The optimum amount of hydride crosslinker and silicone oil used in the crosslinking reaction is found in present study, which allows for designing an optimized system for blocking fractures. The water shutoff performance of the resulting macroscopic PDMS elastomer will be investigated in Chapter 5.

4. Control of PDMS crosslinking by encapsulating a hydride crosslinker in a PMMA microcapsule

As discussed in Section 1.3.3, control of PDMS crosslinking is needed to ensure that macroscopic PDMS elastomer block fractures without affecting the porous rocks. In this chapter, the separation of the mixing and reactive processes, which control PDMS crosslinking, has been achieved by encapsulating hydride crosslinker in a PMMA shell. Microcapsules are mixed with vinyl-terminated PDMS to create a gelation system, which allows for storage at 50°C, without premature gelation, and in addition allows for extensive crosslinking reaction at 120°C. Both visual observations and rheological studies show that a robust PDMS elastomer is obtained upon heating the gelation system. Furthermore, the influence of stoichiometric imbalance on the equilibrium storage modulus of the PDMS network is investigated by utilizing different amount of microcapsules. The results presented in this chapter have been published in RSC advances, Volume 4, Pages 47505-47512 (2014) and is attached as Appendix II.

4.1. Control of PDMS crosslinking reaction

Control crosslinking reaction of PDMS refers to PDMS crosslinking reaction taking place in response to external stimulus and thus yielding PDMS elastomer from it[116]. One way to achieve the control crosslinking reaction is to encapsulate the hydride crosslinker in polymeric microcapsules[102]. When the hydride crosslinker is sequestered inside the polymeric microcapsules, the microcapsules can be mixed with vinyl-terminated PDMS without undergoing a crosslinking reaction, thereby ensuring that the mixture has not reacted[117].

In order to release the hydride crosslinker from the polymeric shell, the shell of the microcapsule should be capable of changing its morphology or structure upon external stimulus[118]. Thermal initiation is one of the most commonly used stimuli which cause changes in the polymer structure of amorphous polymer. At temperatures lower than the glass transition temperature (T_g) of the polymeric shell, the polymeric shell remains rigid and the hydride crosslinker is sequestered inside it; therefore, the mixture containing the microcapsules and vinyl-terminated PDMS will remain liquid-like, due to the absence of a crosslinking reaction[119]. Upon heating up the mixture, the structure of the polymeric shell changes when the temperature is higher than its T_g, resulting in the release of the hydride crosslinker and the initiation of the crosslinking reaction[120]. During the crosslinking reaction, the vinyl-terminated PDMS and the hydride crosslinker convert into one large, infinite molecule. Consequently, the mixture loses its solubility, and its storage modulus starts to rise to a finite value until the completion of the crosslinking reaction.

4.2. Experimental section

4.2.1. Materials

The chemicals employed were: poly (methyl methacrylate) (PMMA) (M_w=15,000g/mol, Aldrich), 25%-35% (methylhydrosiloxane) with 65%-70% (dimethylsiloxane) copolymer (HMS-301) (M_n=2,000g/mol, 8-functional crosslinker, Gelest), platinum cyclovinylmethysiloxane complex (SIP 6832.2 catalyst, Gelest), vinyl-terminated polydimethylsiloxane (DMS-V35) (M_n=49,500g/mol, Gelest), chloroform (>99%, Aldrich), heptane (>99%, Aldrich), methanol (>99%, Aldrich) and deuterated chloroform (>99.8%D, Aldrich).

4.2.2. Apparatus

An air compressor (#1A) and an airbrush (DH-201) were purchased from Sparmax (Germany). The compressor's air flow ranged from 7 to 11 litres per minute, and the maximum pressure provided by the compressor in the air compressing process was 40psi. The diameter of the nozzle in the airbrush was 0.8mm.

The morphology of the PMMA/HMS-301 microcapsules was analysed with a scanning electron microscope (SEM) FEI Inspect S, Oxford Instruments, with an acceleration voltage of 10-20kV.

The size distribution of the PMMA/HMS-301 microcapsules was measured by Mastersizer (Malvern, UK) in a jar tester. The instrument was equipped with a laser at a wavelength of 633nm and a size range of 1µm-1mm.

^{1}H NMR spectra were obtained on a Bruker 250MHz NMR spectrometer in $CDCl_3$ at room temperature. ^{1}H chemical shifts were referenced to tetramethylsilane via a residual non-deuterated solvent signal at δ=7.26ppm.

Rheological measurements were performed in an AR2000 stress-controlled rheometer, while measurements were taken with a strain of 2% to ensure they were within the linear regime of the material[61] as well as to minimize any disruption to the network. Similar to other measurements of in-situ crosslinking reactions of additional curing silicones[104,105], the applied frequency was set to 1Hz.

4.2.3. Microcapsule preparation

The polymeric solution was prepared by dissolving 1.0g of HMS-301 and 1.0g of PMMA in 5.4mL chloroform. The polymeric solution was stirred at 700rpm with a magnetic stirrer for 24 hours at room temperature. Next, the polymeric solution was sprayed with an airbrush into a beaker containing 200mL methanol. The micro droplets formed from the polymeric solution precipitated, resulting in the encapsulation of HMS-301. The microcapsules were then washed with methanol several times, in order to remove any residual HMS-301 on the surface. Finally, the microcapsules were collected by filtration. Figure 4.1 shows the scheme for the spraying setup.

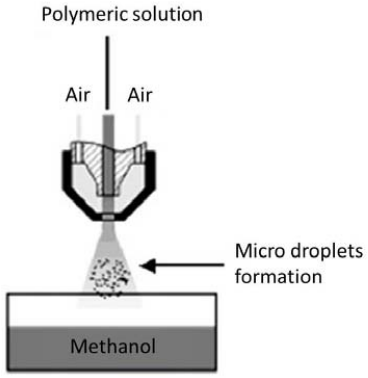

Figure 4.1. Schematic diagram of the spraying setup

In order to compare the encapsulation efficiency of the microcapsules, different concentrations of HMS-301 were used in the preparation as follows: a) 10% (wt) of HMS-301 and 10% (wt) of PMMA in *80% (wt)* chloroform (MP10H10C), b) 15% (wt) of HMS-301 and 10% (wt) of PMMA in *75% (wt)* chloroform (MP10H15C) and c) 20% (wt) of HMS-301 and 10% (wt) of PMMA in *70% (wt)* chloroform (MP10H20C).

For comparison purposes, microcapsules without HMS-301 were prepared using the same procedure from a polymeric solution containing 10% (wt) of PMMA and 90% (wt) of chloroform.

4.2.4. Soluble fraction determination

Approximately 0.5g of network obtained from microcapsule (MP10H10C) + V35 as well as HMS-301 +V35 with different stoichiometric imbalance was swelled in heptane (20-30 times excess, i.e. 15-25mL solvent to a sample of 0.5g; in all experiments, we ensure that the networks were fully covered in heptane) for 48h. After the 48h, the networks were separated from the heptane solution. The residual heptane was removed by evaporation for 48h under atmospheric condition.

4.3. Results and discussion

4.3.1. Morphological characterization

Figure 4.2a and 4.2b show the representative SEM graphs of the outer surfaces and a cross-sectional view of the PMMA/HMS-301 microcapsules which were washed with methanol and heptane, respectively. Figure 4.2a shows that the microcapsules were spherically shaped and only a few were broken after washing with methanol. Due to the low solubility of HMS-301 in methanol, methanol removed any HMS-301 on the surface only, without washing away HMS-301 inside the microcapsules. All the microcapsules in later sections were washed with methanol unless otherwise stated. Figure 4.2b shows that the microcapsules had a core-shell structure with a porous shell. Because of the high solubility of HMS-301 in heptane, heptane passed through the pores in the PMMA shell and entered into the core of the microcapsule. Thus,

heptane removed most HMS-301 and destroyed some of microcapsules during evaporation, thereby leaving a hollow structure in the microcapsules.

The morphology of the PMMA shell was similar to that of the polysulfone (PSU) shell of the PSU/vanillin microcapsule[121]. Similar to our preparation process, the PSU/vanillin microcapsule was also prepared by spraying polymeric solution containing PSU and vanillin into a non-solvent by using an air brush[121,122]. As well as studies on PSU/vanillin microcapsules, several others proved that microcapsules with a porous shell were suitable for stimuli-responsive controlled release, in order to obtain fast response times[121,123,124]. Consequently, PMMA/HMS-301 microcapsules should have a potential for controlled release when stimulated.

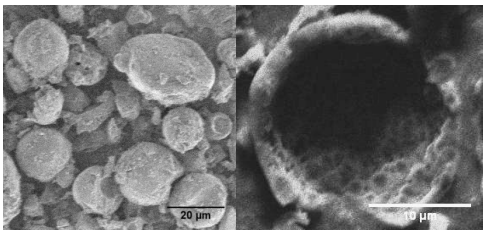

Figure 4.2a (left) and 4.2b (right). SEM image of the outer surface (left) and a cross-section (right) of PMMA/HMS-301 microcapsules. The left- and the right-hand SEM images show the morphology of the MP10H10C microcapsules washed with methanol and heptane, respectively.

4.3.2. Size distribution

As discussed in the previous section, most of the microcapsules were spherical after washing with methanol, and they should also have been identical to those not washed with methanol, as methanol only removed HMS-301 on the surface. The size distribution of the microcapsules could therefore be investigated with Mastersizer, based on laser diffraction. Figure 4.3 shows the size distribution of the microcapsules with a crosslinker inside as well the empty PMMA capsules. As shown in Figure 4.3, microspheres had a mean diameter ranging from 47µm to 58µm and were monomodal and similar in size distribution.

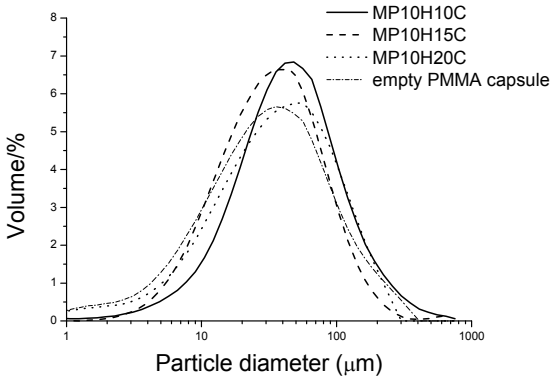

Figure 4.3. Size distribution of MP10H10C, MP10H15C, MP10H20C microcapsules and empty PMMA capsules

4.3.3. Determination of the HMS-301 weight fraction in microcapsules

The weight fraction of HMS-301 was determined through ^{1}H NMR spectroscopy. As the -O-CH_3 groups in PMMA and the Si-H groups in HMS-301 have ^{1}H chemical shifts of 3.6ppm and 4.7ppm, respectively, the mol ratio between the PMMA and HMS-301 could be calculated from the corresponding area of the resonances. Figure 4.4 shows the integrated signals of the -O-CH_3 groups and the Si-H groups in the ^{1}H NMR spectra. The weight fractions of HMS-301, calculated by ^{1}H NMR, were 28%, 21% and 14% in MP10H10C, MP10H15C and MP10H20C, respectively.

According to the information provided by the manufacturer, the HMS-301 has a molecular weight of 2,000g/mol and an average chain length of 28 Si atoms. Eight of these are CH_3HSiO groups. Meanwhile, the PMMA used in the experiment has a molecular weight of 15,000g/mol, consisted of 150 repeating units of –($CH_2C(CH_3)(COOCH_3)$-. Hence, each PMMA molecule contains 450 protons from the methyl ester group. The mol ratio between HMS-301 and PMMA can be obtained by calculating the ratio between 450 times the area of hydride group of the signals at δ=4.7ppm and eight times the area of methyl groups of the signals at δ=3.6ppm by means of the following equation[125]:

$$\frac{n_{HMS-301}}{n_{PMMA}} = \frac{450 \cdot A_1}{8 \cdot A_2} \tag{4.1}$$

where A_1 is area of the signal due to eight protons of the hydride groups in each HMS-301 molecule, A_2 is area of the signal due to 450 protons of the methyl groups in each PMMA molecule. Thus, the weight fraction of HMS-301 in the microcapsule can be obtained by the following equation:

$$\%HMS-301(wt) = \frac{\frac{450 \cdot A_1}{8 \cdot A_2} \cdot M_{n_{HMS-301}}}{\frac{450 \cdot A_1}{8 \cdot A_2} \cdot M_{n_{HMS-301}} + M_{w_{PMMA}}} \tag{4.2}$$

where $M_{n\ \text{HMS-301}}$ and $M_{w\ \text{PMMA}}$ are the molecular weight of HMS-301 and PMMA, respectively. Both the mean diameter and the weight fraction of the HMS-301 of PMMA/HMS-301 microcapsules are summarized and shown in Table 4.1.

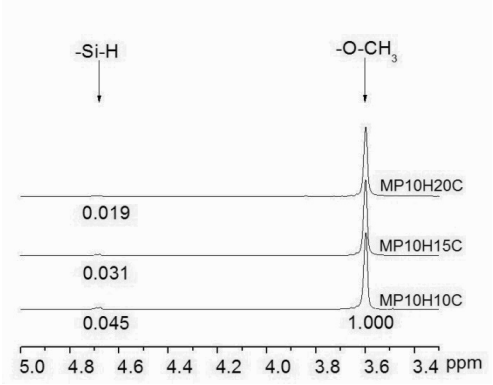

Figure 4.4. ^{1}H NMR spectra of MP10H10C, MP10H15C and MP10H20C microcapsules with an indication of the characteristic peaks for Si-H and -O-CH_3

Table 4.1. Mean diameter and weight fraction of HMS-301 for the PMMA/HMS-301 microcapsules

Sample ID	Concentration in solution before spray (wt%)			Weight fraction of HMS-301 (wt%)	Mean diameter (μm)
	PMMA	HMS-301	*Chloroform*		
MP10H10C	10	10	80	28	48
MP10H15C	10	15	75	21	41
MP10H20C	10	20	70	14	56
empty PMMA capsules	10	0	90	0	41

With the increased HMS-301 concentration, the viscosity of the solution increased, resulting in a delayed breakup process and impeded atomization. Thus the encapsulation efficiency was shown to decrease upon decrease of the shell material concentration.

The size distribution and mean diameter depended on several factors such as the viscosity and surface tension of the solution being atomized as well as the turbulence created[126]. The deviation in the mean diameters was similar to what was observed for other similar systems[127].

4.3.4. Reactivity of PMMA/HMS-301 microcapsules in a vinyl-terminated PDMS polymer

To evaluate the reactivity of the microcapsule in a melt of vinyl-terminated PDMS, a typical mixture containing a 0.01g PMMA/HMS-301 microcapsule (MP10H10C) and 1g V35 was made. All mixtures in the experiments contained 7ppm platinum catalyst. Identical mixtures were placed in two vials, which were then inserted into ovens at 50℃ and 120℃ and cured for several days. Figure 4.5a shows that the mixture

cured at 50℃ was translucent and viscous, with no visible settling of PDMS gel. The mixture remained viscous and of low viscosity, as the HMS-301 remained sequestered inside the rigid PMMA shell, leaving V35 unable to react. In contrast, Figure 4.5b shows that a crosslinked gel was obtained when the mixture was heated to 120℃. This indicates an extensive crosslinking reaction between HMS-301 and V35. After cooling down to room temperature, the material remained in its gel state, indicating that the gelation did not arise from any physical association between the PMMA/HMS-301 microcapsule and V35.

Figure 4.5a (left) and 4.5b (right). Photograph of mixtures containing the PMMA/HMS-301 microcapsule and V35 after curing at 50℃ (left) and 120℃ (right).

To characterize the rheological behavior of the PMMA/HMS-301 microcapsule and V35 mixture quantitatively, time sweep rheological measurements were performed at 50 ℃ and 120 ℃. The measurements were performed with a low amplitude strain, in order to minimise any disruption to the network during the formation process. Table 4.2 shows the composition and stoichiometric imbalance of the mixture in the measurements. The stoichiometric imbalance (*r*) is the ratio between the mol number of the hydride groups and the vinyl groups. *r* is calculated from:

$$r = \frac{n_{hydride}}{n_{vinyl}} = \frac{\frac{m_{HMS-301}}{M_{HMS-301}} \cdot f_{HMS-301}}{\frac{m_{V35}}{M_{V35}} \cdot f_{V35}} \tag{4.3}$$

where *n* is the number of moles, *m* is the mass, *M* is the molecular weight and *f* is the functionality of the respective molecule, and where subscripts HMS-301 and V35 denote the hydride crosslinker and vinyl-terminated PDMS, respectively.

Table 4.2. Compositions and stoichiometric imbalance in rheological measurements

m_{V35}/g	Sample	$m_{microcapsule}$/g	Stoichiometric imbalance (*r*)
1.013	MP10H10C	0.010	0.24
0.992	MP10H15C	0.013	0.24
1.005	MP10H20C	0.020	0.24

Figure 4.6 shows representative curves of the storage modulus of the mixture containing the PMMA/HMS-301 microcapsule and V35 at 50℃ and 120℃, respectively. At 50℃, the storage modulus remained low (~500Pa) and was lower than the loss modulus (not shown in the figure), thereby indicating that the mixture maintained viscous behavior. On the other hand, a slight increase in the storage modulus of the mixture suggests that there was a small degree of crosslinking reaction between HMS-301 and V35, which was related to the leakage of a small amount of HMS-301 from the porous PMMA shell. The porosity of the PMMA shell can be seen in the SEM image in Figure 4.2b. When measurements were made at 120℃, the storage modulus of the mixture increased rapidly, eventually reaching a plateau within 5 hours (~8000Pa), after which any further increase in storage modulus was minimal. 80% of the maximal elasticity (determined from the curve) was obtained within the first 30 minutes. This massive increase in the storage modulus of the mixture not only suggests that there was a substantial degree of crosslinking reaction during the measurement, but also corresponded well with our visual observation of the crosslinked gel obtained in the vial at 120℃ (shown in Figure 4.5b).

Considering the different rheological behaviors of the mixture at 50℃ and 120℃, the results indicates that the reactivity of the PMMA/HMS-301 microcapsule at 120℃ was significantly higher that at 50℃. This difference in reactivity can be explained as follows: at 50℃, most of the HMS-301 was sequestered in the PMMA shell, meaning that the mixture was unable to react. Moving towards the situation at 120℃, the temperature was higher than the T_g of the PMMA (T_g=100℃)[13], resulting in the softening of the PMMA shell in the microcapsule and the release of HMS-301. Consequently, this release of HMS-301 reacted with V35 in the presence of a catalyst, yielding a PDMS network.

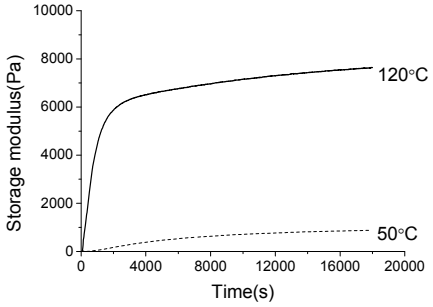

Figure 4.6. Development of elasticity in mixtures containing the PMMA/HMS-301 microcapsule (MP10H10C) and V35 at 50℃ (dash) and 120℃ (solid) over a period of 5 hours.

4.3.5. Soluble fraction

To evaluate the soluble fraction of the network obtained from the MP10H10C+ V35 with different stoichiometric imbalances, swelling experiments were performed. In this and the following section, MP10H10C was selected as a representative microcapsule, as the HMS-301 content was the highest among all the samples. In order to interpret the soluble fraction of the network from MP10H10C + V35, reference networks with identical stoichiometric imbalance as the MP10H10C +V35 network were prepared by mixing HMS-301+ V35 and cured under identical conditions. Table 4.3 shows that the soluble fraction of the

network from MP10H10C + V35 ranged from 14.5% to 27.8% and that of reference samples ranged from 5.6% to 18.2%. The soluble fraction in networks can be attributed to inactive species within the reactants and imperfections arising during the crosslinking of the network. Since the inactive species were identical for all samples, the difference in soluble fraction between the MP10H10C + V35 network and reference network arises from different degrees of imperfections in the networks[107]. The PMMA is not distinguishable soluble in heptane and was thus not washed out of the networks. The difference in the imperfections in the network can be explained as follows: upon the heating of the mixture containing MP10H10C and V35, the HMS-301 diffused out from the microcapsule and reacted with V35, yielding crosslinked PDMS network around the microcapsule. The locally formed network had a much higher viscosity than the vinyl terminated PDMS, eventually impeding the diffusion of HMS-301 and the crosslinking reaction. As a result, the unreacted PDMS remained in the network and increased the imperfections as well as the soluble fraction of the MP10H10C + V35 network.

It is further found that the soluble fraction of the MP10H10C + V35 network decreased from 27.8% to 14.5% when the stoichiometric imbalance increased from 0.8 to 1.4. This trend was similar to that of the reference system, indicating that the increasing amount of microcapsule resulted in the increasing released amount of HMS-301 and yielding stronger network with lower soluble fraction[107,128].

Table 4.3. Soluble fraction of networks obtained from MP10H10C+ V35 and HMS301+ V35

	Stoichiometric imbalance (*r*)			
	0.8	1	1.2	1.4
Soluble fraction of network obtained from MP10H10C+ V35 (%)	27.8	21.5	20.3	14.5
Soluble fraction of network obtained from reference system (HMS-301+ V35) (%)	18.2	10.9	8.4	5.6

4.3.6. Influence of stoichiometric imbalance on the equilibrium storage modulus

The aim of this section is to investigate the influence of stoichiometric imbalance on the equilibrium storage modulus of the network obtained from the crosslinking reaction between the PMMA/HMS-301 microcapsule and V35. Mixtures containing the PMMA/HMS-301 microcapsule and V35 (System A) were characterized by a time sweep rheological measurement at 120℃ within the range $0.2<r<1.4$. In order to interpret the rheological properties of the networks in System A, HMS-301+empty PMMA capsule+V35 (System B) and HMS-301+V35 (System C) with $0.6<r<1.4$ were prepared and then characterized by a time sweep rheological measurement at 120℃. System B was made to simulate the situation whereby all HMS-301 diffused out from the PMMA shell and mixed with V35, while System C consisted of a PDMS elastomer without any filler and was used as a reference sample. (Table 4.4)

Table 4.4. Composition and stoichiometric imbalance of Systems A, B and C

System ID		*r*	$m_{(PMMA/HMS\text{-}301\ microcapsule)}$/g	$m_{(PMMA\ empty\ capsules)}$/g
A	PMMA/HMS-301 microcapsule+V35	0.2	0.010	/
		0.6	0.027	/
		0.8	0.033	/
		1.0	0.045	/
		1.2	0.058	/
		1.4	0.067	/
B	HMS-301+empty PMMA capsules+V35	0.6	/	0.018
		0.8	/	0.023
		1.0	/	0.034
		1.2	/	0.042
		1.4	/	0.045
C	HMS-301+V35	0.6	/	/
		0.8	/	/
		1.0	/	/
		1.2	/	/
		1.4	/	/

The rheological behaviors of Systems A, B and C in a time sweep rheological measurement are shown in Figure 4.7 (a), (b) and (c). The equilibrium storage moduli of Systems A, B and C were obtained from Figure 4.7 (a), (b) and (c) and are shown in Figure 4.8, where we can see that the equilibrium storage modulus of System A increased in line with an increase in stoichiometric imbalance in the range $0.2<r<0.8$, indicating that the crosslinking density of the network increased as more PMMA/HMS-301 microcapsules were used in this range. However, in the range $0.8<r<1.4$, the equilibrium storage modulus of System A remained almost constant. This suggests that the crosslinking density of the network did not increase when an excess amount of PMMA/HMS-301 microcapsules was used in the mixture. In comparison, the maximum equilibrium storage moduli of most commonly applied PDMS networks were obtained in the range $1.2<r<1.4$[41], whereas the maximum equilibrium storage modulus of System A was obtained at $r=0.8$. This indicates that HMS-301 was trapped in the range $0.8<r<1.4$, due to diffusion constriction. The reason for this trapping of HMS-301 is explained in the following: upon heating the mixture containing the PMMA/HMS-301 microcapsule and V35, the PMMA shell softened, thus resulting in the release of HMS-301. Then, the released HMS-301 reacted with V35 around the microcapsule, yielding locally a crosslinked PDMS network. The crosslinked PDMS network around the microcapsule had a much higher viscosity than V35, such that the further diffusion of HMS-301 was significantly hindered by the crosslinked PDMS network. This phenomenon was described by Ndoni and Kramer as 'strangulation within polymer networks'[129]. As the crosslinked PDMS network accumulated around the microcapsule, the diffusion of HMS-301 would eventually stop, resulting in the trapping of HMS-301.

The results of System B and System C clearly show that the equilibrium storage modulus increased as stoichiometric imbalance increased in the interval $0.6<r<1.4$. For most of the PDMS network, the maximum

equilibrium storage modulus was obtained in the range 1.2<*r*<1.4, which was in line with our experimental results. In the comparison of System B and System C, the equilibrium storage modulus of System B was lower than that of System C at identical stoichiometric imbalance. This can be attributed to the immiscibility between the PDMS and the empty PMMA capsule. As such, this immiscibility increased the heterogeneity of the PDMS network, thereby causing the network's lower equilibrium storage modulus.

When comparing the rheological properties of Systems A, B and C, the equilibrium storage modulus of System A was higher than that of Systems B and C in the range 0.2<*r*<0.8. The high storage modulus of System A in this range can be attributed to the reinforcing effect of the PMMA shell from the PMMA/HMS-301 microcapsule[130]. The reinforcing effect is explained as follows: when the mixture containing the PMMA/HMS-301 microcapsule and V35 was heated up to 120℃, HMS-301 diffused out from the PMMA shell. The released HMS-301 reacted with V35 around the microcapsule, yielding crosslinking points around the microcapsules. Locally formed PDMS gel adhered to the porous PMMA shell, eventually anchoring the PDMS chain to the porous PMMA shell, which consequently reinforced the network and increased its storage modulus[131].

In the range 1.0<*r*<1.4, the equilibrium storage modulus of Systems B and C was significantly higher than that of System A with an identical stoichiometric imbalance. This indicates that the equilibrium storage modulus was determined by the homogeneity of the network in this range. The homogeneity of the network of System A was constrained by the trapping of HMS-301, as explained in the previous discussion. The trapping of HMS-301 – caused by the PDMS network around the microcapsule – is envisioned in Figure 4.9.

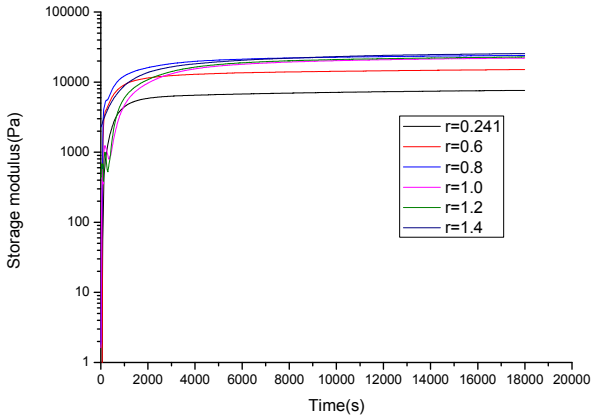

Figure 4.7a. Evolution of storage modulus of mixture containing PMMA/HMS-301 microcapsule+V35 at 120℃ in a period of 5h.

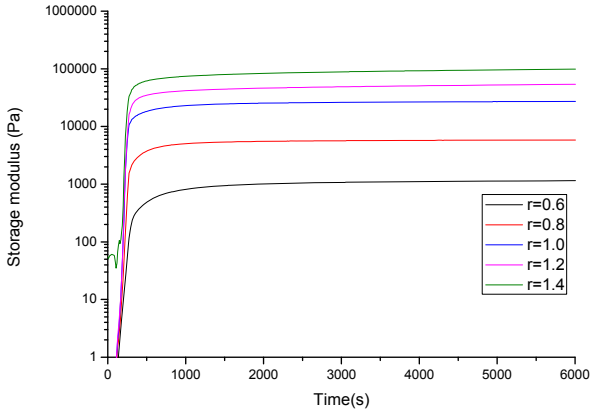

Figure 4.7b. Evolution of storage modulus of mixture containing HMS-301+empty PMMA capsule+V35 at 120℃ in a period of 2h.

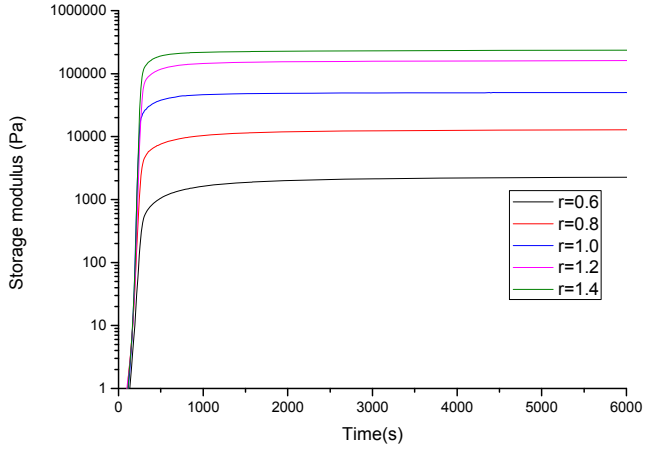

Figure 4.7c. Evolution of storage modulus of mixture containing HMS-301+V35 at 120℃ in a period of 2h.

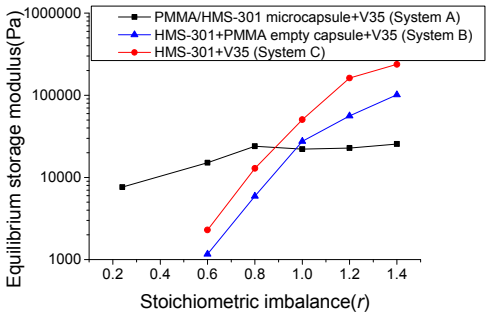

Figure 4.8. Equilibrium storage modulus of the resulting networks from PMMA/HMS-301 microcapsule (MP10H10C) +V35, HMS-301+empty PMMA capsule+V35 and HMS-301+V35 as a function of *r*.

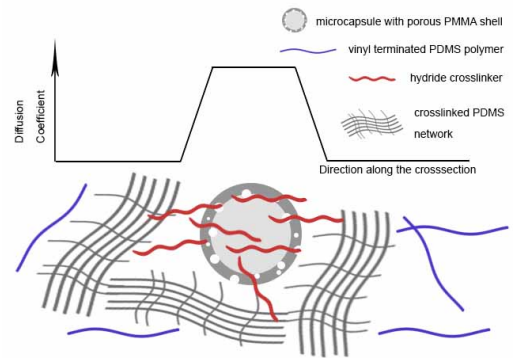

Figure 4.9. Schematic diagram of the formed PDMS network around the microcapsule that leads to the trapping of HMS-301 in the range 0.8<*r*<1.4.

Despite the low storage moduli of the obtained PDMS elastomer (~30kPa), it is comparable to that of so-called heterogeneous bimodal networks developed by Bejenariu *et al* (10-300 kPa)[61] as well as Madsen *et al* (10-100 kPa)[99]. To increase the storage moduli of the network, a natural extension of this study would be to fill the liquid silicone (V35) with fumed silica to reinforce the resulting elastomer. This will increase the storage modulus dramatically and cause elastic moduli comparable to that of commercial silicone elastomer formulations. However, current materials for fracture sealing include hydrogels with significantly lower elastic moduli[45,47,51,132] so for that particular application no further filler reinforcement is deemed necessary.

4.4. Conclusions

Control of the crosslinking reaction between a vinyl-terminated PDMS and a hydride crosslinker has been achieved by encapsulating a HMS-301 hydride crosslinker in a PMMA shell. PMMA/HMS-301 microcapsules are mixed with a V35 vinyl-terminated PDMS to create a stable mixture which remains viscous at 50℃, thereby indicating that the mixture has not reacted and that the HMS-301 is sequestered in the PMMA shell. In contrast, the mixture forms a gel when heated up to 120℃, suggesting that an extensive crosslinking reaction takes place between HMS-301 and V35, due to the release of HMS-301 from the microcapsule. As the amount of HMS-301 released determines the crosslinking density and the storage modulus of the PDMS network, the influence of stoichiometric imbalance on the equilibrium storage modulus of the PDMS network is investigated. It is found that the addition amount of microcapsule increases the equilibrium storage modulus of the PDMS network in the range $0.2<r<0.8$. It is also found that the equilibrium storage modulus of the PDMS network remains constant in the range $0.8<r<1.4$, due to the stalled diffusion of the HMS-301 by the locally formed PDMS network around the microcapsule. This indicates that the equilibrium storage modulus of the PDMS network becomes less sensitive towards stoichiometric imbalance in the control crosslinking reaction.

Control of PDMS crosslinking, which was proposed in Section 1.3.3, has been achieved by the encapsulation of a hydride crosslinker in a PMMA shell in this chapter. The control of PDMS crosslinking enables the crosslinking reaction taking place in response to thermal initiation, thereby ensuring that the macroscopic PDMS elastomer forms inside fractures without affecting the porous rocks.

5. Water shutoff performance of macroscopic PDMS elastomer

In Section 1.3, three criteria were proposed for the healing materials used in the novel shutoff system. These criteria have been satisfied by the PDMS microspheres with moderate size distribution and the control of PDMS crosslinking reaction, which have been discussed in Chapters 2-4. However, the plugging efficiency of the macroscopic PDMS elastomer has not been investigated. In this chapter, the water shutoff performance of macroscopic PDMS elastomer obtained from the crosslinking reaction between PDMS microspheres and hydride crosslinker will be analyzed in a core flow experiment.

5.1. Water permeability

The water permeability of an oil field is essential, as it correlates with the efficiency of oil recovery. The high water permeability of the oil field is unfavorable since it significantly reduces oil recovery efficiency. The high water permeability usually arises from the fractures in reservoir rocks, discussed in detail in Chapter 1.

Due to the high similarity between core samples and reservoir rocks, the petrophysical properties of the core samples are used to represent those of the reservoir rocks. Similarly, the water permeability of the core samples, the fractured core samples and the fractured core samples after treatment is extrapolated to the water permeability of the reservoir rocks, the fractured reservoir rocks and the fractured reservoir rocks after treatment, respectively. Since core samples are only available during the coring process, synthetic core samples are sometimes used as substitutes.

The water permeability of a core sample is calculated by Darcy's Law:

$$k = \frac{Q \cdot \mu \cdot l}{A \cdot \Delta p} \tag{5.1}$$

where k is the water permeability of the core sample, Q is flow rate, μ is the viscosity of water, l is the length of the core sample, A is the cross-sectional area of the core sample and Δp is the pressure difference of the core sample. The pressure difference can be measured by core flow experiment, which will be discussed in detail in Section 5.2. The units in which water permeability is typically expressed are the darcy (D) and millidarcy (mD). A permeability of 1d enables flow of 1cm^3 per second of water with 1cp viscosity through a cross-sectional area of 1cm^2 when a pressure difference of 1atm/cm is applied. The millidarcy (mD), which is one-thousandth of a darcy, is the more common unit in core sample analysis.

5.2. Experimental section

5.2.1. Materials

The chemicals employed were: Sylgard 184 consisting of vinyl terminated PDMS (Batch A) and curing agent (Batch B) (RTV silicone elastomer, Dow Corning), 25-35% (methylhydrosiloxane) with 65%-70% (dimethylsiloxane) copolymer (HMS-301) (M_n=2,000g/mol, 8-functional hydride crosslinker, Gelest), platinum-cyclovinylmethylsiloxane complex (SIP6832.2 catalyst) (Gelest), polyvinyl alcohol (PVA) (M_w=22,000g/mol, Fluka), sodium dodecyl sulphate (SDS) (>99%, BDH), non-reactive silicone oil (20cSt, M_n=2,000g/mol, Dow Corning), deionized water, 80-200 mesh sand (Dansand), phosphoric acid (85%, Aldrich), aluminum hydroxide (Aldrich) and green hydrophilic ink (Oetker).

5.2.2. Apparatus

Core flow instrument

The setup used to conduct core flow experiments is shown in Figure 5.1. It consists of a horizontal core holder, an ISCO pump, an injecting pump, a heater and a pressure transducer. Upon inserting a core sample into the core holder, the ISCO pump was started and the sleeve pressure in the core holder built up. When the system was heated up to the target temperature (80°C in this study), water was pumped into the core sample, and the pressure difference through the core sample was measured by a pressure transducer. A computer equipped with a data acquisition system recorded the pressure difference.

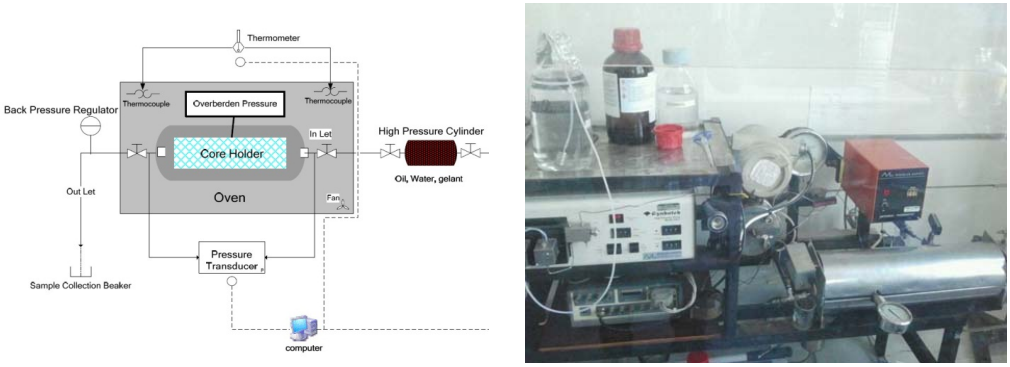

Figure 5.1. Schematic diagram (left) and physical appearance (right) of core flow setup.

Porosity measurement

The porosity of core samples was directly measured by a gas expansion porosimeter (Vinci, Germany) based on Boyle's Law.

5.2.2. Experimental procedure

Preparation of aluminum phosphate gel (APG)

APG was prepared according to the following procedure[133]: 50g aluminum hydroxide was dispersed in 100g 85% phosphoric acid solution in a 500-mL beaker to create a suspension. The suspension was cured in an oven at 120℃ for 1h to obtain the APG. After cooling down to room temperature, the APG was ready for further use.

Preparation of synthetic core samples

Synthetic core samples were prepared as follows[133]: a mixture composed of 200g sand and 120g APG was thoroughly mixed and placed in a 500-mL beaker at 80℃ for 24h to remove the residual water from the APG. Afterwards, the mixture was poured into a cylindrical iron tube and, when the tube was filled, the iron tube was heated to 50℃. The mixture in the iron tube was then subjected to uniaxial pressure of 3MPa to 5MPa by means of a hydraulic piston. Pressure was maintained on the mixture for 30min to ensure that the mixture was bound into a solid that would not disintegrate upon removal from the iron tube. Upon the release of pressure, the mixture was ejected from the iron tube. The mixture was further sintered at 500℃ for 10h to obtain the synthetic core samples. The resulting core samples were then machined at both ends to make flat, smooth surfaces. The schematic diagram and the physical appearance of the synthetic core samples are shown in Figure 5.2.

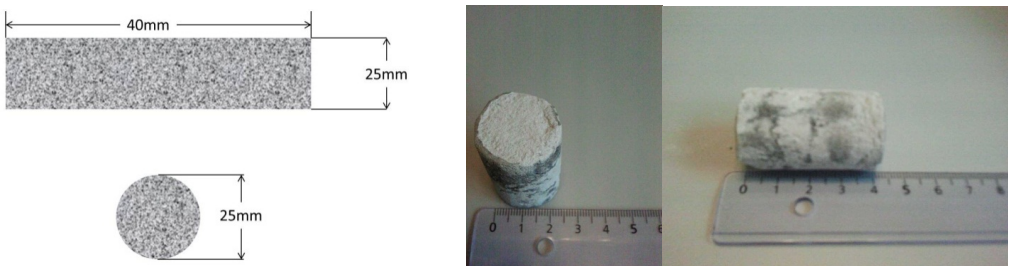

Figure 5.2. Schematic diagram (left) and physical appearance (right) of synthetic core samples.

Preparation of fractured synthetic core samples

Fractured synthetic core samples were prepared from synthetic core samples by creating a simulated fracture by drilling with a diameter of 12mm and a length of 35mm. Figure 5.3 shows the schematic diagram and the physical appearance of the fractured synthetic core samples.

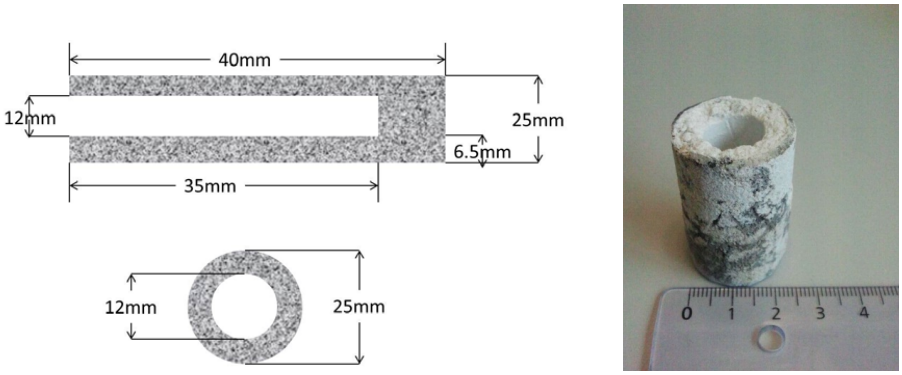

Figure 5.3. Schematic diagram (left) and physical appearance (right) of fractured core samples.

Petrophysical properties of the synthetic core samples

The petrophysical properties of synthetic core samples and fractured core samples played an important role in the evaluation of the water shutoff performance of macroscopic PDMS elastomer. Several parameters, including pore volume (PV), fracture volume (FV) and the water permeability of synthetic core samples (k_c) and fractured core samples (k_f), should be considered with respect to the petrophysical properties. PV and FV are calculated by using the following equations:

$$PV = \pi \cdot (\frac{d_c}{2})^2 \cdot l_c \cdot \phi \tag{5.2}$$

$$FV = \pi \cdot (\frac{d_f}{2})^2 \cdot l_f \tag{5.3}$$

where d, l and ϕ are the diameter, length and porosity of core samples, respectively. Subscripts c and f denote synthetic core samples and fractured core samples, respectively. The water permeability of the synthetic core samples and fractured core samples is calculated according to Darcy's Law:

$$k_c = \frac{Q \cdot \mu \cdot l_c}{A \cdot \Delta p_c} \tag{5.4}$$

$$k_f = \frac{Q \cdot \mu \cdot l_c}{A \cdot \Delta p_f} \tag{5.5}$$

where k is the water permeability of core samples, Q is flow rate, μ is viscosity of water, l_c is the length of synthetic core samples, A is the cross-sectional area of synthetic core samples and Δp is the pressure difference obtained by core flow experiment. Table 5.1 shows that the porosity of the core samples deviated only slightly, ensuring that the synthetic core samples are reproducible. Depending on the porosity and the dimensions of the synthetic core samples, the PV ranged from (7-8)·10^3mm^3, which was in line with the results in the literature[134,135]. It can also be seen that the FV of the fractured core samples ranged from (2-3)·10^3mm^3, indicating that the volume of macroscopic PDMS elastomer required in the

treatment was moderate[134,136]. k_c was fairly low and deviated slightly in different core samples, ensuring that the k_c was within the range of the permeability of the reservoir rock and that the core samples were suitable for used as simulated core samples[9]. Furthermore, the k_f was much higher than k_c, indicating that the permeability increased significantly upon fracture[7].

Table 5.1. Petrophysical properties of synthetic core samples and fractured core samples.

Core	Fracture aperture (mm)	Length (mm)	Diameter (mm)	Porosity (%)	PV (mm^3)	FV (mm^3)	k_c (mD)*	k_f (mD)*
S1P6L1	12.0	32.2	25.3	46.0	7442	2467	14.4	349.5
S1P6L2	12.0	37.8	25.3	47.1	8734	3142	18.6	482.8

*Permeability measurements determining k_c and k_f were performed at a sleeve pressure of 15 bar at 80℃ by core flow experiment.

Preparation of PDMS microspheres

For the preparation of PDMS microspheres, see Section 3.3.3. In this chapter, only PDMS microspheres prepared from a mixing ratio of 20:1 (ratio between Batch A to Batch B from Sylgard 184) were used.

5.3. Results and discussion

5.3.1. Properties of PDMS microspheres and their crosslinking reaction

The properties of PDMS microspheres were investigated systematically in Chapters 2 and 3. For the size distribution and the surface vinyl concentration of the PDMS microspheres, refer to Sections 3.4.1 and 3.4.3. Regarding the crosslinking reaction of the PDMS microspheres, see Sections 3.4.4 and 3.4.5.

5.3.2. Mechanism of water shutoff using macroscopic PDMS elastomer

Macroscopic PDMS elastomer was obtained from the crosslinking reaction between PDMS microspheres and hydride crosslinker. Figure 5.4 shows the schematic diagram and the physical appearance of the macroscopic PDMS elastomer in a treated core sample. It can be seen that the macroscopic PDMS elastomer filled up the fracture without leaving a macro-scale gap. The condensed packaging of the macroscopic PDMS elastomer could prevent water channeling between the macroscopic PDMS elastomer and the sidewall of the core sample, thus improving the plugging efficiency of the macroscopic PDMS elastomer. Moreover, the hydrophobicity of the macroscopic PDMS elastomer could also prevent water penetration.

Figure 5.4. Schematic diagram (left) and physical appearance (right) of treated core sample filled up with macroscopic PDMS elastomer. The macroscopic PDMS elastomer is within the red circle.

To further investigate the water flow in a treated core sample, an ink flow experiment was performed using diluted green hydrophilic ink solution. Figure 5.5 shows the representative photograph of the residual pigment in the treated core sample after flushing with the ink solution. The pattern of the residual pigment, which was generated by the evaporation of the water in the ink solution, indicates that water flowed only through the core sample without penetrating the macroscopic PDMS elastomer due to its hydrophobicity. This corresponds to the mechanism in the previous discussion.

Figure 5.5 Representative photograph of residual pigment in treated core sample after flow of ink solution.

5.3.3. Evaluation of water shutoff performance of macroscopic PDMS elastomer

In the evaluation of the water shutoff performance of macroscopic PDMS elastomer, a typical mixture containing 2g of PDMS microsphere, 0.1g of HMS-301 and 1g of non-reactive silicone oil was made. The mixture was poured into the fractured core sample and cured at 80℃ for 3h to obtain macroscopic PDMS elastomer in the fracture. The treated core sample was then subjected to core flow experiment at 80℃ with a sleeve pressure of 15bar. The water permeability of the treated core sample was recorded as a function of the accumulative injection volume of water. As the water permeability could not reflect the plugging efficiency of the macroscopic PDMS elastomer directly, water residual resistance factor (F_{rrw}), which was widely used in the evaluation of the water shutoff performance of healing materials, was introduced. It is defined as follows[137]:

$$F_{rrw} = \frac{k_f}{k_h} \tag{5.6}$$

where k_f and k_h are the water permeability of fractured core samples and treated core samples, respectively. The F_{rrw} reflects the plugging efficiency as well as the reduction in permeability after treatment. In most studies, the F_{rrw} in fractured cores with fractures not extending through ranged from 3 to 50[138]. A high value of F_{rrw}, preferably above 10, indicates successful treatment with excellent plugging properties.

In oil recovery, the volume of water injected into the oil field depended on many parameters, including the volume and the porosity of the reservoir rocks in the oil field. Thus, the volume of water injected into the oil field was divided by the pore volume of the reservoir rocks to compare oil recovery efficiency in different reservoirs[9]. Similarly, the volume of water injected into the treated core sample in the experiment was divided by the pore volume of the core sample to ease the comparison of the treatment stability between different cores as well as the comparison between the simulated cores and the reservoirs. It has been shown that the injection of 5PV water required exposure to reservoir conditions for at least two years[7]. Thus, to ensure the validity of the treatment, the shutoff performance of the treated core sample was required to persist longer than the injection of 5PV water in the core flow experiment.

Figure 5.6 shows the evolution of F_{rrw} as a function of accumulated water injected during the core flow experiment. Upon the injection of the first PV of water, the F_{rrw} increased from 5 to 12. During this period, the increase of F_{rrw} arises from the building up of a pressure difference due to the injection of water. The F_{rrw} then reached a plateau at approximately 18 after the injection of 5PV water. This indicates that the pressure difference did not increase with the injection of water after injecting 5PV water, and the pressure difference became constant in this period. As a result, the plugging efficiency of macroscopic PDMS elastomer could be determined. The high value of the F_{rrw} clearly indicates the excellent water shutoff performance of the macroscopic PDMS elastomer. Furthermore, the F_{rrw} remained constant during the injection of 25PV water, indicating that the macroscopic PDMS elastomer was stable within this period and that the treatment was durable.

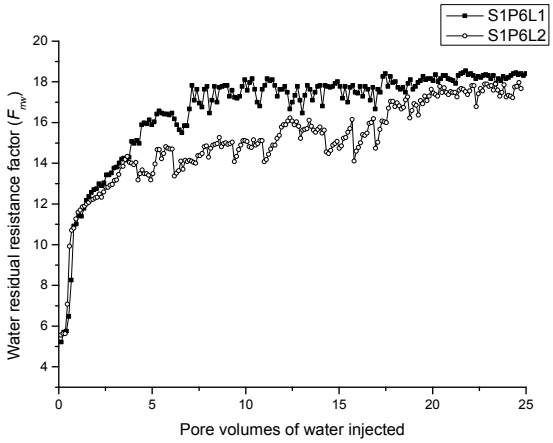

Figure 5.6. Water residual resistance factor (F_{rrw}) versus pore volumes of water injected in treated core samples (S1P6L1 and S1P6L2). The core flow experiment was performed at 80℃ with a sleeve pressure of 15bar.

5.3.4. Comparison with other water shutoff systems

An ideal water shutoff treatment should satisfy the following criteria[37,135]: first of all, the water permeability of a treated core sample should be much lower than that of a fractured core sample, thereby ensuring the high plugging efficiency of the treatment. Quantitatively speaking, the F_{rrw} of the treatment should be greater than 10. Secondly, the water permeability of the treated core sample should be similar to that of core sample without fracture. This requires the k_h/k_c to be close to 1, where k_h and k_c are the permeability of the treated core sample and the core sample without fracture, respectively. Finally, the healing materials should be durable and withstand the high pressure difference for extended periods of time. This requires the water permeability of the treated core sample to remain constant for a period longer than that involving injection of 5PV water.

The water shutoff performance of macroscopic PDMS elastomer, like many other healing materials, was evaluated by core flow experiment. The differences in the experimental conditions of the core flow experiment, including sleeve pressure, temperature and the flow rate of water, did not affect the water permeability of core samples significantly. Therefore, a fair comparison can be made between the water shutoff performances of different materials.

In order to compare water shutoff performance by using different systems, the permeability of core samples before fracturing (k_c), permeability of fractured core samples (k_f), permeability of treated core samples (k_h) from the literature and this study are summarized in Table 5.2. Concerning the first criterion, it can be seen that the k_h was significantly lower than k_f in all treatments, indicating that the value of F_{rrw} was much larger than 10 (data not shown) and that the treatments were successful in blocking fracture. Regarding the second criterion, the k_h/k_c from Zhao *et al*[7], Abbasy *et al*[138] and Simjoo *et al*[23] were significantly lower than 1, indicating that the permeability of the treated core sample was much lower than

the permeability of the original core sample. The decrease in water permeability arises from the healing materials in these studies blocking the fractures and some of the pores in the core sample simultaneously. In comparison, the results of Seright *et al*[134–136] in 1994, 1995 and 1999[134–136] and the results in this study showed that k_h/k_c was close to 1, indicating that the treatment successfully blocked fracture without affecting the pores in the rock. With respect to the third criterion, the healing materials from Simjoo *et al*[23], Abbasy *et al*[21] and this study were stable longer than the injection of 25PV water, while the healing materials used by Seright *et al*[134–136] had significantly lower stability.

From the comparison between other water shutoff systems and our system, it can be seen that our system maintained the permeability of the core sample after blocking the fracture and had long validity. The reasons for this macroscopic PDMS elastomer performance are explained as follows: first of all, the PDMS microspheres have a mean diameter of approximately 100μm, which is larger than the pore size of the core sample. The PDMS microspheres were prevented from penetrating the pores, resulting in the permeability of the treated core sample being similar to that of the core sample without fracture. Secondly, the high stability of macroscopic PDMS elastomer arises from its hydrophobicity and highly crosslinked structure. The hydrophobicity prevented water penetration, while the highly crosslinked structure contributed to the high durability of the macroscopic PDMS elastomer.

Table 5.2. Water permeability of core samples without fracture, fractured core samples and treated core samples as well as the stability of the treatment.

	k_c	k_f	k_h	k_h/k_c	Polymer	crosslinker	stability
Zhao *et al*[7], 2011	140	8100	12	0.09	PAM	polyethylene imine	>2PV
Simjoo *et al*[23], 2009	280	28000	<30	<0.1	PAM sodium acrylate	chromium acetate	>25PV
Abbasy *et al*[138], 2008	950	2100	190	0.20	PAM copolymer	none	>25PV
Seright *et al*[135,136], 1994, 1995	650	27000	550	0.85	PAM	Cr^{3+}	1PV
Seright *et al*[134], 1999	50	5100	<81	<1.6	PAM	Cr^{3+}	4PV
This study	17	420	19	1.1	PDMS microspheres	hydride crosslinker	>25PV

5.4. Conclusions

In this chapter, the water shutoff performance of macroscopic PDMS elastomer has been evaluated by core flow experiment. It is found that the water permeability of the treated core sample is similar to the core sample without fracture, suggesting that the macroscopic PDMS elastomer blocked fracture without affecting the pores in the core sample. The high plugging efficiency can be attributed to the hydrophobicity of the macroscopic PDMS elastomer, which prevents water from flowing through, while the isolation of pores arises from the size of the PDMS microspheres being larger than the diameter of the pores. Moreover, it is further found that the PDMS elastomer has higher stability than the injection of 25PV water, ensuring the long validity of the treatment.

6. Conclusions and future work

6.1. Conclusions

For water shutoff systems, it is essential to block fracture selectively and efficiently. In Chapter 1, three main criteria were discussed for selective plugging, namely the size of the PDMS microspheres falling between the size of pores and the width of fractures, high surface vinyl concentration on the PDMS microspheres allowing for a strong macroscopic PDMS elastomer, and initiation of crosslinking reaction upon stimulus allowing for fast and efficient delivery of the plug to the fracture. Moving towards the efficient plugging, the macroscopic PDMS elastomer should reduce the water permeability of the fractured core sample significantly and withstand the pressure difference for a long period.

To satisfy the first criterion of selective plugging, PDMS microspheres with diameters ranging from 2µm-500µm have been prepared by emulsion polymerization in surfactant solution. The size of the PDMS microspheres falls between the size of the pores (diameter<1µm) and the width of the fracture (width between 1µm and 4mm), allowing the PDMS microspheres to flow into the fracture without affecting the pores. The experimental size distribution of the PDMS microspheres is further compared with the theoretical size distribution predicted by the population balance model and maximum entropy formalism. There is noticeable correlation between the experimental and theoretical results.

The second criterion—high surface vinyl concentration on the PDMS microspheres—has been satisfied by increasing the ratio of vinyl-terminated PDMS during the preparation of PDMS microspheres. The excess vinyl-terminated PDMS gives the PDMS microspheres' vinyl groups on the surface. To determine the surface vinyl concentration of the PDMS microspheres, a novel titration method using monofunctional hydride is employed for the following reasons. First, the silicone-based monofunctional hydride is miscible with the PDMS microspheres and will not alter the surface properties of the PDMS microspheres. Secondly, the monofunctional hydride can efficiently bind to the vinyl groups on the surface of the PDMS microspheres via hydrosilylation reaction in a ratio of 1:1. Not only can the novel titration method be applied to PDMS microspheres to determine the vinyl concentration, but, based on the titration method, should be applicable for commercial crosslinked silicone systems, where vinyl concentration is of importance. According to the titration method, the PDMS microspheres have a vinyl concentration of approximately $2 \cdot 10^{-5}$mol/g, which allows for extensive crosslinking reaction and, thus, allows for a macroscopic network. A maximum storage modulus of the macroscopic network was found in the presence of a moderate amount of hydride crosslinker and non-reactive silicone oil.

Regarding the third criterion of selective plugging, the healing material should not react until initiated, i.e. controlled crosslinking reaction. The controlled crosslinking reaction has been facilitated by the encapsulation of hydride crosslinker in the PMMA shell. The mixture containing the PMMA microcapsules and the vinyl-terminated PDMS allows for storage at 50℃, as the hydride crosslinker is sequestered inside the PMMA shell, leaving the mixture unable to react. Upon heating to 120℃, the hydride crosslinker is released and the crosslinking reaction is thereby initiated, yielding PDMS elastomer. The PDMS elastomer has a storage modulus of 30kPa, which is significantly higher than that of the currently applied hydrogels (<1kPa) for fracture treatment. It is further found that the PDMS elastomer can be obtained within a period of 2h after initiation, allowing for fast delivery of the elastomeric plug to the fracture.

As discussed above, the three main criteria of selective plugging have been satisfied. Meanwhile, it is also important to block fracture efficiently and withstand the pressure difference for a long period. Therefore, the macroscopic PDMS elastomer obtained from the crosslinking reaction between PDMS microspheres and hydride crosslinker will be used to evaluate plugging efficiency.

In the evaluation of plugging efficiency of the macroscopic PDMS elastomer, core flow experiments are performed. Initially, the water permeability of the core sample is approximately 20mD. By drilling a fracture with a diameter of 12mm, the water permeability of the fractured core sample increases up to 400mD, suggesting that the water permeability of the core sample is significantly affected by the fracture. Afterwards, the fractured core sample is healed by the macroscopic PDMS elastomer obtained from the crosslinking reaction between PDMS microspheres and hydride crosslinker. The water permeability of the treated core sample decreases to 23mD, indicating that the macroscopic elastomer block fracture efficiently without affecting the pores in the core sample. Moreover, the water permeability of the treated core sample remains constant after the injection of 25PV water.

6.2. Future work

As discussed in Chapter 5, the PDMS elastomer obtained from the crosslinking reaction between PDMS microspheres and hydride crosslinker blocks the fracture selectively and efficiently. However, the combination of mixing and reactive process of the microspheres and the crosslinker limits the fast and efficient delivery of PDMS elastomer to the fracture. To resolve this problem, encapsulated hydride crosslinker, rather than crosslinker without encapsulation, should be employed to react with PDMS microspheres in a controlled manner.

The objective of this encapsulation is to investigate the water shutoff performance of PDMS elastomer obtained in a controlled manner. The PDMS microspheres and microcapsule should be inserted into the fractured core sample at room temperature. The water permeability of the filled-up core sample is expected to be similar to that of the fractured core sample due to the PDMS microspheres and the microcapsule remaining separate, with no macroscopic PDMS elastomer being obtained. The filled-up core sample could then be heated up to 120℃ to release the hydride crosslinker from the microcapsule, yielding macroscopic PDMS elastomer to block fracture (referred to Chapter 4). Therefore, the water permeability of the treated core sample is expected to be significantly lower than that of the fractured core sample.

Given that the macroscopic PDMS elastomer obtained in a controlled manner blocks fracture efficiently and rapidly, the system could be further subjected to water shutoff in the oil field. After treatment, excessive water production is expected to decrease and oil recovery efficiency will therefore increase.

References

1 R. Cosse, Basics of reservoir engineering. Editions Technip, Paris, France, **1993**.

2 W. M. Ahr, Geology of carbonate reservoirs. Wiley, Hoboken, New Jersey, **2008**.

3 M. Lesage, P. Hall, J. R. A. Pearson, and M. J. Thlercelln, Pore-pressure and fracture gradient predictions. *Journal of Petroleum Technology*, **1991**, 43, 652–654.

4 T. D. Van Golf-Racht, Fundamentals of fractured reservoir engineering. Elsevier Inc., Amsterdam, Netherlands, **1982**.

5 L. Lacy, A. Rickards, and D. Bilden, Fracture width and embedment testing in soft reservoir sandstone. in *SPE Drilling & Completion*, Denver, U.S., **1998**, pp. 25–29.

6 S. Vickers, A. Hutton, and R. Main, Drilling highly fractured limestone reservoirs: is it a particle bridge too far? in *SPE Annual Technical Conference and Exhibition*, Florence, Italy, **2010**, pp. 19–22.

7 J. Zhao, H. Jia, W. Pu, and R. Liao, Influences of fracture aperture on the water-shutoff performance of polyethyleneimine cross-linking partially hydrolyzed polyacrylamide gels in hydraulic fractured reservoirs. *Energy & Fuels*, **2011**, 25, 2616–2624.

8 C. E. Cook Jr, Conductivity of fracture proppants in multiple layers. in *SPE Annual Technical Conference and Exhibition*, San Antonio, U.S., **1973**, pp. 1101–1107.

9 T. Ahmed, Reservoir engineering handbook. Elsevier, Oxford, UK, **2010**.

10 A. Dyes, C. Kemp, and B. Caudle, Effect of fractures on sweep-out pattern. *Petroleum Trasnsactions, AIME*, **1958**, 213, 245–249.

11 M. K. Fisher, C. A. Wright, and B. M. Davidson, Integrating fracture mapping technologies to optimize stimulations in the barnett shale. in *SPE Annual Technical Conference and Exhibition*, San Antonio, U.S., **2002**, pp. 1–7.

12 W. McGuire and V. Sikora, The effect of vertical fractures on well productivity. *Journal of Petroleum Technology*, **1960**, 72–73.

13 M. Prats, P. Hazebroek, and W. R. Strickler, Effect of vertical fractures on reservoir behavior-incompressible fluid case. *Society of Petroleum Engineers Journal*, **1961**, 1, 87–94.

14 W. Olsson, The effect of slip on the flow of fluid through a fracture. *Geophysical Research Letters*, **1992**, 19, 541–543.

15 R. D. Sydansk, Y. Xiong, A. M. Al-Dhafeeri, R. J. Schrader, and R. S. Seright, Characterization of partially formed polymer gels for application to fractured production wells for water-shutoff purposes. in *SPE/DOE Symposium on Improved Oil Recovery*, Society of Petroleum Engineers, Tulas, U.S., **2004**, pp. 1–11.

16 R. Ruhland, Methode detude de la fracturation naturelle des roches, associete divers modeles structuraux. *Geology Society Bulletin*, **1973**, 26, 91–113.

17 O. Joseph, G. Saleem, and F. Alhasan, Stochastic simulation of fracture density for permeability field estimation. in *SPE International*, Manama, Bahrain, **1997**, pp. 121–136.

18 J. Vasquez, I. Jurado, and A. Santillan, Organically crosslinked polymer system for water reduction treatments in mexico. in *First International Oil Conference and Exhibition in Mexico*, Cancun, Mexico, **2006**, pp. 1–8.

19 A. Kabir, Chemical water & gas shutoff technology-an overview. in *SPE Asia Pacific Improved Oil Recovery Conference*, Kuala Lumpur, Malaysia, **2001**, pp. 1–14.

20 H. A. Nasr-El-Din and K. C. Taylor, Evaluation of sodium silicate/urea gels used for water shut-off treatments. *Journal of Petroleum Science and Engineering*, **2005**, 48, 141–160.

21 S. Bauer, P. Gronewald, J. Hamilton, D. Laplant, and A. Mansure, High-temperature plug formation with silicates. in *SPE international Symposium on Oilfield chemistry*, Houston, U.S., **2005**, pp. 1–6.

22 A. El-Sayed, N. A.-A. Musaed, and A.-H. Emad S, Potential use of blast furnace slag and steel making slag for consolidation of friable sandstone reservoirs. *Journal of King Saud University*, **2000**, 13, 271–285.

23 A. Moradi-Araghi, G. Bjornson, and P. Doe, Thermally stable gels for near-wellbore permeability contrast corrections. *SPE Advanced Technology Series*, **1993**, 1, 140–145.

24 S. L. Bryant, M. Bartosek, and T. P. Lockhart, Laboratory evaluation of phenol—formaldehyde/polymer gelants for high-temperature applications. *Journal of Petroleum Science and Engineering*, **1997**, 17, 197–209.

25 A. Izumi, T. Nakao, and M. Shibayama, Gelation and cross-link inhomogeneity of phenolic resins studied by 13C-NMR spectroscopy and small-angle X-ray scattering. *Soft Matter*, **2013**, 9, 4188–4197.

26 E. Larry, G. Funkhouser, and C. Mike, High-density monomer system for formation consolidation/water shutoff applications. in *SPE international Symposium on Oilfield chemistry*, Houston, U.S., **1999**, pp. 1–13.

27 D. Dalrymple, J. Tarkington, and J. Hallock, A gelation system for conformance technology. in *SPE Annual Technical Conference and Exhibition*, **1994**, pp. 397–404.

28 P. Shriwal and R. Lane, Impacts of timing of crosslinker addition on water shutoff polymer gel properties. in *Proceedings of SPE Improved Oil Recovery Symposium*, Society of Petroleum Engineers, Tulas, U.S., **2012**, pp. 1–15.

29 Z. Hua, M. Lin, J. Guo, F. Xu, Z. Li, and M. Li, Study on plugging performance of cross-linked polymer microspheres with reservoir pores. *Journal of Petroleum Science and Engineering*, **2013**, 105, 70–75.

30 M. Al-Anazi, S. Al-Mutairi, M. Al-Khaldi, A. Al-Zahrani, I. Al-Yami, and M. Gurmen, Laboratory evaluation of organic water shut-off gelling system for carbonate formations. in *SPE European Formation Damage Conference*, **2011**, pp. 1–21.

31 H. Jia, W. F. Pu, J. Z. Zhao, and F. Y. Jin, Research on the gelation performance of low toxic PEI cross-linking PHPAM gel systems as water shutoff agents in low temperature reservoirs. *Industrial & Engineering Chemistry Research*, **2010**, 49, 9618–9624.

32 C. Guy, T. Rene, C. Bon, and R. Michel, In-depth permeability control by adsorption of soft size-controlled microgels. in *SPE European Formation Damage Conference*, SPE, Hague, Netherlands, **2003**, pp. 1–8.

33 Y. Wu and B. Bai, Modeling particle gel propagation in porous media. in *SPE Annual Technical Conference and Exhibition*, Denver, U.S., **2008**, pp. 1–10.

34 G. Chauveteau, A. Omari, R. Tabary, M. Renard, and J. Veerapen, New size-controlled microgels for oil production. in *SPE international Symposium on Oilfield chemistry*, Houston, U.S., **2001**, pp. 1–8.

35 H. Zhang and B. Bai, Preformed particle gel transport through open fractures and its effect on water flow. in *SPE Improved Oil Recovery Symposium*, Society of Petroleum Engineers, Tulsa, U.S., **2010**, pp. 1–15.

36 D. Dwyann, L. Eoff, and J. Vasquez, Shallow penetration particle-gel system for water and gas shutoff applications. in *SPE Russian Oil and Gas Technical Conference and Exhibition*, Moscow, Russia, **2008**, pp. 1–7.

37 B. Bai, F. Huang, Y. Liu, R. S. Seright, and Y. Wang, Case study on prefromed particle gel for in-depth fluid diversion. in *SPE/DOE Improved Oil Recovery Symposium*, Tulsa, U.S., **2008**, pp. 1–18.

38 A. Al-Ibadi and F. Civan, Experimental study of gel particles transport through porous media. in *SPE Latin America and Caribbean Petroleum Engineering Conference*, Mexico City, Mexico, **2012**, pp. 1–27.

39 C. Yao, G. Lei, L. Li, and X. Gao, Selectivity of pore-scale elastic microspheres as a novel profile control and oil displacement agent. *Energy & Fuels*, **2012**, 26, 5092–5101.

40 R. Mukhopadhyay, When PDMS is not the best. *Anal. Chem.*, **2007**, 3248–3253.

41 A. L. Larsen, K. Hansen, O. Hassager, A. Bach, S. Ndoni, and M. Jørgensen, Elastic properties of nonstoichiometric reacted PDMS networks. *Macromolecules*, **2003**, 36, 10063–10070.

42 K. E. Polymanteer, Silicon rubber, its development and technological progress. in *Rubber Division, American Chemical Society*, Cleverland, U.S., **1987**, pp. 470–502.

43 P. Jerschow, Silicone Elastomers. Springer, Shropshire, UK, **2001**, vol. 12.

44 A. C. C. Esteves, J. Brokken-Zijp, J. Laven, H. P. Huinink, N. J. W. Reuvers, M. P. Van, and G. de With, Influence of cross-linker concentration on the cross-linking of PDMS and the network structures formed. *Polymer*, **2009**, 50, 3955–3966.

45 B. Sengupta, V. P. Sharma, and G. Udayabhanu, Gelation studies of an organically cross-linked polyacrylamide water shut-off gel system at different temperatures and pH. *Journal of Petroleum Science and Engineering*, **2012**, 81, 145–150.

46 A. Moradi-Araghi, A review of thermally stable gels for fluid diversion in petroleum production. *Journal of Petroleum Science and Engineering*, **2000**, 26, 1–10.

47 M. Rafipoor, M. V. Sefti, F. Salimi, K. Jarrahian, and S. S. Ghorashi, Investigation of rheological properties of polyacrylamide/ chromium triacetate hydrogels performed for water shutoff treatment in oil reservoirs. *Journal of Dispersion Science and Technology*, **2013**, 6, 1–31.

48 M. Simjoo, M. Vafaie, and A. Dadvand, Polyacrylamide gel polymer as water shut-off system: preparation and investigation of physical and chemical properties in one of the Iranian oil reservoirs. *Iranian Journal of Chemistry and Chemical Engineering*, **2007**, 26, 99–108.

49 G. Dupuis and A. Al-Maamari, Mechanical and thermal stability of polyacrylamide-based microgel products for EOR. in *SPE international Symposium on Oilfield chemistry Symposium on Oilfield*, Woodlands, U.S., **2013**, pp. 1–11.

50 D. Broseta, O. Marquer, N. Blin, and A. Zaitoun, Rheological screening of low-molecular-weight polyacrylamide/chromium (III) acetate water shutoff gels. in *SPE/DOE Improved Oil Recovery Symposium*, Tulas, U.S., **2000**, pp. 1–11.

51 G. A. Al-Muntasheri, I. A. Hussein, H. A. Nasr-El-Din, and M. B. Amin, Viscoelastic properties of a high temperature cross-linked water shut-off polymeric gel. *Journal of Petroleum Science and Engineering*, **2007**, 55, 56–66.

52 Shin-Etsu, Characteristic properties of silicone rubber compounds. Shin-Etsu Chemical Co., Ltd., Tokyo, Japan, **2012**.

53 A. Colas, Silicones: preparation, properties and performance. Nova Science, Seneffe, Belgium, **2000**.

54 R. D. Shupe, Chemical stability of polyacrylamide polymers. in *Society of Petroleum Engineers of AIME*, Dallas, U.S., **1981**, pp. 1513–1529.

55 S. H. Yang and L. E. Treiber, Chemical stability of polyacrylamide under simulated field conditions. in *SPE Annual Technical Conference and Exhibition*, Society of Petroleum Engineers, Las Vegas, U.S., **1985**, pp. 1–12.

56 A. Colas, Inorganic polymers. Nova Science, Seneffe, Belgium, **1994**, vol. 38.

57 A. Mata, A. J. Fleischman, and S. Roy, Characterization of polydimethylsiloxane (PDMS) properties for biomedical micro/nanosystems. *Biomedical Microdevices*, **2005**, 7, 281–93.

58 J. Lee, J. Kim, H. Kim, Y. M. Bae, K. H. Lee, and H. J. Cho, Effect of thermal treatment on the chemical resistance of polydimethylsiloxane for microfluidic devices. *Journal of Micromechanics and Microengineering*, **2013**, 23, 035007.

59 I. Klammer, M. C. Hofmann, A. Buchenauer, W. Mokwa, and U. Schnakenberg, Long-term stability of PDMS-based microfluidic systems used for biocatalytic reactions. *Journal of Micromechanics and Microengineering*, **2006**, 16, 2425–2428.

60 S. Kakadjian, O. Rauseo, and F. Mejias, Dynamic rheology as a method for quantify gel strength of water shutoff systems. in *SPE international Symposium on Oilfield chemistry*, Houston, U.S, **1999**, pp. 1–11.

61 A. G. Bejenariu, L. Yu, and A. L. Skov, Low moduli elastomers with low viscous dissipation. *Soft Matter*, **2012**, 8, 3917–3923.

62 A. Mennella and L. Chiappa, Candidate and chemical selection rules for water shutoff polymer treatments. in *SPE European Formation Damage Conference*, Hague, Netherlands, **1999**, pp. 1–10.

63 C. Yao, G. Lei, L. M. Cathles, and T. S. Steenhuis, Pore-scale investigation of micron-size polyacrylamide elastic microspheres (MPEMs) transport and retention in saturated porous media. *Environmental Science & Technology*, **2014**, 48, 5329–5335.

64 J. Hinze, Fundamentals of the hydrodynamic mechanism of splitting in dispersion processes. *AIChE Journal*, **1955**, 1, 289–295.

65 R. A. Ghotli, A. Raman, S. Ibrahim, and S. Baroutian, Liquid-liquid mixing in stirred vessels: a review. *Chemical Engineering Communications*, **2013**, 200, 595–627.

66 R. V Calabrese, T. K. Chang, and P. T. Dang, Drop breakup in turbulent stirred-tank contactors. Part I: effect of dispersed-phase viscosity. *AIChE Journal*, **1986**, 32, 657–666.

67 H. T. Chen and S. Middleman, Drop size distribution in agitated liquid-liquid systems. *AIChE Journal*, **1967**, 13, 989–995.

68 D. Ramkrishna, Population balances: theory and applications to particulate systems in engineering. Academic Press, Minnesota, U.S., **2000**.

69 J. Boxall, C. Koh, E. D. Sloan, A. K. Sum, and D. T. Wu, Droplet size scaling of water-in-oil emulsions under turbulent flow. *Langmuir*, **2012**, 28, 104–110.

70 J. A. Boxall, C. A. Koh, E. D. Sloan, A. K. Sum, and D. T. Wu, Measurement and calibration of droplet size distributions in water-in-oil emulsions by particle video microscope and a focused beam reflectance method. *Industrial & Engineering Chemistry Research*, **2010**, 49, 1412–1418.

71 C. Liu, M. Li, C. Liang, and W. Wang, Measurement and analysis of bimodal drop size distribution in a rotor-stator homogenizer. *Chemical Engineering Science*, **2013**, 102, 622–631.

72 A. EL-Hamouz, Drop size distribution in a standard twin-impeller batch mixer at high dispersed-phase volume fraction. *Chemical Engineering & Technology*, **2009**, 32, 1203–1210.

73 K. Binder and D. W. Heermann, Monte Carlo simulation in statistical physics: an introduction. Springer, Mainz, Germany, **2010**.

74 P. M. Bapat, L. L. Tavlarides, and G. W. Smith, Monte Carlo simulation of mass transfer in liquid-liquid dispersions. *Chemical Engineering Science*, **1982**, 38, 2003–2013.

75 D. Mondal, A. Datta, and A. Sarkar, Prediction of drop size distribution in a spray from a pressure swirl atomizer using maximum entropy formalism. *Proceedings of the Institution of Mechanical Engineers, Part C: Journal of Mechanical Engineering Science*, **2003**, 217, 831–838.

76 J. Cousin, S. J. Yoon, and C. Dumouchel, Coupling of classical linear theory and maximum entropy formalism for prediction of drop size distribution in sprays. *Atomization and Sprays*, **1996**, 6, 601–622.

77 Y. Mlynek and W. Resnick, Drop sizes in an agitated liquid-liquid system. *AIChE Journal*, **1972**, 18, 122–127.

78 J. S. Lagisetty, P. K. Das, R. Kumar, and K. S. Gandhi, Breakage of viscous and non-newtonian in stirred drops. *Chemical Engineering Science*, **1986**, 41, 65–72.

79 R. D. Cohen, Steady-state cluster size distribution in stirred suspensions. *Journal of the Chemical Society, Faraday Transactions*, **1990**, 86, 2133–2138.

80 R. D. Cohen, Evolution of the cluster-size distribution in stirred suspensions. *Journal of the Chemical Society, Faraday Transactions*, **1991**, 87, 1163–1168.

81 M. Kostoglou and A. J. Karabelas, On the self-similarity of the aggregation–fragmentation equilibrium particle size distribution. *Journal of Aerosol Science*, **1999**, 30, 157–162.

82 S. Maaß, N. Paul, and M. Kraume, Influence of the dispersed phase fraction on experimental and predicted drop size distributions in breakage dominated stirred systems. *Chemical Engineering Science*, **2012**, 76, 140–153.

83 S. Kumar and D. Ramkrishna, On the solution of population balance equations by discretization—III. Nucleation, growth and aggregation of particles. *Chemical Engineering Science*, **1997**, 52, 4659–4679.

84 M. Attarakih and H. J. Bartb, On the constrained maximum entropy solution of the population balance equation. in *Proceedings of the 22nd European Symposium on Computer Aided Process Engineering*, London, UK, **2012**, pp. 1–5.

85 A. Huan, Statistical mechanics. Royal Society of Chemistry, Cambridge,UK, **1975**, vol. 2.

86 P. Harremoës, Binomial and poisson distributions as maximum entropy distributions. *Information Theory, IEEE Transactions*, **2001**, 47, 2039–2041.

87 C. E. Shannon and W. Weaver, The mathematical theory of communication. University of Illinois Press, Urbana, U.S., **1964**.

88 B. Osbaeck and V. Johansen, Particle size distribution and rate of strength development of Portland cement. *Journal of the American Ceramic Society*, **1989**, 72, 197–201.

89 C. Y. Wang and R. V Calabrese, Drop breakup in turbulent stirred-tank contactors. Part II: relative influence of viscosity and interfacial tension. *AIChE Journal*, **1986**, 32, 667–676.

90 N. Vankova, S. Tcholakova, N. D. Denkov, I. B. Ivanov, V. D. Vulchev, and T. Danner, Emulsification in turbulent flow 1. Mean and maximum drop diameters in inertial and viscous regimes. *Journal of Colloid and Interface Science*, **2007**, 312, 363–380.

91 N. J. Alvarez, L. M. Walker, and S. L. Anna, A non-gradient based algorithm for the determination of surface tension from a pendant drop: application to low Bond number drop shapes. *Journal of Colloid and Interface Science*, **2009**, 333, 557–562.

92 T. Ma, Y. Huang, J. Yang, J. He, and L. Zhao, Preparation of spherical zirconia powder in microemulsion system and its densification behavior. *Materials & Design*, **2004**, 25, 515–519.

93 C. Dumouchel, The maximum entropy formalism and the prediction of liquid spray drop size distribution. *Entropy*, **2009**, 11, 713–747.

94 M. Gaborieau, L. Nebhani, R. Graf, L. Barner, and C. Barner-Kowollik, Accessing quantitative degrees of functionalization on solid substrates via solid-state NMR spectroscopy. *Macromolecules*, **2010**, 43, 3868–3875.

95 H. So, A. S. Fawcett, H. Sheardown, and M. A. Brook, Surface-active copolymer formation stabilizes PEG droplets and bubbles in silicone foams. *Journal of Colloid and Interface Science*, **2013**, 390, 121–128.

96 J. Downey, R. Frank, W. Li, and H. Stöver, Growth mechanism of poly (divinylbenzene) microspheres in precipitation polymerization. *Macromolecules*, **1999**, 32, 2838–2844.

97 Y. Yamamoto, M. Okubo, and Y. Iwasaki, Estimation of distribution of vinyl groups in micron-sized monodisperse polymer microspheres by bromine titration method. *Colloid & Polymer Science*, **1991**, 269, 1126–1132.

98 F. B. Madsen, I. Dimitrov, A. E. Daugaard, S. Hvilsted, and A. L. Skov, Novel cross-linkers for PDMS networks for controlled and well distributed grafting of functionalities by click chemistry. *Polymer Chemistry*, **2013**, 4, 1700–1707.

99 F. B. Madsen, A. E. Daugaard, C. Fleury, S. Hvilsted, and A. L. Skov, Visualisation and characterisation of heterogeneous bimodal PDMS networks. *RSC Advances*, **2014**, 4, 6939–6945.

100 X. Hu, J. Zhou, N. Zhang, H. Tan, and C. Gao, Preparation and properties of an injectable scaffold of poly(lactic-co-glycolic acid) microparticles/chitosan hydrogel. *Journal of the Mechanical Behavior of Biomedical Materials*, **2008**, 1, 352–359.

101 L. J. Fetters, D. J. Lohse, S. T. Milner, and W. W. Graessley, Packing length influence in linear polymer melts on the entanglement, critical, and reptation molecular weights. *Macromolecules*, **1999**, 32, 6847–6851.

102 L. Gonzalez, K. Malgorzata, B. Ma, L. Li, H. J. Hansen, S. Hvilsted, and A. L. Skov, Preparation and characterization of silicone liquid core/polymer shell microcapsules by using internal phase separation as methodology. *Macromolecular Materials and Engineering*, **2014**, 299, 1259–1267.

103 B. Ma, J. H. Hansen, S. Hvilsted, and A. L. Skov, Control of PDMS crosslinking by encapsulationg a hydride crosslinker in a PMMA microcapsule. *RSC advances*, **2014**, 4, 47505–47512.

104 E. Westhaus and P. B. Messersmith, Triggered release of calcium from lipid vesicles: a bioinspired strategy for rapid gelation of polysaccharide and protein hydrogels. *Biomaterials*, **2001**, 22, 453–462.

105 T. J. Sanborn, P. B. Messersmith, and A. E. Barron, In situ crosslinking of a biomimetic peptide-PEG hydrogel via thermally triggered activation of factor XIII. *Biomaterials*, **2002**, 23, 2703–2710.

106 L. González, B. Ma, L. Li, J. H. Hansen, S. Hvilsted, and A. L. Skov, Encapsulated PDMS microspheres with reactive handles. *Macromolecular Materials and Engineering*, **2014**, 299, 729–738.

107 S. M. G. Frankær, M. K. Jensen, A. G. Bejenariu, and A. L. Skov, Investigation of the properties of fully reacted unstoichiometric polydimethylsiloxane networks and their extracted network fractions. *Rheologica Acta*, **2012**, 51, 559–567.

108 E. Denkbaş, E. Kiliçay, C. Birlikseven, and E. Ozturk, Magnetic chitosan microspheres: preparation and characterization. *Reactive and Functional Polymers*, **2002**, 50, 225–232.

109 L. Marcus, Organic Reactions in Water. Blackwell, Oxford, UK, **2007**.

110 T. Gisler and D. A. Weitz, Scaling of the microrheology of semidilute F-actin solutions. *Physical Review Letters*, **1999**, 82, 1606–1609.

111 V. Trappe and D. Weitz, Scaling of the viscoelasticity of weakly attractive particles. *Physical review letters*, **2000**, 85, 449–452.

112 C. A. Bonino, J. E. Samorezov, O. Jeon, E. Alsberg, and S. A. Khan, Real-time in situ rheology of alginate hydrogel photocrosslinking. *Soft Matter*, **2011**, 7, 11510–11517.

113 F. Chambon and H. H. Winter, Linear viscoelasticity at the gel point of a crosslinking PDMS with imbalanced stoichiometry. *Journal of Rheology*, **1987**, 31, 683–697.

114 R. A. Mrozek, P. J. Cole, K. J. Otim, K. R. Shull, and J. L. Lenhart, Influence of solvent size on the mechanical properties and rheology of polydimethylsiloxane-based polymeric gels. *Polymer*, **2011**, 52, 3422–3430.

115 L. Valette, J. P. Pascault, and B. Magny, Rheological properties of (meth)acrylic cross-linked polymer microparticles, 1. comparison with linear polymers in bulk and in non-reactive solvents. *Macromolecular Materials and Engineering*, **2002**, 287, 41–51.

116 A. P. R. Johnston, G. K. Such, and F. Caruso, Triggering release of encapsulated cargo. *Angewandte Chemie (International ed. in English)*, **2010**, 49, 2664–2666.

117 Y. Deyrail, N. Zydowicz, and P. Cassagnau, Polymer crosslinking controlled by release of catalyst encapsulated in polycarbonate micro-spheres. *Polymer*, **2004**, 45, 6123–6131.

118 A. P. Esser-Kahn, S. A. Odom, N. R. Sottos, S. R. White, and J. S. Moore, Triggered release from polymer capsules. *Macromolecules*, **2011**, 44, 5539–5553.

119 S. H. Cho, S. R. White, and P. V. Braun, Self-healing polymer coatings. *Advanced Materials*, **2009**, 21, 645–649.

120 C. L. Mangun, C. Mader, N. R. Sottos, and S. R. White, Self-healing of a high temperature cured epoxy using poly(dimethylsiloxane) chemistry. *Polymer*, **2010**, 51, 4063–4068.

121 B. Peña, C. Panisello, G. Aresté, R. Garcia-Valls, and T. Gumí, Preparation and characterization of polysulfone microcapsules for perfume release. *Chemical Engineering Journal*, **2012**, 179, 394–403.

122 C. Panisello and R. Garcia-Valls, Polysulfone/vanillin microcapsules production based on vapor-induced phase inversion precipitation. *Industrial & Engineering Chemistry Research*, **2012**, 51, 15509–15516.

123 L. Chu, S. Park, T. Yamaguchi, and S. Nakao, Preparation of micron-sized monodispersed thermoresponsive core-shell microcapsules. *Langmuir*, **2002**, 18, 1856–1864.

124 L. Chu, S. Park, T. Yamaguchi, and S. Nakao, Preparation of thermo-responsive core-shell microcapsules with a porous membrane and poly (N-isopropylacrylamide) gates. *Journal of Membrane Science*, **2001**, 192, 27–39.

125 U. Holzgrabe, R. Deubner, C. Schollmayer, and B. Waibel, Quantitative NMR spectroscopy-applications in drug analysis. *Journal of Pharmaceutical and Biomedical Analysis*, **2005**, 38, 806–812.

126 A. H. Lefebvre, Atomization and sprays. Hemisphere publishing corporation, West lafayette, U.S., **1989**.

127 E. Herrero, E. Valle, and M. Galan, Development of a new technology for the production of microcapsules based in atomization processes. *Chemical Engineering Journal*, **2006**, 117, 137–142.

128 M. Villar, M. Bibbo, and E. Valles, Influence of pendant chains on mechanical properties of model poly (dimethylsiloxane) networks. 1. Analysis of the molecular structure of the network. *Macromolecules*, **1996**, 29, 4072–4080.

129 S. Ndoni and O. Kramer, Longest relaxation time of linear polybutadiene chains trapped in rubber networks. *Europhysics Letters*, **1997**, 39, 165–170.

130 M. I. Aranguren, E. Mora, J. V. DeGroot Jr, and C. W. Macosko, Effect of reinforcing fillers on the rheology of polymer melts. *Journal of Rheology*, **1992**, 36, 1165–1182.

131 D. Ciprari, K. Jacob, and R. Tannenbaum, Characterization of polymer nanocomposite interphase and its impact on mechanical properties. *Macromolecules*, **2006**, 39, 6565–6573.

132 L. González, A. L. Skov, and S. Hvilsted, Ionic networks derived from the protonation of dendritic amines with carboxylic acid end-functionalized PEGs. *Journal of Polymer Science Part A: Polymer Chemistry*, **2013**, 51, 1359–1371.

133 L. Ma and M. Men, Method for making man-made rock core target. **2012**, 1–2.

134 R. Seright, Mechanism for gel propagation through fractures. in *SPE Rocky Mountain regional meeting*, Wyoming, U.S., **1999**, pp. 1–9.

135 R. S. Seright, Gel placement in fractured systems. in *SPE Production & Facilities*, Tulsa, U.S., **1995**, pp. 241–248.

136 R. S. Seright and J. Liang, A survey of field applications of gel treatments for water shutoff. in *Latin American/Caribbean Petroleum Engineering Conference*, Buenos, Argentina, **1994**, pp. 221–231.

137 T. Yongqiang, H. Jirui, and L. Chenghui, Water shut off in a horizontal well: lab experiments with starch graft copolymer agent. *Journal of Petroleum Science and Engineering*, **2013**, 108, 230–238.

138 I. Abbasy, J. Vasquez, L. Eoff, and D. Dalrymple, Laboratory evaluation of water swellable materials for fracture shutoff. in *SPE North Africa Technical Conference and Exhibition*, Marrakech, Morocco, **2008**, pp. 1–13.

Symbols and abbreviations

AM	acrylamide
APG	aluminum phosphate gel
DMF	dimethylformamide
DMS-V35	vinyl terminated polydimethylsiloxane
FV	fracture volume
HMS-301	8-functional hydride crosslinker
HTV	high temperature vulcanizing
MCR-H21	monofunctional hydride
NMR	nuclear magnetic resonance
PAM	polyacrylamide
PDMS	polydimethylsiloxane
PMMA	Poly (methyl methacrylate)
PSU	polysulfone
PV	pore volume
PVA	polyvinyl alcohol
RTV	room temperature vulcanizing
SDS	sodium dodecyl sulphate
SEM	scanning electron microscope
TGA	thermogravimetric analysis
bar	atmospheric air pressure (1bar=10^5Pa)
mD	millidarcy
ppm	parts per million
rpm	rotations per minute
Δp	pressure difference
A	cross-sectional area of core
A_i	surface area of PDMS microsphere with diameter of di
A_{PM}	surface area of PDMS microsphere
$c_{vinyl}(surface)$	surface vinyl concentration by surface area
$c_{vinyl}(wt)$	vinyl concentration of PDMS microsphere by weight
D	impeller diameter
D_{20}	mean surface diameter
D_{30}	mean volumetric diameter
D_{32}	Sauter mean diameter
d_c	diameter of core
d_f	diameter of fracture
d_i	particle diameter
d_{min}	primary particle size
$f(D)$	normal distribution
$f_{HMS-301}$	functionality of HMS-301 hydride crosslinker
f_i	volume frequency of PDMS microsphere with

	diameter of d_i
$f_n(D_p)$	number-based particle size distribution
f_{PDMS}	functionality of PDMS
F_{rrw}	water residual resistance factor
$f_v(D_p)$	volume-based particle size distribution
f_{V35}	functionality of V35
G'	storage modulus
$G'(0)$	initial storage modulus
$G'(terminal)$	terminal storage modulus
$G'(terminal)/G'(0)$	normalized terminal storage modulus
G''	loss modulus
k_B	Boltzmann constant
k_c	water permeability of synthetic core
k_f	water permeability of fractured core
k_h	water permeability of treated core
l_c	length of core
l_f	length of fracture
m_1,m_2	mass of PDMS microsphere before and after swelling in heptane
m_3,m_4	mass of PDMS microsphere before and after titration
m_A, m_B	mass of Batch A and Batch B in Sylgard 184
$m_{HMS-301}$	mass of HMS-301 hydride crosslinker
$M_{HMS-301}$	molecular weight of HMS-301 hydride crosslinker
$m_{hydride}$	mass of monofunctional hydride
$M_{hydride}$	molecular weight of monofunctional hydride
M_{PDMS}	molecular weight of PDMS
m_{PM}	mass of PDMS microspheres
m_{tot}	mass of vinyl functional PDMS and curing agent
m_{V35}	mass of V35
M_{V35}	molecular weight of V35
N	number of particles
N_0	number of primary particles
N_i	number of particles with diameter of d_i
n_i	number of PDMS microsphere
$n^{\#}_{v,tot}$	mol number of vinyl groups after crosslinking reaction
$n_{v,tot}$	total mole number of vinyl groups before reaction
n_{vA}, n_{vB}	initial mole number of vinyl groups from Batch A and Batch B in Sylgard 184
$n_{hydride}$	mol number of monofunctional hydride
n_{vinyl}	mol number of vinyl groups on PDMS microspheres
$p(i)$	Poisson distribution
q	fitting parameter in Rosin-Rammler distribution
Q	flow rate
Q_i	cumulative volume fraction for particle smaller than d_i
r	stoichiometric imbalance

S	entropy function
S'	Shannon's entropy function
T_g	glass transition temperature
V_i	viscosity number or volume of PDMS microsphere with diameter of d_i
V_{PM}	volume of PDMS microsphere
We	Weber number
$w_{sol\%}$	soluble fraction
Y	size parameter in Rosin-Rammler distribution
Y_{PM}	yield of PDMS microspheres
Z	characteristic parameter of N_0
Γ	Gamma function
λ_1, λ_2, a_0, a_1	Lagrange multiplier
μ	viscosity of water
μ_d	viscosity of continuous phase
ρ	density
ρ_{PM}	density of PDMS microsphere
σ	surface tension
σ_d	standard deviation
φ	volume fraction or porosity of core sample
ω	rotational speed
Ω	degeneracy

Publication list

1. **B. Ma**, J. H. Hansen, S. Hvilsted, and A. L. Skov, Control of PDMS crosslinking by encapsulationg a hydride crosslinker in a PMMA microcapsule.*RSC advances*, **2014**, 4, 47505–47512.

2. **B. Ma**, J. H. Hensen, S. Hvilsted, and A. L. Skov, PDMS microspheres with PMMA coating: modeling, preparation and characterization.*Canadian Journal of Chemical Engineering*, **2014**. Submitted manuscript.

3. L. González, **B. Ma**, L. Li, J. H. Hansen, S. Hvilsted, and A. L. Skov, Encapsulated PDMS microspheres with reactive handles.*Macromolecular Materials and Engineering*, **2014**, 299, 729–738.

4. L. Gonzalez, K. Malgorzata, **B. Ma**, L. Li, H. J. Hansen, S. Hvilsted, and A. L. Skov, Preparation and characterization of silicone liquid core/polymer shell microcapsules by using internal phase separation as methodology.*Macromolecular Materials and Engineering*, **2014**, 299, 1259–1267.

Copyright

RSC | Advancing the Chemical Sciences

Royal Society of Chemistry
Thomas Graham House
Science Park
Milton Road
Cambridge
CB4 0WF

Tel: +44 (0)1223 420 066
Fax: +44 (0)1223 423 623
Email: contracts-copyright@rsc.org

www.rsc.org

Acknowledgements to be used by RSC authors

Authors of RSC books and journal articles can reproduce material (for example a figure) from the RSC publication in a non-RSC publication, including theses, without formally requesting permission providing that the correct acknowledgement is given to the RSC publication. This permission extends to reproduction of large portions of text or the whole article or book chapter when being reproduced in a thesis.

The acknowledgement to be used depends on the RSC publication in which the material was published and the form of the acknowledgements is as follows:

- For material being reproduced from an article in *New Journal of Chemistry* the acknowledgement should be in the form:
    - [Original citation] - Reproduced by permission of The Royal Society of Chemistry (RSC) on behalf of the Centre National de la Recherche Scientifique (CNRS) and the RSC
- For material being reproduced from an article *Photochemical & Photobiological Sciences* the acknowledgement should be in the form:
    - [Original citation] - Reproduced by permission of The Royal Society of Chemistry (RSC) on behalf of the European Society for Photobiology, the European Photochemistry Association, and RSC
- For material being reproduced from an article in *Physical Chemistry Chemical Physics* the acknowledgement should be in the form:
    - [Original citation] - Reproduced by permission of the PCCP Owner Societies
- For material reproduced from books and any other journal the acknowledgement should be in the form:
    - [Original citation] - Reproduced by permission of The Royal Society of Chemistry

The acknowledgement should also include a hyperlink to the article on the RSC website.

The form of the acknowledgement is also specified in the RSC agreement/licence signed by the corresponding author.

Except in cases of republication in a thesis, this express permission does not cover the reproduction of large portions of text from the RSC publication or reproduction of the whole article or book chapter.

A publisher of a non-RSC publication can use this document as proof that permission is granted to use the material in the non-RSC publication.

VAT Registration Number: GB 342 1764 71 Registered Charity Number: 207890

Appendix I

PDMS microspheres with PMMA coating: modeling, preparation and characterization

The Canadian Journal of Chemical Engineering (2014)

The Canadian Journal of Chemical Engineering

PDMS microspheres with PMMA coating: modeling, preparation and characterization

Journal:	*The Canadian Journal of Chemical Engineering*
Manuscript ID:	CJCE-14-0694
Wiley - Manuscript type:	Article
Date Submitted by the Author:	24-Aug-2014
Complete List of Authors:	Ma, Baoguang; DTU, Chemical Engineering Hansen, Jens; Maersk, Maersk Oil Research and Technology Centre Hvilsted, Søren; DTU, Chemical Engineering Skov, Anne; DTU, Chemical Engineering
Keywords:	Materials processing/fabrication < Materials science and technology, Polymers, rubber and plastics, Fluid-particle dynamics < Fluid mechanics

Highlights:

1. Polydimethylsiloxane microspheres with excess vinyl groups have been prepared

2. The Hinze-Kolmogorov theory has been shown applicable for the reactive system

3. Efficient encapsulation of polydimethylsiloxane microspheres was obtained

PDMS microspheres with PMMA coating: modeling, preparation and characterization

Baoguang Ma[‡], *Jens Henrik Hansen*[§], *Søren Hvilsted*[‡], *Anne Ladegaard Skov*[‡*]

[‡] Danish Polymer Centre, Department of Chemical and Biochemical Engineering & Center for Energy Resources Engineering, DTU, DK-2800 Kgs. Lyngby, Denmark

[§]Maersk Oil Research and Technology Centre, Education City, P.O. Box 210112, Doha, Qatar

Abstract:

Polydimethylsiloxane (PDMS) microspheres are prepared by mixing homogeneous dispersions of vinyl-functional PDMS and curing agent with mechanical stirring in a series of aqueous solutions, and curing at 80°C for 2h. In order to verify the experimental diameter and size distribution of the PDMS microspheres, the Hinze-Kolmogorov theory is applied to predict the mean diameter, and population balance model as well as the maximum entropy formalism are used to describe the size distribution. Good agreement is found between experiments and theories. Furthermore, vinyl functional PDMS microspheres were coated with PMMA by spin coating with different concentrations of PMMA solutions. The quality of the resulting PMMA shell is investigated by rheological measurements at 50°C with a time-sweep procedure. The results strongly imply that PMMA-coated PDMS microspheres react much slower than the uncoated ones, and that the PMMA shell significantly hinders the reaction between the PDMS microsphere and cross-linker. Thus the thin PMMA shells are very efficient in protecting the reactive PDMS microsphere.

Key words: PDMS microspheres, silicone, modeling, coating

Highlights:

1. Polydimethylsiloxane microspheres with excess vinyl groups have been prepared
2. The Hinze-Kolmogorov theory has been shown applicable for the reactive system
3. Efficient encapsulation of polydimethylsiloxane microspheres was obtained

1. Introduction

Polydimethylsiloxane (PDMS) has attracted much attention due to its excellent properties, such as water repellency, low surface energy and non-toxity[1]. Crosslinked PDMS microspheres not only possess the excellent properties of PDMS, but also has the potential for versatile applications, such as drug delivery[2], enzyme immobilization[3] and environmental technology[4]. Due to the excellent properties and the attractive potentials applications, the preparation of PDMS microsphere has been investigated in several studies[5]-[7]. However, most of the studies focus on producing the monodisperse functional PDMS microspheres of the order of milligram by using microfluidic systems. The low productivity of PDMS microspheres from the microfluidic system constrains the potential applications of the PDMS microsphere in industrial scale. Hence, it will be of considerable interest to prepare large quantities of PDMS microspheres in a facile way[8]. In this study, the preparation of PDMS microspheres by emulsion technique will be demonstrated from emulsions with varying concentrations of surfactant solutions, and the resulting particle distribution of the PDMS microspheres will be further investigated.

In the preparation of the PDMS microspheres, the process involves with the dispersion of the PDMS in a turbulent system. A vast amount of theoretical and experimental works can be found concerning the mean diameter and size distribution of the droplets in turbulent systems[9]-[11]. However, the droplets in the previous studies are obtained from physical mixtures of two

immiscible liquids, which allow for no further reaction, meaning that the droplets can not be separated from the emulsion. In our study, we prepare crosslinked PDMS microspheres which can be separated and used in other applications. In order to interpret the mean diameter and the size distribution of the PDMS microspheres, the experimental results are compared with the theoretical mean diameter predicted by the Hinze-Kolmogorov theory and the size distribution described by the population balance model as well as the maximum entropy formalism.

By changing the mixing ratio between vinyl terminated PDMS and hydride crosslinker in the preparation process, the resulting PDMS microsphere can be functionalized with vinyl groups, which allow for further crosslinking reaction at the presence of additional hydride crosslinker. Thus, the protection of the active vinyl groups by encapsulation, which is similar to the encapsulation of hydride crosslinker in PMMA[12],[13], has been achieved by solvent evaporation technique. Similarly, the reactive PDMS microsphere will be encapsulated by spin coating technique and time sweep rheological measurements are performed to investigate the quality of the PMMA coating.

2. Theory

2.1 Hinze-Kolmogorov theory

Many industrial processes involve liquid-liquid dispersion in stirred vessels and the knowledge of the resulting drop size distribution characteristic with changes of external mechanical energy input. Much work has been done to investigate the mean diameter and the size distribution in turbulent liquid-liquid dispersions subjected to mechanical stirring, and most of these investigate the concept of turbulent energy cascades to predict the mean diameter of the droplets, referring to the Hinze-Kolmogorov theory[14]. This theory presents a decreasing power law for the dependence of the diameter on the average turbulent energy dissipation. Applying this approach, similar equations have been derived for systems where viscous energy dissipation occurs[9],[10],[15]–[17]. A recent version of the resulting formula is:

$$\frac{D_{32}}{D} = k \cdot We^{-0.6}(1 + a \cdot Vi(\frac{D_{32}}{D})^{\frac{1}{3}})^{0.6}(1 + b \cdot \phi) \quad (1)$$

where We is the Weber number given by eq.(2) and Vi is the viscosity number given by eq. (3)

$$We = \frac{\rho \cdot \omega^2 \cdot D^3}{\sigma} \quad (2)$$

$$Vi = \frac{\mu_d \cdot \omega \cdot D}{\sigma} \quad (3)$$

where D_{32} is the Sauter mean diameter, D is impeller diameter, k is an empirical constant, a is a proportionality factor, b is an empirical system-dependent constant, ρ is the density of the continuous phase, φ is the volume fraction of the dispersed phase, μ_d is the viscosity of the continuous phases, ω is the rotational speed of the impeller and σ is the surface tension of the aqueous solution.

2.2 Size distribution in turbulent systems

The particle size distribution has been predicted by many methods in turbulent systems. Amongst the methods, population balance model, Monte Carlo simulation and maximum entropy formalism are most commonly used. The population balance model deals with systems containing particles in a continuous phase. In this model, the basic assumption is that there exists a number density of particles in a continuous phase[18]. By coupling conservation equations with this assumption, the population balance model is used to depict the number density and the size distribution of particles at given conditions. The population balance model has been applied in various studies, in which the number density and the particle distribution play an important role[19]. For instance, this model has successfully predicted the size distribution of droplets in water-in-oil systems[20],[21] and oil-in-water systems[22],[23]. As the population balance model is concerned about the particle size distribution on a macroscopic level, Monte Carlo simulation has also been used for describing the particle size distribution by means of statistics[24]. Compared to the other methods, the Monte Carlo simulation

describes the particles with various degrees of freedom, such as temperature, pressure and density. Also, the simulation can provide a realistic way to understand a system in a dynamic way. For instance, Monte Carlo simulation has been used to predict the particle size distribution by combining the behavior of individual particle in the system[25]. While the Monte Carlo simulation describes the particle size distribution in a dynamic way, maximum entropy formalism depicts the particle size distribution in a thermodynamic way[26]. The maximum entropy formalism suggests the least biased solution in the prediction of the particle size distribution, given that the statistical entropy in the system is maximized. For instance, the drop size distribution in a spraying process has been successfully predicted by this formalism[27]. In our study, the population balance model and the maximum entropy formalism will be used to describe the size distribution of the PDMS microspheres.

2.2.1 Population balance model

Consider a suspension that contains a large number of clusters, each consisting of a number of primary particles. Due to the high speed mechanical stirring in the vessel, there is a great possibility that the clusters will collide with each other and form larger clusters in the suspension; but it is also possible that the clusters will break and divide into smaller clusters or primary particles due to the mechanical stirring until a dynamic equilibrium is established[15],[28].

In the investigated system, the effect of the mechanical stirring is dominating such that other effects such as Brownian motion, surface interactions and slow chemical reactions are overwhelmed[29].

Let the number of clusters in the system be N, the number of primary particles be N_0 and the number of clusters with size equal to i be N_i. Then we can write:

$$N = \sum_{i=1} N_i$$
$$N_0 = \sum_{i=1} i \cdot N_i \quad (4)$$

where i is the number of primary particles in a cluster. By assuming that the fragmentation and the aggregation process of the clusters occur randomly and independently, the particle size distribution is determined solely by the stochastic combination of the primary particles[11],[29]. When the dynamic equilibrium has been achieved, the particle size distribution can be predicted by using various methods or assumptions, such as self-similarity[30], breakage-domination[31], aggregation-domination[32] or maximum entropy[33]. Here, we use the maximum entropy assumption to depict the particle size distribution in the dynamic equilibrium in our system. From Boltzmann's equation, S can be expressed as:

$$S = k_B \ln \Omega \quad (5)$$

where k_B is the Boltzmann constant and Ω is the degeneracy or the total number of ways in which the particles can be distributed into all clusters. According to the statistical mechanics[34], Ω can be expressed as:

$$\Omega(N_1, N_2, N_3 \ldots) = \frac{N_0!}{\prod_{i=1}^{N_0} N_i![i!]^{N_i}} \quad (6)$$

Since the value of Ω is constrained by (4) and (6), the Lagrange multipliers λ_1 and λ_2 are introduced in order to obtain the maximum value of Ω.

$$\frac{\partial}{\partial N_i}(\ln \Omega + \lambda_1 N_0 + \lambda_2 N) = 0 \quad (7)$$

In an isotropic turbulent system, where all particles are primary particles or a single large cluster in the solution, Ω is minimized. When the number of particles is suitable, Ω becomes maximized. By solving eqs. (4)-(7), we obtain the Poisson type size-distribution probability function[35]:

$$p(i) = \exp(-Z)\frac{Z^i}{i!} \tag{8}$$

where Z is the characteristic parameter of N_0, and it satisfies the following equation:

$$N_0 = Z \exp Z \tag{9}$$

The primary particle size is denoted d_{min} to describe the relation between drop size distribution and cluster size using the mathematical definition of D_{32}:[11],[29]

$$\frac{\sum_{i=1}^{N_0} i \cdot p(i)}{\sum_{i=1}^{N_0} i^{2/3} \cdot p(i)} = \frac{D_{32}}{d_{\min}} \tag{10}$$

2.2.2 Maximum entropy formalism

In the prediction of the particle size distribution in a turbulent system, an alternative way is to use Shannon's entropy function[36]. The relation between the Shannon entropy S' and the particle diameter D_p can be expressed as:

$$S' = -k\int_0^\infty f_n(D_p)\ln[f_n(D_p)]dD_p \tag{11}$$

where $f_n(D_p)$ is the number-based particle size distribution. Here, we assume that the entropy function S' is maximized in the dynamic equilibrium in our system. In order to obtain the maximum value of the entropy function S', the relation between the mean diameters D_{q0} and the particle diameter D_p is used as constraint[27]:

$$\int_0^\infty f_n(D_p)D_p^q dD_p = D_{q0}^q \tag{12}$$

According to the definition of $f_n(D_p)$, another constraint exists:

$$\int_0^\infty f_n(D_p)dD_p = 1 \tag{13}$$

By solving eqs. (11), (12) and (13), we get:

$$f_n(D_p) = \exp(-a_0 - a_1 D_p^q) \tag{14}$$

where a_0 and a_1 are Lagrange multipliers, which satisfy the following equations:

$$\exp(a_0) = q^{\frac{1-q}{q}} D_{q0} \Gamma(\frac{1}{q}) \tag{15}$$

$$a_1 = \frac{1}{qD_{q0}^q} \tag{16}$$

where Γ is the Gamma function. In order to compare the experimental data with the simulation data, $f_v(D_p)$ is introduced as the volume based distribution. The relation between the $f_v(D_p)$ and the $f_n(D_p)$ is

$$f_v(D_p) = \frac{D_p^3}{D_{30}^3} f_n(D_p) \tag{17}$$

where D_{30} is the mean volumetric diameter. Therefore, we can obtain the final expression for volume-based distribution by assuming that the Shannon's entropy function is maximized:

$$f_v(D_p) = q^{\frac{q-4}{q}} \frac{D_p^3}{D_{q0}^4 \Gamma(4/q)} \exp(-\frac{D_q}{qD_{q0}^q}) \tag{18}$$

From the Hinze-Kolmogorov theory, we obtain the Sauter mean diameter D_{32}. From the definition of D_{32}, we have:

$$D_{32} = \frac{D_{30}^3}{D_{20}^2} \tag{19}$$

where D_{20} is the mean surface diameter. Then we can obtain the relation between the D_{32} and the D_{q0} by combining eq. (12) and (19):

$$D_{32} = D_{q0} \cdot \sqrt[q]{q} \frac{\Gamma(4/q)}{\Gamma(3/q)} \tag{20}$$

Here, the parameter q is related to the width of the distribution and equals the distribution parameter of the Rosin-Rammler distribution[27]. In order to estimate the value of q, the Rosin-Rammler distribution is introduced:

$$1-Q_i = \exp(-\frac{d_i}{Y})^q \quad (21)$$

where Q_i is cumulative volume fraction for particle smaller than d_i. Y is a size parameter, which measures the particle size below 63.2% of total volume[26],[37]. By plotting $\ln(1\text{-}Qi)^{-1}$ versus d_i/Y , we can obtain the value of q.

2.2.3 Normal distribution

In order to compare with the size distribution predicted by the population balance model and the maximum entropy formalism, normal distribution is introduced. Several studies [10],[38],[39] show that the normal distribution fits the experimental size distribution in the turbulent system well:

$$f(D) = \frac{1}{\sqrt{2\pi}\sigma_d}\exp[-\frac{(D-D_{32})^2}{2\sigma_d^{\,2}}] \quad (22)$$

where $f(D)$ is the particle size distribution, D_{32} is the mean diameter and σ_d is the standard deviation.

3. Materials and methods

3.1 Materials

Sylgard 184 consisting of vinyl functional PDMS (Batch A) and curing agent (Batch B) (RTV silicone elastomer, Dow Corning), 25-35% (methylhydrosiloxane) with 65%-70% (dimethylsiloxane) copolymer (HMS-301) (Mw=2,000g/mol 8-functional crosslinker, Gelest), platinum-cyclovinylmethylsiloxane complex (SIP6832.2 catalyst) (Gelest), polyvinyl alcohol (PVA) (Mw=22,000g/mol, Fluka), poly (methyl methacrylate) (PMMA) (Mw=15,000g/mol, Aldrich), dimethyl fomamide (DMF) (>99%, Aldrich), sodium dodecyl sulphate (SDS) (>99%, BDH), non-reactive silicone oil (20cSt, Dow Corning), deionized water

3.2 Experimental procedure

PDMS microsphere preparation: 8g Sylgard 184 vinyl functional PDMS and appropriate amount of curing agent were mixed in a polystyrene cup in a ratio of 10:1 or 20:1 at 1000rpm for 2min to yield a mixture. 7g of this mixture was then poured into a conical flask with 200g of aqueous surfactant solution. The choice of geometry is discussed in Supplementary Info 1. A 2.0 cm diameter impeller with two inclined blades was used to stir for 2min at 2000rpm to produce an emulsion. After the emulsion was formed, the system was inserted into an oven at 80°C for 2h to cure the PDMS microspheres. The system was then filtered using a vacuum filter and washed with deionized water for several times to remove the residual surfactant. The PDMS microspheres were then dried in an oven at 80°C°C for 2h and weighed to calculate the microsphere yield.

PDMS microsphere coated with PMMA: 0.4g PDMS microsphere with a ratio of vinyl functional PDMS to curing of 20:1 were added to a watch glass (radius 22mm). PMMA was dissolved in DMF to yield a solution of 10%, 20%, 50% (by weight), which was dropped into the watch glass with a syringe. The watch glass was then placed in the spin coater. Spin coating was performed at 5000rpm for 1min, with an acceleration of 1000rpm/s from 0 to 5000rpm. After the coating, the coated PDMS microsphere was inserted into an oven at 80°C to remove the residual DMF.

3.3 Apparatus

PDMS microsphere size distribution was measured by Mastersizer (Malvern, UK) in a jar tester. In this measurement, PDMS microspheres in aqueous solution were pumped through a transparent tubing with an internal diameter of 5mm by a peristaltic pump at a flow rate of 10mL/min and then back to the conical flask. The instrument was equipped with a laser with a wavelength of 633nm, and the size range is 1μm~1000μm in the measurement.

The surface tension was measured by Nelder-Mead simplex method using a Data Physics OCA20 tension meter. The sample was loaded into a syringe mounted to a stepper motor, which was used to control the rate of the advancing and receding drop front. 10μl samples were dispensed at a rate of 2μl/s using a needle with a diameter of 1.67mm. The pendant drop was illuminated from behind by a white-light projector. A CCD camera was used to capture the images for analysis.

The viscosity of PDMS emulsion was measured using an AR-2000 Rheometer (TA Instruments, USA) at room temperature using a conical tank. 100mL PDMS emulsion was tested at shear rates ranging from $100s^{-1}$ to $0.1s^{-1}$.

Spin coating was performed by using Spin150 (SPS coating, Netherland). 0.4g PDMS microspheres on a watch glass were subjected to spin-coating with different concentration PMMA solution in DMF for 1min at 5000rpm.

The thermogravimetric behavior of coated PDMS microsphere was analyzed by using a TGA Q500 (TA Instruments, USA). Typically 20~50mg sample was used. The measurement was made from 30°C to 800°C in nitrogen at a heating rate of 10°C/min.

The rheological behavior of coated and uncoated PDMS microsphere was investigated by using AR-2000 using a time sweep procedure. 0.4g PDMS microspheres were mixed with 0.01g hydride 8-functional crosslinker (HMS-301) and 0.1g non-reactive silicone oil. Measurement were made using a parallel plate geometry consisting of a pair of 25mm plates at 50°C with a strain rate of 2% (within the linear viscoelastic region), while the normal force was around 9N.

4. Modeling

The mean diameter of PDMS microsphere can be calculated from eqs. (1)—(3) with the following parameters:

k is an empirical number equal to 0.100 for the systems with a viscosity ranging from 0.005 to 4 Pa·s[15],[28], a equals to 11.5 for the silicone oil-water system[10],[16], b is an empirical number equal to 4.47 for the system with concentrations between 1.5% and 5%[10],[28]. The values of k, a and b are from the literatures while the following parameters are determined from the measurements. D is the impeller diameter (D=0.02m), ρ is the density of the continuous phase (993kg/m^3), φ is the volume fraction of PDMS mixture, $\varphi \approx 3.5\%$ as 7g PDMS mixture is dispersed in 200g solution, ω is the rotational speed of the impeller (2000rpm), μ_d is the viscosity of the continuous phase (μ_d =0.00528Pa·s, measured by AR-2000) and σ is the surface tension of the aqueous surfactant solution (σ=36.2mN·m^{-1})[40].

For the population balance model, the size distribution of PDMS microsphere can be described from eq. (10). The primary particle size (d_{min}) is measured by using Mastersizer 2000 in the experiment. After substituting the value of D_{32} and d_{min}, the particle size distribution can be obtained.

For maximum entropy formalism, the size distribution of PDMS microsphere can be described from eq. (18). The parameter q is estimated from a plot of $\ln(1-Q_i)^{-1}$ versus d_i/Y.

For normal distribution, the size distribution of the PDMS microsphere can be described from eq. (22). Similar to the population balance model, the standard deviation (σ_d) equals to the primary particle size (d_{min}).

5. Results and discussion

5.1 PDMS microsphere size distribution from experiment

In order to investigate the PDMS microsphere size distribution with respect to diameter and the yield of the PDMS microspheres, eight samples are prepared by mixing Sylgard 184 in a recommended ratio of 10:1 with different surfactant concentrations. Sample ID, surfactant

concentration, mean diameter and microsphere yield are listed in Table 1. The Sample ID indicates the surfactant concentration, e.g. S3P1 means that 3% (wt) SDS and 1% (wt) PVA are added to the aqueous solution.

The yield of the PDMS microsphere is calculated from eq. (23). As shown in Table 1, the yield of the PDMS microsphere ranges from 25.3% to 71.4%, a maximum yield of 71.4% is obtained in Sample S5P1. Meanwhile, the yield of the PDMS microsphere depends on the surfactant concentration in the solution. This is in line with the yield of the poly(divinylbenzene) microspheres in surfactant solution[41], indicating that the yield of the PDMS microsphere not only depends on the external mechanical energy input in the turbulent system, but also related to the surfactant concentration in the solution[42].

$$Y_{PM} = \frac{m_{PM}}{m_{tot}} \cdot 100\% \tag{23}$$

where Y_{PM} is the yield of PDMS microsphere, m_{PM} is the mass of PDMS microsphere and m_{tot} is the mass of vinyl functional PDMS and curing agent.

Table 1. PDMS microsphere mean size and yield from varying surfactant concentrations

Sample ID	SDS (%)	PVA (%)	σ (mN/m)	D_{32} (μm)	Y_{PM} (%)
S0P0	0	0	72.9	/	0
S1P0	1	0	37.3	120	41.6
S3P0	3	0	32.3	104	47.4
S5P0	5	0	32.0	102	54.4
S0P1	0	1	52.4	/	0
S1P1	1	1	37.9	105	25.3
S3P1	3	1	36.2	107	69.4

S5P1	5	1	36.1	89	71.3

Figure 1 and Figure 2 show the volume frequency and the accumulated volume frequency of the PDMS microsphere in different surfactant solutions. As shown in Figure 1, the diameter of the PDMS microsphere falls between 30μm and 300μm and the mean diameter is ca. 100μm. The high polydispersity of the PDMS microsphere demonstrates that the size distribution of the crosslinked PDMS microsphere is different from the narrow size distribution of the silicone oil droplets in water emulsion[23].

Amongst the samples in our study, the samples with PVA exhibit narrower size distribution than those without PVA, indicating that the emulsions created from the mechanical stirring are more stable at the presence of PVA. This is in agreement with that the stability of the emulsion can be increased by using PVA as an assistant surfactant[43]. On the other hand, Sample S0P1 shows that no PDMS microsphere can be obtained, meaning that the PVA can not be used solely in the preparation of the PDMS microsphere and should be added to the solution as assistant surfactant.

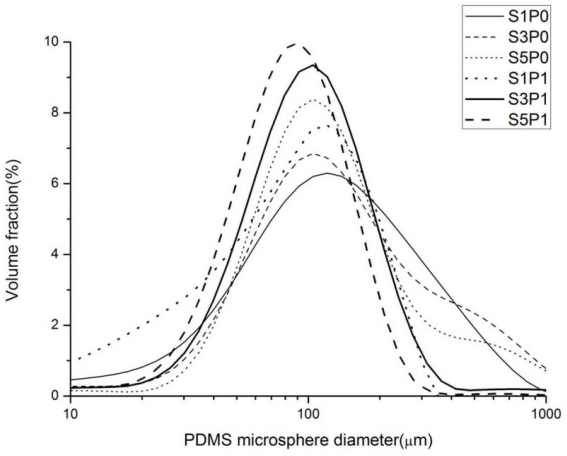

Figure 1. Experimental relative volume fraction versus microsphere diameter for different surfactant concentrations

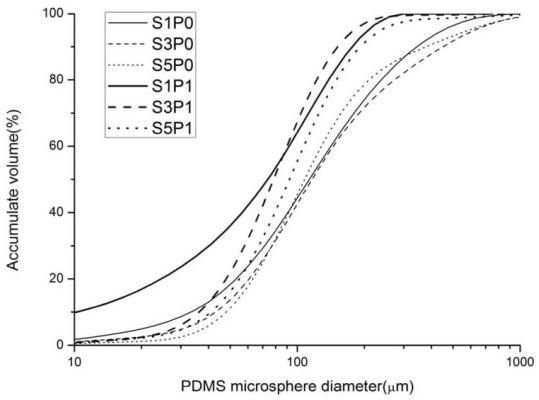

Figure 2. Experimental accumulated volume fraction versus microsphere diameter for different surfactant concentrations

5.2 Comparison of theoretical predictions with experimental results

5.2.1 Comparison of the population balance model simulation with the experimental results

As discussed in Section 2.1, the theoretical mean diameter of the PDMS microsphere can be calculated from eq. (1). By substituting the parameters from the measurements and the literatures, the theoretical mean diameter of the PDMS microspheres can be obtained. Table 2 shows the experimental mean diameter as well as the theoretical mean diameter of the PDMS microsphere. As we can see, the experimental mean diameter varies from 89μm to 120μm, while the predicted mean diameter is around 99μm. The maximum deviation between the experimental value and the

theoretical value is 20μm and the average deviation is around 7μm, indicating that the theoretical values fits the experimental results quite well.

Table 2. Comparison between the experimental and the theoretical mean diameter of the PDMS microspheres in different surfactant solutions

Sample ID	S1P0	S3P0	S5P0	S1P1	S3P1	S5P1
Exp. mean diameter (μm)	120	104	102	105	107	89
Theo. mean diameter (μm)	98.1	99.5	99.6	97.9	98.4	98.4
Deviation between exp. and theo. (μm)	21.9	4.5	2.4	7.1	8.6	9.4

In Section 2.2, population balance model is used to describe the size distribution of the PDMS microspheres based on eq. (10). Normal distribution is introduced in order to compare with the size distribution predicted by the population balance model. Table 3 shows the volume frequency of the most probable distribution from the experiment, the population balance model and the normal distribution. It can be seen that the deviation of the volume frequency of the most probable distribution between the experiment and the population balance model is around 5%, while the deviation between the experiment and the normal distribution is substantial, indicating that the population balance model provides realistic solution in prediction of the volume frequency of the most probable distribution.

Table 3. Comparison of the volume frequency of the most probable distribution between the experiment, the population balance model and the normal distribution of the PDMS microsphere in different surfactant solutions

Sample ID	S1P0	S3P0	S5P0	S1P1	S3P1	S5P1
Exp. most probable distribution (%)	6.3	6.9	8.4	7.6	9.4	10
Theo. most probable distribution (%)	8.3	11	11	6.6	11	11
Normal distribution (%)	36.4	36.4	36.4	36.4	36.4	36.4

The size distribution of the PDMS microspheres between the experiment, the population balance model and the normal distribution are compared and shown in Figure.3. It can be seen that the size distribution obtained from the population balance model is similar to that from the experiment. Meanwhile, the experimental distribution indicated that there is small possibility of primary particles forming clusters smaller than 30μm or larger than 300μm, which can not be predicted by the population balance model.

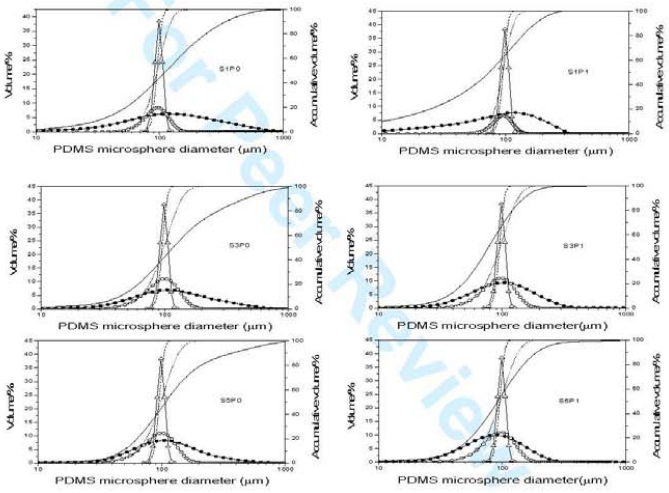

Figure 3. Comparison between experimental, population balance model simulation and normal distribution of the PDMS microsphere in size distribution and cumulative volume fraction. The solid circle, open circle and open triangle represent the size distribution of the experiments, the population balance model simulations and the normal distribution, while the solid line, dotted lines

and dash lines represent the cumulative distribution of the experiments, the population balance model simulations and the normal distribution.

There is good agreement between the experimental values and the modeling values, demonstrating that the Hinze-Kolmogorov theory and population balance model based on dilute systems provide realistic values for the mean diameter and size distribution of the PDMS microspheres. A lot of experiments and simulations based on the Hinze-Kolmogorov theory have been reported[15],[16],[28], however, to the best of our knowledge, none of them involve chemical reactions and irreversible crosslinking in the system. The good agreement between the experimental and the theoretical values in our experiment show that the applicability of the Hinze-Kolmogorov theory to determine mean diameter can be fairly broadened.

5.2.2 Comparison of the maximum entropy formalism simulation with the experimental results

As described in section 2.2.2, the mean diameter and the size distribution of the PDMS microspheres can also be predicted by the maximum entropy formalism using eq. (18). The mean diameter obtained from the simulation is compared with the experimental values and shown in Table.4. As shown in Table.4, the deviation of the mean diameter of the PDMS microsphere between the experiment and the simulation is around 20μm, meaning that the agreement between the experiment and the simulation is reasonably good.

Table 4. Comparison between the experimental and the theoretical mean diameter of the PDMS microspheres in different surfactant solutions

	S1P0	S3P0	S5P0	S1P1	S3P1	S5P1
Exp. mean diameter (μm)	120	104	102	105	107	89
Theo. mean diameter (μm)	118	120	121	120	138	122
Deviation between exp. and theo. (μm)	2	16	19	15	29	33

In eq. (18), the size distribution predicted by the maximum entropy formalism is relevant to the distribution parameter q. In some studies, the value of q is arbitrarily set to 1, providing the size distribution in terms of linear mean diameter[27],[44]. Meanwhile, the value of q can also be determined by using eq. (21), namely that q equals to the slope of $\ln(1-Qi)^{-1}$ versus d_i/Y[26],[37]. The value of the size parameter Y and the distribution parameter q are shown in Table 5.

In order to compare with the maximum entropy formalism model, the normal distribution is also introduced. Table 5 shows the volume frequency of the most probable distribution of the PDMS microsphere from the experiment, the maximum entropy formalism and the normal distribution in different surfactant solutions. It can be seen that the deviation of the volume frequency of the most probable distribution between the experiment and the maximum entropy formalism is around 5%, while the deviation between the experiment and the normal distribution is phenomenal, demonstrating that the maximum entropy formalism also provides fairly realistic solution in the prediction of the volume frequency of the most probable distribution.

Table 5. Comparison of the volume frequency of the most probable distribution between the experiment, the population balance model and the normal distribution of the PDMS microsphere as well as the value of the size parameter Y and the distribution parameter q in different surfactant solutions

	S1P0	S3P0	S5P0	S1P1	S3P1	S5P1
Exp. most probable distribution (%)	6.3	6.9	8.4	7.6	9.4	10
Theo. most probable distribution (%)	11	9.7	8.4	8.4	11	8.4
Normal distribution (%)	36.4	36.4	36.4	36.4	36.4	36.4
Y value (size below 63.2%) (μm)	152	158	135	184	124	113
q (slope of $\ln(1-Qi)^{-1}$ versus d_i/Y)	1.1	0.8	0.6	2.7	1.0	0.6

Figure 4 shows the size distribution of the PDMS microsphere from the experiment, the maximum entropy formalism and the normal distribution. It can be seen that the normal distribution show a remarkable difference in distribution trend, thus is not suitable to describe the experimental data. Meanwhile, the size distribution predicted by the maximum entropy formalism can describe the distribution trend of the experimental data as well as the shows inevitable difference in the peak. This demonstrates that the entropy in the experimental systems is not maximized, resulting in the deviation between the predicted values and the experimental values.

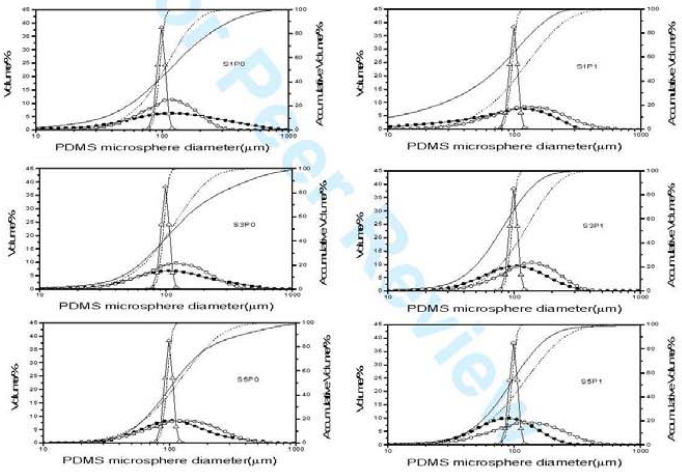

Figure 4. Comparison between experimental, maximum entropy formalism simulation and normal distribution of the PDMS microsphere in size distribution and cumulative volume fraction. The solid circle, open circle and open triangle represent the size distribution of the experiments, the maximum entropy formalism simulation and the normal distribution, while the solid line, dotted

lines and dash lines represent the cumulative distribution of the experiments, the maximum entropy formalism simulation and the normal distribution

5.3 PMMA coated PDMS microsphere characterization

5.3.1 Thermogravimetric analysis

In order to investigate the content of PMMA in the coated PDMS microspheres, four samples are coated in presence of various concentrations of PMMA. Sample ID, PMMA concentrations and char yield at 800°C are summarized in Table 6. The sample ID indicates the coating concentration of PMMA, e.g. 10PD mean the coating solution is 10% PMMA in DMF, while PM is the abbreviation of PDMS microsphere.

In the TGA measurement, the PDMS microsphere degrades simultaneously with the PMMA. Since the PMMA degrades completely at 430°C, the char yield at 800°C only depends on the content of the PDMS microsphere. As shown in Table 6, the char yield of the coated PDMS microsphere decreases when higher concentration of PMMA is used in the spin coating process. This indicates that the content of the PMMA in the coated PDMS microsphere increases at the presence of high concentration of PMMA in the solution.

Table 6. Thermogravimetric analysis (TGA) of PDMS microspheres coated with different concentration of PMMA by spin coating

Sample ID	PMMA	non-coated PM	PM-10PD	PM-20PD	PM-50PD
PMMA concentration in solution (%)	/	0	10	20	50
Char yield at 800°C (wt%)	0	37.7	27.5	18.3	11.4

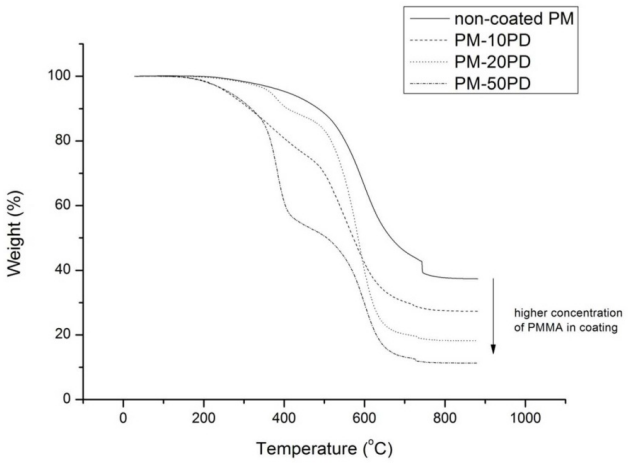

Figure 5. TGA thermograms in a N_2 atmosphere of PDMS microspheres coated with PMMA and non-coated sample

As a commercial available technique, spin coating has been used for decades to produce thin films on a planar substrate. However, it has not been reported that spin coating can be used to produce coated microspheres. There is no solid evidence to prove that PMMA can be coated perfectly onto PDMS microspheres, and further studies (e.g. rheology) are required.

5.3.2 Rheological measurement

In the preparation of the PDMS microspheres, excess vinyl terminated PDMS is added to the mixture to obtained the vinyl functional PDMS microspheres. The vinyl groups on the surface of the PDMS microsphere are able to react with the crosslinker at the presence of catalyst. The reaction between the PDMS microsphere and the crosslinker will increase the crosslinking density of the system, resulting in the increase of the storage modulus.

The objective of the rheological measurement is to investigate the quality of the coated PMMA layer, namely that whether the coated PMMA is sufficient to prevent the vinyl functional PDMS microsphere from reacting with the crosslinker. If the PDMS microspheres are completely coated with PMMA, the crosslinker can not penetrate the PMMA shell and the modulus will remain constant, vice versa.

In the measurement, 0.4g PMMA-coated vinyl functional PDMS microsphere is mixed with 0.01g HMS-301 crosslinker and 0.1g non-reactive silicone oil. The uncoated PDMS microspheres are used as a control sample. For details of the applied amount see Supplementary Info 2. Meanwhile, the rheological measurements are made at 50°C for two reasons: first, the measuring temperature is lower than the T_g of the PMMA such that the coated PMMA remains rigid; secondly, the PDMS microspheres reacts with the crosslinker at a moderate rate if the crosslinking reaction occurs.

Figure 6 shows the rheological behavior of the PDMS microspheres with and without coating over a period of 10h. For the PDMS microspheres without coating, the storage modulus increases from

10kPa to 38kPa, indicating that the PDMS microspheres undergo crosslinking reaction with the crosslinker. The slope of the storage modulus curve is relatively steep at first hour, showing a relatively high rate of the crosslinking reaction. Afterwards, the storage modulus levels out, meaning that the vinyl groups on the surface of the PDMS microsphere have been consumed. For the coated PDMS microspheres, the storage modulus increases slightly, demonstrating that the crosslinking reaction occurs to a small degree. In the comparison of the uncoated and the coated PDMS microsphere, the difference in rheological behavior suggests that the PMMA shell hinders the crosslinking reaction greatly.

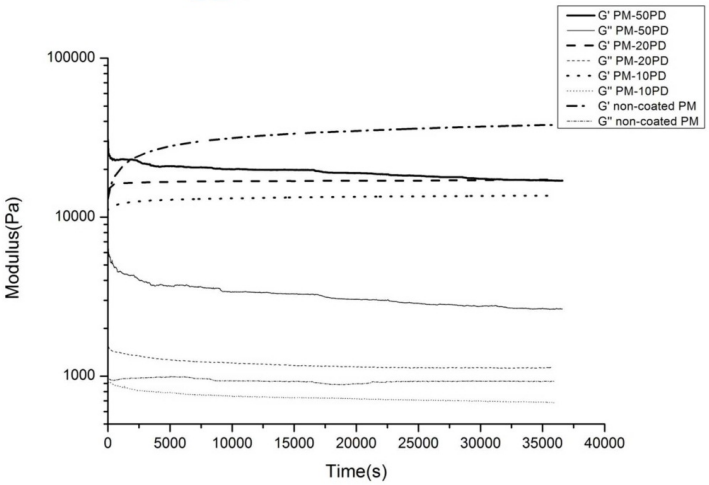

Figure 6. Rheological behavior of PDMS microspheres with and without PMMA coating in silicone oil at 50℃

6. Conclusions

PDMS microspheres have been prepared by mechanical stirring using a series of surfactant solutions. The size distribution of the PDMS microsphere has been investigated, and it is found that the diameter of 90% PDMS microsphere falls between 30μm and 300μm while the mean diameter of the PDMS microsphere is around 100μm in all samples. The broad distribution of the PDMS microsphere in diameter suggests that high polydisperse PDMS microspheres have been obtained.

As the preparation process of the PDMS microsphere involves with the dispersion of the PDMS in the aqueous surfactant solution, the mean diameter of the PDMS microsphere has been predicted by using Hinze-Kolmogorov theory. The agreement between the experimental value and the calculated value is excellent. This indicates that the applicability of the Hinze-Kolmogorov theory can be fairly broadened in the prediction of the mean diameter of droplets in turbulent system. Furthermore, the size distribution of the PDMS microsphere has been described by using the population balance model and the maximum entropy formalism. Compared to the experimental results, it is shown that both population balance model and maximum entropy formalism provide realistic results.

The PDMS microspheres with residual vinyl groups on the surface have been further coated by PMMA in a newly developed spin coating procedure. The coated PDMS microspheres show very slow reaction rates compared to those without coating, indicating that the reaction has been significantly hindered by the PMMA shell. Such properties may provide a potential for designing responsive materials.

AUTHOR INFORMATION

Corresponding Author. Anne Ladegaard Skov

*Email: al@kt.dtu.dk Tel +45 4525 2825

References:

[1] P. Jerschow, *Silicone Elastomers*, Springer, Shropshire, UK, **2001**, vol. 12.

[2] R. A. Ramli, W. A. Laftah, and S. Hashim, *RSC Adv.*, **2013**, *3*, 15543.

[3] D. Brady and J. Jordaan, *Biotechnol. Lett.*, **2009**, *31*, 1639–1650.

[4] N. J. Fendinger, D. C. McAvoy, W. S. Eckhoff, and B. B. Price, *Environ. Sci. Technol.*, **1997**, *31*, 1555–1563.

[5] M. T. Gokmen and F. E. Du Prez, *Prog. Polym. Sci.*, **2011**, *37*, 365–405.

[6] S. Shojaei-Zadeh, J. F. Morris, A. Couzis, and C. Maldarelli, *J. Colloid Interface Sci.*, **2011**, *363*, 25–33.

[7] S. Peng, M. Zhang, X. Niu, W. Wen, P. Sheng, Z. Liu, and J. Shi, *Appl. Phys. Lett.*, **2008**, *92*, 012108.

[8] L. González, M. Baoguang, L. Li, J. H. Hansen, S. Hvilsted, and A. L. Skov, *Macromol. Mater. Eng.*, **2014**, *299*, 729–738.

[9] J. Bałdyga, J. Bourne, and A. Pacek, *Chem. Eng. Sci.*, **2001**, *56*, 3377–3385.

[10] H. Chen and S. Middleman, *AIChE J.*, **1967**, *13*, 989–995.

[11] R. Cohen, *J. Chem. Soc. Faraday Trans.*, **1990**, *86*, 2133–2138.

[12] L. Gonzalez, B. Ma, K. Malgorzata, L. Li, H. J. Hansen, S. Hvilsted, and A. L. Skov, *Macromol. Mater. Eng.*, **2014**. DOI: 10.1002/mame.201400020

[13] B. Ma, J. H. Hensen, S. Hvilsted, and A. L. Skov, *RSC Adv.*, **2014**. Submitted Manuscript

[14] J. Hinze, *AIChE J.*, **1955**, *1*, 289–295.

[15] Y. Mlynek and W. Resnick, *AIChE J.*, **1972**, *18*, 122–127.

[16] R. V. Calabrese, T. P. K. Chang, and P. T. Dang, *AIChE J.*, **1986**, *32*, 657–666.

[17] R. Afshar Ghotli, A. Raman, S. Ibrahim, and S. Baroutian, *Chem. Eng. Commun.*, **2013**, *200*, 595–627.

[18] D. Ramkrishna, *Population Balances: Theory and Applications to Particulate Systems in Engineering*, Academic Press, Minnesota, **2000**.

[19] J. Solsvik, Z. Borka, P. J. Becker, N. Sheibat-Othman, and H. a. Jakobsen, *Can. J. Chem. Eng.*, **2014**, *92*, 234–249.

[20] J. Boxall, C. Koh, E. D. Sloan, A. K. Sum, and D. T. Wu, *Langmuir*, **2012**, *28*, 104–110.

[21] J. Boxall, C. Koh, E. D. Sloan, A. K. Sum, and D. T. Wu, *Ind. Eng. Chem. Res.*, **2010**, *49*, 1412–1418.

[22] C. Liu, M. Li, C. Liang, and W. Wang, *Chem. Eng. Sci.*, **2013**, *102*, 622–631.

[23] A. EL-Hamouz, *Chem. Eng. Technol.*, **2009**, *32*, 1203–1210.

[24] K. Binder and D. Heermann, *Monte Carlo simulation in statistical physics: an introduction*, Springer, Mainz, **2010**.

[25] P. M. Bapat, L. L. Tavlarides, and G. W. Smith, *Chem. Eng. Sci.*, **1982**, *38*, 2003–2013.

[26] D. Mondal, a Datta, and a Sarkar, *Proc. Inst. Mech. Eng. Part C J. Mech. Eng. Sci.*, **2003**, *217*, 831–838.

[27] J. Cousin and C. Dumouchel, *At. sprays*, **1996**, *6*, 601–622.

[28] J. S. Lagisetty and P. K. Das, *Chem. Eng. Sci.*, **1986**, *41*, 65–72.

[29] R. D. Cohen, *J. Chem. Soc. Faraday Trans.*, **1991**, *87*, 1163–1168.

[30] M. Kostoglou and A. Karabelas, *J. Aerosol Sci.*, **1999**, *30*, 157–162.

[31] J. Baldyga and W. Podgórska, *Can. J. Chem. Eng.*, **1998**, *76*, 456–470.

[32] S. Kumar and D. Ramkrishna, *Chem. Eng. Sci.*, **1997**, *52*, 4659–4679.

[33] M. Attarakih and H. Bartb, in *Proceedings of the 22nd European Symposium on Computer Aided Process Engineering*, Elsevier B.V., London, **2012**.

[34] A. Huan, *Statistical mechanics*, Royal Society of Chemistry, Cambridge,UK, **1975**, vol. 2.

[35] P. Harremoës, *Inf. Theory, IEEE Trans.*, **2001**, *47*, 2039–2041.

[36] C. Shannon and W. Weaver, *The mathematical theory of communication*, University of Illinois Press, Urbana, **1964**.

[37] B. Osbaeck and V. Johansen, *J. Am. Ceram. Soc.*, **1989**, *72*, 197–201.

[38] C. Y. Wang and R. V. Calabrese, *AIChE J.*, **1986**, *32*, 667–676.

[39] N. Vankova, S. Tcholakova, N. D. Denkov, I. B. Ivanov, V. D. Vulchev, and T. Danner, *J. Colloid Interface Sci.*, **2007**, *312*, 363–380.

[40] N. J. Alvarez, L. M. Walker, and S. L. Anna, *J. Colloid Interface Sci.*, **2009**, *333*, 557–562.

[41] Q. Yan, Y. Bai, Z. Meng, and W. Yang, *J. Phys. Chem. B*, **2008**, *112*, 6914–22.

[42] A. Khakpay, H. Abolghasemi, and M. M. Montazer-Rahmati, *Can. J. Chem. Eng.*, **2010**, *88*, 101–108.

[43] T. Ma, Y. Huang, J. Yang, J. He, and L. Zhao, *Mater. Des.*, **2004**, *25*, 515–519.

[44] C. Dumouchel, *Entropy*, **2009**, *11*, 713–747.

[45] A. Colas and L. Aguadisch, *Chim. Nouv.*, **1997**, 1–5.

[46] A. L. Larsen, K. Hansen, O. Hassager, A. Bach, S. Ndoni, and M. Jørgensen, *Macromolecules*, **2003**, *36*, 10063–10070.

Appendix II

Control of PDMS crosslinking by encapsulating a hydride crosslinker in a PMMA microcapsule

RSC Advances (2014)

RSC Advances

PAPER

View Article Online
View Journal | View Issue

Cite this: RSC Adv., 2014, 4, 47505

Control of PDMS crosslinking by encapsulating a hydride crosslinker in a PMMA microcapsule†

Baoguang Ma,[a] Jens Henrik Hansen,[b] Søren Hvilsted[a] and Anne Ladegaard Skov*[a]

In the preparation of PDMS elastomers, a combination of mixing and reactive processes constrains the applicability of the PDMS elastomer in research and applications. Separation of the mixing and reactive processes, which control PDMS crosslinking, has been achieved by encapsulating a hydride crosslinker in a PMMA shell. Microcapsules are mixed with vinyl-terminated PDMS to create a gelation system, which allows for storage at 50 °C, without premature gelation, and in addition allows for extensive crosslinking reaction at 120 °C. Both visual observations and rheological studies show that a robust PDMS elastomer is obtained upon heating the gelation system. Furthermore, the influence of stoichiometric imbalance on the equilibrium storage modulus of the PDMS network is investigated, by employing different amounts of microcapsules in vinyl-terminated PDMS. It has been found that adding microcapsules increases the equilibrium storage modulus of the PDMS elastomer until the diffusion of the hydride crosslinker is constricted. An optimum amount of crosslinker used in the control crosslinking reaction has also been found. However, compared to the pure PDMS elastomer, the modulus of the PDMS elastomer from the encapsulated system is less sensitive in relation to the stoichiometry of the system than the corresponding polymer network. This broadens the applicability range of silicone elastomers.

Received 23rd July 2014
Accepted 19th September 2014

DOI: 10.1039/c4ra07513g

www.rsc.org/advances

Introduction

A controlled crosslinking reaction, which takes place in response to external stimulus,[1] is of considerable interest in applications. Amongst all research on and applications of silicone elastomers, controlling the crosslinking reaction (*e.g.* between a vinyl-terminated PDMS and a hydride crosslinker) attracts most attention, due to the fascinating properties of PDMS elastomers obtained from the reaction.[2] One potential application where control of PDMS crosslinking reaction is required is in the delivery of elastic seals to fractures in oil reservoirs. In the sealing process, the crosslinking reaction needs to be postponed until the elastomer reactants are placed inside the fracture. One way to solve the problem is to encapsulate the crosslinker in polymeric microcapsules.[3] When the hydride crosslinker is sequestered inside the polymeric microcapsules, the microcapsules can be mixed with the vinyl-terminated PDMS, without undergoing a crosslinking reaction, thereby ensuring the mixture has not reacted.[4]

In order to release the hydride crosslinker from the polymeric shell, the shell of the microcapsule should be capable of changing its morphology or structure upon external stimulus.[5] Thermal initiation is one of the most commonly used stimuli which causes changes in the polymer structure of amorphous polymer.[6] At temperatures lower than the glass transition temperature (T_g) of the polymeric shell, the polymeric shell remains rigid and the hydride crosslinker is sequestered inside it; therefore, the mixture containing the microcapsules and vinyl-terminated PDMS will remain liquid-like, due to the absence of a crosslinking reaction. Upon heating up the mixture,[7] the structure of the polymeric shell changes when the temperature is higher than its T_g, resulting in the release of the hydride crosslinker and the initiation of the crosslinking reaction.

Traditionally so-called model networks are prepared from silicone networks obtained by silylation reactions.[8–10] A (usually short) hydride functional crosslinker is reacted with long, linear, end-linked vinyl functional silicones to yield a network. The silylation reaction is catalyzed by platinum. During the crosslinking reaction, the vinyl-terminated PDMS and the hydride crosslinker convert into one large, infinite molecule.[11] Consequently, the mixture loses its solubility, and its storage modulus starts to rise to a finite value until the completion of the crosslinking reaction.[12] The storage modulus at the completion of the crosslinking reaction refers to the equilibrium storage modulus, which is determined by stoichiometric imbalance and the crosslinking density of the network. Many studies show that the equilibrium storage modulus of the PDMS network is sensitive to the stoichiometric imbalance as well as

[a]Danish Polymer Centre, Department of Chemical and Biochemical Engineering, Technical University of Denmark, Søltofts Plads Building 227, DK-2800 Kgs. Lyngby, Denmark. E-mail: al@kt.dtu.dk

[b]Maersk Oil Research and Technology Centre, Education City, P.O. Box 210112, Doha, Qatar

† Electronic supplementary information (ESI) available. See DOI: 10.1039/c4ra07513g

the perfection of the PDMS network.[11,13–16] Thus, the influence of stoichiometric imbalance on the equilibrium storage modulus will be investigated, in order to determine the optimum amount of microcapsules and sensitivity of the storage modulus on stoichiometric imbalance in controlled PDMS crosslinking reaction.

This paper, which is devoted to studying the crosslinking reaction between a hydride crosslinker and a vinyl-terminated PDMS polymer controlled by releasing the hydride crosslinker from a PMMA shell, is divided into the following parts: in the first part, we describe the preparation and the characterisation of a PMMA microcapsule containing a multifunctional methylhydrosiloxane-dimethylsiloxane copolymer crosslinker. Following this, the reactivity of the PMMA/crosslinker microcapsule is evaluated in the presence of a vinyl-terminated PDMS at 50 °C and 120 °C, respectively. To characterise the system quantitatively, time sweep rheological analyses are used, which determine the storage modulus of the mixture containing the PMMA/crosslinker microcapsule and the vinyl-terminated PDMS. In the last part of the paper, mixtures with different stoichiometric imbalances are characterised through time sweep rheological measurements, and the rheological properties of the obtained network are compared with those of a pure PDMS elastomer.

Experimental section

Materials

The chemicals employed are: poly (methyl methacrylate) (PMMA) (M_w = 15 000 g mol^{-1}, Aldrich), 25–35% (methylhydrosiloxane) with 65–70% (dimethylsiloxane) copolymer (HMS-301) (M_n = 2000 g mol^{-1}, 8-functional crosslinker, Gelest), platinum cyclovinylmethysiloxane complex (SIP 6832.2 catalyst, Gelest), vinyl-terminated polydimethylsiloxane (DMS-V35) (M_n = 49 500 g mol^{-1}, Gelest), chloroform (>99%, Aldrich), heptane (>99%, Aldrich), methanol (>99%, Aldrich) and deuterated chloroform (>99.8%D, Aldrich).

Apparatus

An air compressor (#1A) and an airbrush (DH-201) were purchased from Sparmax (Germany). The compressor's air flow ranged from 7 to 11 litres per minute, and the maximum pressure provided by the compressor in the air compressing process was 40 psi. The diameter of the nozzle in the airbrush was 0.8 mm.

The morphology of the PMMA/HMS-301 microcapsules was analysed with a scanning electron microscope (SEM) FEI Inspect S, Oxford Instruments, with an acceleration voltage of 10–20 kV.

The size distribution of the PMMA/HMS-301 microcapsules was measured by Mastersizer (Malvern, UK) in a jar tester. The instrument was equipped with a laser at a wavelength of 633 nm and a size range of 1 μm–1 mm.

^{1}H NMR spectra were obtained on a Bruker 250 MHz NMR spectrometer in $CDCl_3$ at room temperature. ^{1}H chemical shifts were referenced to TMS *via* a residual non-deuterated solvent signal at $\delta = 7.26$ ppm.

Rheological measurements were performed in an AR2000 stress-controlled rheometer, while measurements were taken with a strain of 2% to ensure they were within the linear regime of the material[17] as well as to minimise any disruption to the network. Similar to other measurements of *in situ* crosslinking reactions of additional curing silicones,[18,19] the applied frequency was set to 1 Hz.

Microcapsule preparation

The polymeric solution was prepared by dissolving 1.0 g of HMS-301 and 1.0 g of PMMA in 5.4 mL chloroform. The polymeric solution was stirred at 700 rpm with a magnetic stirrer for 24 hours at room temperature. Next, the polymeric solution was sprayed with an airbrush into a beaker containing 200 mL methanol. The micro droplets formed from the polymeric solution precipitated, resulting in the encapsulation of HMS-301. The microcapsules were then washed with methanol several times, in order to remove any residual HMS-301 on the surface. Finally, the microcapsules were collected by filtration. Fig. 1 shows the scheme for the spraying setup.

Microcapsule preparation with different HMS-301 concentrations

In order to compare the encapsulation efficiency of the microcapsules, different concentrations of HMS-301 were used in the preparation as follows: (a) 10% (wt) of HMS-301 and 10% (wt) of PMMA in 80% (wt) chloroform (MP10H10C), (b) 15% (wt) of HMS-301 and 10% (wt) of PMMA in 75% (wt) chloroform (MP10H15C) and (c) 20% (wt) of HMS-301 and 10% (wt) of PMMA in 70% (wt) chloroform (MP10H20C).

For comparison purposes, microcapsules without HMS-301 were prepared using the same procedure from a polymeric solution containing 10% (wt) of PMMA and 90% (wt) of chloroform.

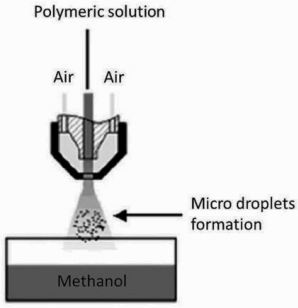

Fig. 1 Schematic diagram of the spraying setup.

Soluble fraction determination

Approximately 0.5 g of network obtained from microcapsule (MP10H10C) + V35 as well as HMS-301 + V35 with different stoichiometric imbalance was swelled in heptane (20–30 times excess, *i.e.* 15–25 mL solvent to a sample of 0.5 g; in all experiments, we ensure that the networks were fully covered in heptane) for 48 h. After the 48 h, the networks were separated from the heptane solution. The residual heptane was removed by evaporation for 48 h under atmospheric condition.

Results and discussion

Morphological characterisation

Fig. 2a and b show the representative SEM graphs of the outer surfaces and a cross-sectional view of the PMMA/HMS-301 microcapsules which were washed with methanol and heptane, respectively. Fig. 2a shows that the microcapsules were spherically shaped and only a few were broken after washing with methanol. Due to the low solubility of HMS-301 in methanol, methanol removed any HMS-301 on the surface only, without washing away HMS-301 inside the microcapsules. All the microcapsules in later sections were washed with methanol unless otherwise stated. Fig. 2b shows that the microcapsules had a core–shell structure with a porous shell. Because of the high solubility of HMS-301 in heptane, heptane passed through the pores in the PMMA shell and entered into the core of the microcapsule. Thus, heptane removed most HMS-301 and destroyed some of microcapsules during evaporation, thereby leaving a hollow structure in the microcapsules.

The morphology of the PMMA shell was similar to that of the polysulfone (PSU) shell of the PSU/vanillin microcapsule.[20] Similar to our preparation process, the PSU/vanillin microcapsule was also prepared by spraying polymeric solution containing PSU and vanillin into a non-solvent by using an air brush.[20,21] As well as studies on PSU/vanillin microcapsules, several others have proven that microcapsules with a porous shell are suitable for stimuli-responsive controlled release, in order to obtain fast response times.[20,22,23] Consequently, PMMA/HMS-301 microcapsules should have a potential for controlled release when stimulated.

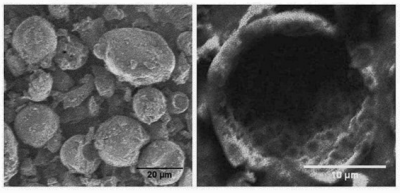

Fig. 2 (a (left) and b (right)). SEM image of the outer surface (left) and a cross-section (right) of PMMA/HMS-301 microcapsules. The left- and the right-hand SEM images show the morphology of the MP10H10C microcapsules washed with methanol and heptane, respectively.

Size distribution of PMMA/HMS-301 microcapsules and empty PMMA capsules

As discussed in the previous section, most of the microcapsules were spherical after washing with methanol, and they should also have been identical to those not washed with methanol, as methanol only removed HMS-301 on the surface. The size distribution of the microcapsules could therefore be investigated with Mastersizer, based on laser diffraction. Fig. 3 shows the size distribution of the microcapsules with a crosslinker inside as well the empty PMMA capsules. As shown in Fig. 3, microspheres had a mean diameter ranging from 47 μm to 58 μm and were monomodal and similar in size distribution.

Determination of the HMS-301 weight fraction in microcapsules

The weight fraction of HMS-301 was determined through ^{1}H NMR spectroscopy. As the –O–CH_3 groups in PMMA and the Si–H groups in HMS-301 have ^{1}H chemical shifts of 3.6 ppm and 4.7 ppm, respectively, the mol ratio between the PMMA and HMS-301 could be calculated from the corresponding area of the resonances. Fig. 4 shows the integrated signals of the –O–CH_3 groups and the Si–H groups in the ^{1}H NMR spectra. The weight fractions of HMS-301, calculated by ^{1}H NMR, were 28%, 21% and 14% in MP10H10C, MP10H15C and MP10H20C, respectively. For more details on the method used in determining the content of HMS-301, see ESI.†

Both the mean diameter and the weight fraction of the HMS-301 of PMMA/HMS-301 microcapsules are summarized and shown in Table 1.

With the increased HMS-301 concentration, the viscosity of the solution decreased, resulting in a delayed breakup process and impeded atomization. Thus the encapsulation efficiency was shown to decrease upon decrease of the shell material concentration.

The size distribution and mean diameter depend on several factors such as the viscosity and surface tension of the solution being atomized as well as the turbulence created.[24] The

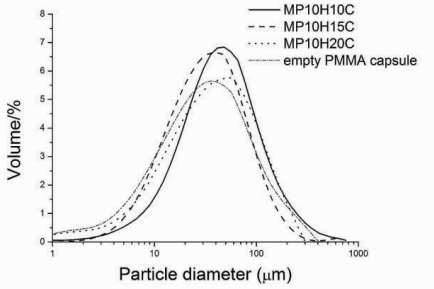

Fig. 3 Size distribution of MP10H10C, MP10H15C, MP10H20C microcapsules and empty PMMA capsules.

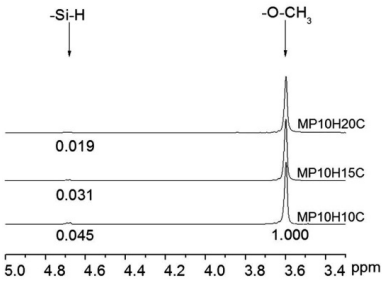

Fig. 4 ^{1}H NMR spectra of MP10H10C, MP10H15C and MP10H20C microcapsules with an indication of the characteristic peaks for Si–H and –O–CH_3.

Fig. 5 (a (left), 5b (right)). Photograph of mixtures containing the PMMA/HMS-301 microcapsule and V35 after curing at 50 °C (left) and 120 °C (right).

deviation in the mean diameters is similar to what is observed for other similar systems.[25]

Reactivity of PMMA/HMS-301 microcapsules in a vinyl-terminated PDMS polymer

To evaluate the reactivity of the microcapsule in a melt of vinyl-terminated PDMS, a typical mixture containing a 0.01 g PMMA/HMS-301 microcapsule (MP10H10C) and 1 g V35 was made. All mixtures in the experiments contained 7 ppm platinum catalyst. Identical mixtures were placed in two vials, which were then inserted into ovens at 50 °C and 120 °C and cured for several days. Fig. 5a shows that the mixture cured at 50 °C was translucent and viscous, with no visible settling of PDMS gel. The mixture remained viscous and of low viscosity, as the HMS-301 remained sequestered inside the rigid PMMA shell, leaving V35 unable to react. In contrast, Fig. 5b shows that a crosslinked gel was obtained when the mixture was heated to 120 °C. This indicated an extensive crosslinking reaction between HMS-301 and V35. After cooling down to room temperature, the material remained in its gel state, indicating that the gelation did not arise from any physical association between the PMMA/HMS-301 microcapsule and V35.

To characterise the rheological behaviour of the PMMA/HMS-301 microcapsule and V35 mixture quantitatively, time sweep rheological measurements were performed at 50 °C and 120 °C. The measurements were performed with a low amplitude strain, in order to minimise any disruption to the network during the formation process. Table 2 shows the composition and stoichiometric imbalance of the mixture in the measurements. The stoichiometric imbalance (r) is the ratio between the mol number of the hydride groups and the vinyl groups. r is calculated from:

$$r = \frac{n_{\text{hydride}}}{n_{\text{vinyl}}} = \frac{\frac{m_{\text{HMS-301}}}{M_{\text{HMS-301}}} f_{\text{HMS-301}}}{\frac{m_{\text{V35}}}{M_{\text{V35}}} f_{\text{V35}}}$$

where n is the number of moles, m is the mass, M is the molecular weight and f is the functionality of the respective molecule, and where subscripts HMS-301 and V35 denote the hydride crosslinker and vinyl-terminated PDMS, respectively.

Fig. 6 shows representative curves of the storage modulus of the mixture containing the PMMA/HMS-301 microcapsule and

Table 2 Compositions and stoichiometric imbalance in rheological measurements

m_{V35}/g	Sample	$m_{\text{microcapsule}}$/g	Stoichiometric imbalance (r)
1.013	MP10H10C	0.010	0.24
0.992	MP10H15C	0.013	0.24
1.005	MP10H20C	0.020	0.24

Table 1 Mean diameter and weight fraction of HMS-301 for the PMMA/HMS-301 microcapsules

	Concentration in solution before spray (wt%)				
Sample ID	PMMA	HMS-301	Chloroform	Weight fraction of HMS-301 (wt%)	Mean diameter (μm)
MP10H10C	10	10	80	28	48
MP10H15C	10	15	75	21	41
MP10H20C	10	20	70	14	56
Empty PMMA capsules	10	0	90	0	41

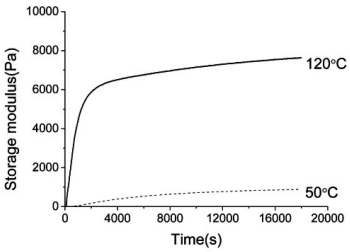

Fig. 6 Development of elasticity in mixtures containing the PMMA/HMS-301 microcapsule (MP10H10C) and V35 at 50 °C (dash) and 120 °C (solid) over a period of 5 hours.

V35 at 50 °C and 120 °C, respectively. At 50 °C, the storage modulus remained low (~500 Pa) and was lower than the loss modulus (not shown in the figure), thereby indicating that the mixture maintained viscous behaviour. On the other hand, a slight increase in the storage modulus of the mixture suggested that there was a small degree of crosslinking reaction between HMS-301 and V35, which was related to the leakage of a small amount of HMS-301 from the porous PMMA shell. The porosity of the PMMA shell can be seen in the SEM image in Fig. 2b. When measurements were made at 120 °C, the storage modulus of the mixture increased rapidly, eventually reaching a plateau within 5 hours (~8000 Pa), after which any further increase in storage modulus was minimal. 80% of the maximal elasticity (determined from the curve) was obtained within the first 30 minutes. This massive increase in the storage modulus of the mixture not only suggested that there was a substantial degree of crosslinking reaction during the measurement, but also corresponded well with our visual observation of the crosslinked gel obtained in the vial at 120 °C (shown in Fig. 5b).

Considering the different rheological behaviours of the mixture at 50 °C and 120 °C, the results indicated that the reactivity of the PMMA/HMS-301 microcapsule at 120 °C was significantly higher that at 50 °C. This difference in reactivity could be explained as follows: at 50 °C, most of the HMS-301 was sequestered in the PMMA shell, meaning the mixture was unable to react. Moving towards the situation at 120 °C, the temperature was higher than the T_g of the PMMA ($T_g = 100$ °C),[13] resulting in the softening of the PMMA shell in the microcapsule and the release of HMS-301. Consequently, this release of HMS-301 reacted with V35 in the presence of a catalyst, yielding a PDMS network.

Soluble fraction

To evaluate the soluble fraction of the network obtained from the MP10H10C + V35 with different stoichiometric imbalances, swelling experiments were performed. In this and the following section, MP10H10C was selected as a representative microcapsule, as the HMS-301 content was the highest among all the samples. In order to interpret the soluble fraction of the network from MP10H10C + V35, reference networks with identical stoichiometric imbalance as the MP10H10C + V35 network were prepared by mixing HMS-301 + V35 and cured under identical conditions. Table 3 shows that the soluble fraction of the network from MP10H10C + V35 ranged from 14.5% to 27.8% and that of reference samples ranged from 5.6% to 18.2%. The soluble fraction in networks can be attributed to inactive species within the reactants and imperfections arising during the crosslinking of the network. Since the inactive species were identical for all samples, the difference in soluble fraction between the MP10H10C + V35 network and referenced network arises from different degrees of imperfections in the networks.[13] The PMMA is not distinguishable soluble in heptane and is thus not washed out of the networks. The difference in the imperfections in the network could be explained as follows: Upon the heating of the mixture containing MP10H10C and V35, the HMS-301 diffused out from the microcapsule and reacted with V35, yielding crosslinked PDMS network around the microcapsule. The locally formed network has a much higher viscosity than the vinyl terminated PDMS, eventually impeding the diffusion of HMS-301 and the crosslinking reaction. As a result, the unreacted PDMS remained in the network and increased the imperfections as well as the soluble fraction of the MP10H10C + V35 network.

It was further found that the soluble fraction of the MP10H10C + V35 network decreased from 27.8% to 14.5% when the stoichiometric imbalance increased from 0.8 to 1.4. This trend was similar to that of the referenced system, indicating that the increasing amount of microcapsule resulted in the increasing released amount of HMS-301 and yielding stronger network with lower soluble fraction.[13,14]

Influence of stoichiometric imbalance on the equilibrium storage modulus

The aim of this section is to investigate the influence of stoichiometric imbalance on the equilibrium storage modulus of the network obtained from the crosslinking reaction between the PMMA/HMS-301 microcapsule and V35. Mixtures containing the PMMA/HMS-301 microcapsule and V35 (System A) were characterised by a time sweep rheological measurement at 120 °C within the range $0.2 < r < 1.4$. In order to interpret the rheological properties of the networks in System A, HMS-301 + empty PMMA capsule + V35 (System B) and HMS-301 + V35 (System C) with $0.6 < r < 1.4$ were prepared and then characterised by a time sweep rheological measurement at 120 °C. System B was made to simulate the situation whereby all HMS-301 diffused out from the PMMA shell and mixed with V35, while System C consisted of a PDMS elastomer without any filler and was used as a reference sample (Table 4).

The rheological behaviours of Systems A, B and C in a time sweep rheological measurement are shown in ESI S2.† The equilibrium storage moduli of Systems A, B and C were obtained from Fig. S2 in ESI S2† and are shown in Fig. 7, where we can see that the equilibrium storage modulus of System A increased in line with an increase in stoichiometric imbalance in the range $0.2 < r < 0.8$, indicating that the crosslinking density

Table 3 Soluble fraction of networks obtained from MP10H10C + V35 and HMS301 + V35

	Stoichiometric imbalance (r)			
	0.8	1	1.2	1.4
Soluble fraction of network obtained from MP10H10C + V35 (%)	27.8	21.5	20.3	14.5
Soluble fraction of network obtained from reference system (HMS-301 + V35) (%)	18.2	10.9	8.4	5.6

of the network increased as more PMMA/HMS-301 microcapsules were used in this range. However, in the range $0.8 < r < 1.4$, the equilibrium storage modulus of System A remained almost constant. This suggested that the crosslinking density of the network did not increase when an excess amount of PMMA/HMS-301 microcapsules was used in the mixture. In comparison, the maximum equilibrium storage moduli of most commonly applied PDMS networks are obtained in the range $1.2 < r < 1.4$,[15] whereas the maximum equilibrium storage modulus of System A was obtained at $r = 0.8$. This indicated that HMS-301 was trapped in the range $0.8 < r < 1.4$, due to diffusion constriction. The reason for this trapping of HMS-301 is explained in the following: upon heating the mixture containing the PMMA/HMS-301 microcapsule and V35, the PMMA shell softened, thus resulting in the release of HMS-301. Then, the released HMS-301 reacted with V35 around the microcapsule, yielding locally a crosslinked PDMS network. The crosslinked PDMS network around the microcapsule had a much higher viscosity than V35, such that the further diffusion of HMS-301 was significantly hindered by the crosslinked PDMS network. This phenomenon was described by Ndoni and Kramer as 'strangulation within polymer networks'.[26] As the crosslinked PDMS network accumulated around the microcapsule, the diffusion of HMS-301 would eventually stop, resulting in the trapping of HMS-301.

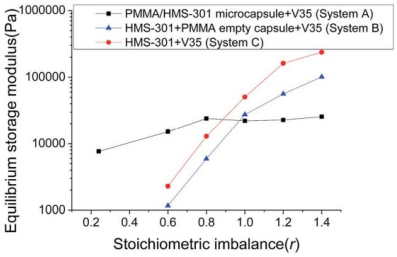

Fig. 7 Equilibrium storage modulus of the resulting networks from PMMA/HMS-301 microcapsule (MP10H10C) +V35, HMS-301 + empty PMMA capsule + V35 and HMS-301 + V35 as a function of r.

The results of System B and System C clearly showed that the equilibrium storage modulus increased as stoichiometric imbalance increased in the interval $0.6 < r < 1.4$. For most of the PDMS network, the maximum equilibrium storage modulus was obtained in the range $1.2 < r < 1.4$, which was in line with our experimental results. In the comparison of System B and System C, the equilibrium storage modulus of System B was lower than that of System C at identical stoichiometric imbalance. This could be attributed to the immiscibility between the PDMS and the empty PMMA capsule. As such, this immiscibility increased the heterogeneity of the PDMS network, thereby causing the network's lower equilibrium storage modulus.

When comparing the rheological properties of Systems A, B and C, the equilibrium storage modulus of System A was higher than that of Systems B and C in the range $0.2 < r < 0.8$. The high storage modulus of System A in this range could be attributed to the reinforcing effect of the PMMA shell from the PMMA/HMS-301 microcapsule.[27] The reinforcing effect is explained as follows: when the mixture containing the PMMA/HMS-301 microcapsule and V35 was heated up to 120 °C, HMS-301

Table 4 Composition and stoichiometric imbalance of Systems A, B and C

System ID		r	$m_{(\text{PMMA/HMS-301 microcapsule})}$/g	$m_{(\text{PMMA empty capsules})}$/g
A	PMMA/HMS-301 microcapsule + V35	0.2	0.010	—
		0.6	0.027	—
		0.8	0.033	—
		1.0	0.045	—
		1.2	0.058	—
		1.4	0.067	—
B	HMS-301 + empty PMMA capsules + V35	0.6	—	0.018
		0.8	—	0.023
		1.0	—	0.034
		1.2	—	0.042
		1.4	—	0.045
C	HMS-301 + V35	0.6	—	—
		0.8	—	—
		1.0	—	—
		1.2	—	—
		1.4	—	—

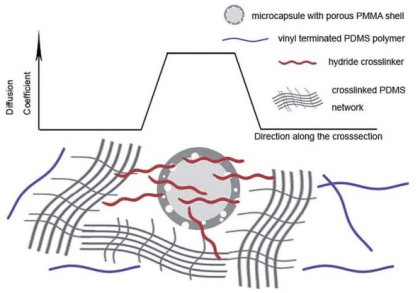

Fig. 8 Schematic diagram of the formed PDMS network around the microcapsule that leads to the trapping of HMS-301 in the range $0.8 < r < 1.4$.

diffused out from the PMMA shell. The released HMS-301 reacted with V35 around the microcapsule, yielding crosslinking points around the microcapsules. Locally formed PDMS gel adhered to the porous PMMA shell, eventually anchoring the PDMS chain to the porous PMMA shell, which consequently reinforced the network and increased its storage modulus.[28]

In the range $1.0 < r < 1.4$, the equilibrium storage modulus of Systems B and C was significantly higher than that of System A with an identical stoichiometric imbalance. This indicated that the equilibrium storage modulus was determined by the homogeneity of the network in this range. The homogeneity of the network of System A was constrained by the trapping of HMS-301, as explained in the previous discussion. The trapping of HMS-301 – caused by the PDMS network around the microcapsule – is envisioned in Fig. 8.

Despite the low storage moduli of the obtained PDMS elastomer (~30 kPa), it is comparable to that of so-called heterogeneous bimodal networks developed by Bejenariu *et al.* (10–300 kPa)[17] as well as Madsen *et al.* (10–100 kPa).[29] To increase the storage moduli of the network, a natural extension of this study would be to fill the liquid silicone (V35) with fumed silica to reinforce the resulting elastomer. This will increase the storage modulus dramatically and cause elastic moduli comparable to that of commercial silicone elastomer formulations. However, current materials for fracture sealing include hydrogels with significantly lower elastic moduli[30–33] so for that particular application no further filler reinforcement is deemed necessary.

Conclusions

Control of the crosslinking reaction between a vinyl-terminated PDMS and a hydride crosslinker has been achieved by encapsulating a HMS-301 hydride crosslinker in a PMMA shell. This PMMA/HMS-301 microcapsule was mixed with a V35 vinyl-terminated PDMS to create a stable mixture which remained viscous at 50 °C, thereby indicating that the mixture did not react and that the HMS-301 was sequestered in the PMMA shell. In contrast, the mixture formed a gel when heated up to 120 °C, suggesting that an extensive crosslinking reaction took place between HMS-301 and V35, due to the release of HMS-301 from the microcapsule. As the amount of HMS-301 released determined the crosslinking density and the storage modulus of the PDMS network, the influence of stoichiometric imbalance on the equilibrium storage modulus of the PDMS network was investigated. It was found that the addition amount of a microcapsule increased the equilibrium storage modulus of the PDMS network in the range $0.2 < r < 0.8$. It was also found that the equilibrium storage modulus of the PDMS network remained constant in the range $0.8 < r < 1.4$, due to the stalled diffusion of the HMS-301 by the locally formed PDMS network around the microcapsule. This indicated that the equilibrium storage modulus of the PDMS network became less sensitive towards stoichiometric imbalance in the control crosslinking reaction.

In applications where high modulus and transparency are not required, soft PDMS elastomer obtained from controlled crosslinking reaction can be utilized, *e.g.* as elastomeric plugs in oil fields. Furthermore, the optimum amount of microcapsules used in the controlled crosslinking reaction was found in the present study, which allows for designing an optimised controlled crosslinking system.

References

1 A. P. R. Johnston, G. K. Such and F. Caruso, *Angew. Chem., Int. Ed. Engl.*, 2010, **49**, 2664–2666.
2 B. J. Blaiszik, S. L. B. Kramer, S. C. Olugebefola, J. S. Moore, N. R. Sottos and S. R. White, *Annu. Rev. Mater. Res.*, 2010, **40**, 179–211.
3 L. Gonzalez, B. Ma, K. Malgorzata, L. Li, H. J. Hansen, S. Hvilsted and A. L. Skov, *Macromol. Mater. Eng.*, 2014, DOI: 10.1002/mame.201400020.
4 Y. Deyrail, N. Zydowicz and P. Cassagnau, *Polymer*, 2004, **45**, 6123–6131.
5 A. P. Esser-Kahn, S. A. Odom, N. R. Sottos, S. R. White and J. S. Moore, *Macromolecules*, 2011, **44**, 5539–5553.
6 S. H. Cho, S. R. White and P. V. Braun, *Adv. Mater.*, 2009, **21**, 645–649.
7 C. L. Mangun, C. Mader, N. R. Sottos and S. R. White, *Polymer*, 2010, **51**, 4063–4068.
8 J. E. Mark and J. L. Sullivan, *J. Chem. Phys.*, 1977, **66**, 1006–1011.
9 K. Urayama, T. Kawamura and S. Kohjiya, *J. Chem. Phys.*, 1996, **105**, 4833–4840.
10 S. Patel, S. Malone and C. Cohen, *Macromolecules*, 1992, **25**, 5241–5251.
11 F. Chambon and H. H. Winter, *J. Rheol.*, 1987, **31**, 683–697.
12 H. H. Winter and F. Chamson, *J. Rheol.*, 1986, **30**, 367–382.
13 S. M. G. Frankær, M. K. Jensen, A. G. Bejenariu and A. L. Skov, *Rheol. Acta*, 2012, **51**, 559–567.
14 M. Villar, M. Bibbo and E. Valles, *Macromolecules*, 1996, **29**, 4072–4080.

15 A. L. Larsen, K. Hansen, O. Hassager, A. Bach, S. Ndoni and M. Jørgensen, *Macromolecules*, 2003, **36**, 10063–10070.
16 D. Dasgupta, S. Manna and A. Garai, *Macromolecules*, 2008, **41**, 779–787.
17 A. Bejenariu, L. Yu and A. Skov, *Soft Matter*, 2012, **8**, 3917–3923.
18 T. J. Sanborn, P. B. Messersmith and A. E. Barron, *Biomaterials*, 2002, **23**, 2703–2710.
19 E. Westhaus and P. B. Messersmith, *Biomaterials*, 2001, **22**, 453–462.
20 B. Peña, C. Panisello, G. Aresté, R. Garcia-Valls and T. Gumí, *Chem. Eng. J.*, 2012, **179**, 394–403.
21 C. Panisello and R. Garcia-Valls, *Ind. Eng. Chem. Res.*, 2012, **51**, 15509–15516.
22 L. Chu, S. Park, T. Yamaguchi and S. Nakao, *Langmuir*, 2002, **18**, 1856–1864.
23 L. Chu, S. Park, T. Yamaguchi and S. Nakao, *J. Membr. Sci.*, 2001, **192**, 27–39.
24 A. H. Lefebvre, *Atomization and sprays*, ed. N. Chigier, Hemisphere publishing corporation, West lafayette, US, 1989, pp. 14–25.
25 E. Herrero, E. Valle and M. Galan, *Chem. Eng. J.*, 2006, **117**, 137–142.
26 S. Ndoni and O. Kramer, *Europhys. Lett.*, 1997, **39**, 165–170.
27 M. I. Aranguren, E. Mora and J. V. DeGroot Jr, *J. Rheol.*, 1992, **36**, 1165–1182.
28 D. Ciprari, K. Jacob and R. Tannenbaum, *Macromolecules*, 2006, **39**, 6565–6573.
29 F. B. Madsen, A. E. Daugaard, C. Fleury, S. Hvilsted and A. L. Skov, *RSC Adv.*, 2014, **4**, 6939.
30 G. A. Al-Muntasheri, I. A. Hussein, H. A. Nasr-El-Din and M. B. Amin, *J. Pet. Sci. Eng.*, 2007, **55**, 56–66.
31 M. Rafipoor, M. V. Sefti, F. Salimi, K. Jarrahian and S. S. Ghorashi, *J. Dispersion Sci. Technol.*, 2013, **6**, 1–31.
32 B. Sengupta, V. P. Sharma and G. Udayabhanu, *J. Pet. Sci. Eng.*, 2012, **81**, 145–150.
33 L. González, A. L. Skov and S. Hvilsted, *J. Polym. Sci., Part A: Polym. Chem.*, 2013, **51**, 1359–1371.

The Danish Polymer Centre
Department of Chemical and Biochemical Engineering
Technical University of Denmark
Søltofts Plads, Building 227
DK-2800 Kgs. Lyngby
Denmark

Phone: +45 4525 6801
Web: www.dpc.kt.dtu.dk

ISBN : 978-87-93054-59-2